# ELECTRO-QUASISTATIC HUMAN BODY COMMUNICATION: FROM BIO-PHYSICAL MODELING TO BROADBAND CIRCUITS AND HCI APPLICATIONS

A Dissertation

Submitted to the Faculty

of

Purdue University

by

Shovan Maity

In Partial Fulfillment of the

Requirements for the Degree

of

Doctor of Philosophy

August 2019

Purdue University

West Lafayette, Indiana

# THE PURDUE UNIVERSITY GRADUATE SCHOOL
# STATEMENT OF DISSERTATION APPROVAL

Dr. Shreyas Sen, Chair

Department of Electrical and Computer Engineering

Dr. Kaushik Roy

Department of Electrical and Computer Engineering

Dr. Anand Raghunathan

Department of Electrical and Computer Engineering

Dr. Byunghoo Jung

Department of Electrical and Computer Engineering

**Approved by:**

Dr. Dimitrios Peroulis

Head of Electrical and Computer Engineering

To *Ma* and *Baba* who have been the greatest source of inspiration, encouragement, and support in my life

Smt Sujata Maity and Shri Mukul Maity

# ACKNOWLEDGMENTS

There have been numerous times on which I have gone through this page on my head. I am now able to write this due the generous support of so many people around me. First of all I would like to thank my advisor Prof. Shreyas Sen for his guidance, support throughout the course of my stay at Purdue. From a technical standpoint I have learned a lot from through the numerous discussion we had over the years. As a person I have grown a lot from the numerous interesting conversations we had away from our regular field of work. I am truly grateful for his help on the multiple occasions when he has helped me hands on to solve problems. To me he has been way more than just my PhD. advisor. I hope I have lived up to his expectations.

I would also like to thank my thesis committee members, Prof. Kaushik Roy, Prof. Anand Raghunathan, Prof. Byunghoo Jung for their guidance and useful suggestions for my PhD. Thesis.

I would like to thank Air Force Office of Scientific Research, National Science Foundation, Semiconductor Research Corporation for funding my research throughout my PhD.

I would like to thank all my colleagues at SPARC Lab, Debayan Das, Baibhab Chatterjee, Donghyun Seo, David Yang, Mayukh Nath, Scott Redford, Gregory Chang, Nirmoy Modak, Parikha Mehrotra, Shitij Avlani, Gargi Bhattacharya, Xinyi Jiang, Mingxuan He, Shreeya Sriram, Abhishek Srivastava, Chun Tao, Mananga Mutombo for their professional and personal support throughout my stay at Purdue. I have learned a lot from them and their company has made my stay at Purdue an enjoyable journey. I am thankful to Mohit Singh, Weeseong Seo for taking the role of senior mentors when I started the journey of a PhD. student in a new lab.

I would also like to thank my friends Arnab Raha, Indranil Chakraborty, Punyashloka Debashis, Sibendu Paul, Deboleena Roy for helping me start off my life at a new coun-

try and being there throughout the journey. A special thanks to David, Punyashloka, Donghyun, Arnab, Gregory, Mananga for giving me numerous rides back home during the late night stays in lab which played a crucial role in shaping my PhD.

Finally, I would like to thank my parents for their unconditional support and love which has made me worthy of writing this thesis.

TABLE OF CONTENTS

Page

Page

Page

Page

Page

# LIST OF TABLES

# LIST OF FIGURES

Figure Page

Figure Page

Figure Page

Figure Page

Figure Page

Figure Page

Figure Page

Figure Page

Figure Page

Figure Page

Figure Page

# ABSTRACT

Maity, Shovan PhD student, Purdue University, August 2019. Electro-Quasistatic Human Body Communication: from Bio-physical modeling to Broadband Circuits and HCI Applications . Major Professor: Shreyas Sen.

Decades of scaling in semiconductor technology has resulted in a drastic reduction in the cost and size of unit computing. This has enabled computing capabilities in small form factor wearable and implantable devices. These devices communicate with each other to form a network around the body, commonly known as the Wireless Body Area Network (WBAN). Radio wave transmission over air is the commonly used method of communication among these devices. However, the human body can be used as the communication medium by utilizing its electrical conductivity property. This has given rise to Human Body Communication (HBC), which provides higher energy efficiency and enhanced security compared to over the air radio wave communication enabling applications like remote health monitoring, secure authentication. In this thesis we characterize the human body channel characteristics at low frequencies, utilize the insight obtained from the channel characterization to build high energy-efficiency, interference-robust circuits and demonstrate the security and selectivity aspect of HBC through a Common Off the Shelf (COTS) component-based system. First, we characterize the response of the human body channel in the 10KHz1MHz frequency range with wearable transmitter/ receiver to study the feasibility of using it as a broadband communication channel. Voltage mode measurements with capacitive termination show almost flat-band response in this frequency range, establishing the body as a broadband channel. The body channel response is also measured across different interaction scenario between two wearable devices and a wearable and a computer. A bio- physical model of the HBC channel is developed to explain the

measurement results and the wide discrepancies found in previous studies.We analyze the safety aspect of different type of HBC by carrying out theoretical circuit and FEM based simulations. A study is carried out among multiple subjects to assess the effect of HBC on the vital parameters of a subject. A statistical analysis of the results shows no significant change in the vital parameters before and during HBC transmission, validating the theoretical simulations showing ¿1000x safety margin compared to the established ICNIRP guidelines. Next, an HBC transceiver is built utilizing the wire-like, broadband human body channel to enable high energy efficiency. The transceiver also provides robustness to ambient interference picked up by the human body through integration followed by periodic sampling. The transceiver achieves 6.3pJ/bit energy efficiency while operating at a maximum data rate of 30 Mbps, while providing -30dB interference tolerant operation. Finally, a COTS based HBC prototype is developed, which utilizes low frequency operation to enable selective and physically secure communication strictly during touch for Human Computer Interaction (HCI) between two wearable devices for the first time. A thorough study of the effect of different parameters such as environment, posture, subject variation, on the channel loss has also been characterized to build a robust HBC system working across different use cases. Applications such as secure authentication (e.g. opening a door, pairing a smart device) and information exchange (e.g. payment, image, medical data, personal profile transfer) through touch is demonstrated to show the impact of HBC in enabling new human-machine interaction modalities.

# 1. INTRODUCTION

Decades of scaling following Moore's law has led to the exponential decrease in the cost and size of unit computing. This has enabled the development of small form factor wearable, implantable devices which reside on and around the body. These devices communicate among each other to form a network of devices around the body commonly referred to as the Wireless Body Area Network (WBAN). Wireless radio frequency electromagnetic waves are the communication method of choice for these devices to communicate among themselves. However, the proximity of these devices to the human body along with the body's electrical conductivity properties can be utilized to use the human body as the electrical communication medium between these devices. This has led to the development of Human Body Communication (HBC), also commonly referred to as Body Coupled Communication (BCC) or Intra-Body Communication (IBC).

## 1.1 Key Advantages

HBC provides potential advantage compared to wireless radio wave communication in terms of energy-efficiency and security as shown in 1.1. The energy-efficiency aspect is enabled due to the low-loss, broadband nature of the human body channel. Radio wave communication suffers high loss around the body due to absorption and multi-path reflection effects. Hence, the transmission loss during HBC is lower compared to radio waves during transmission around close proximity of the human body. This results in higher received signals and hence less stringent sensitivity requirement on the receiver. A higher sensitivity receiver requires higher power for its operation, which reduces the battery life of small form factor wearable devices. Also, for radio wave transmission the operating frequency is limited by the size of the antenna, which

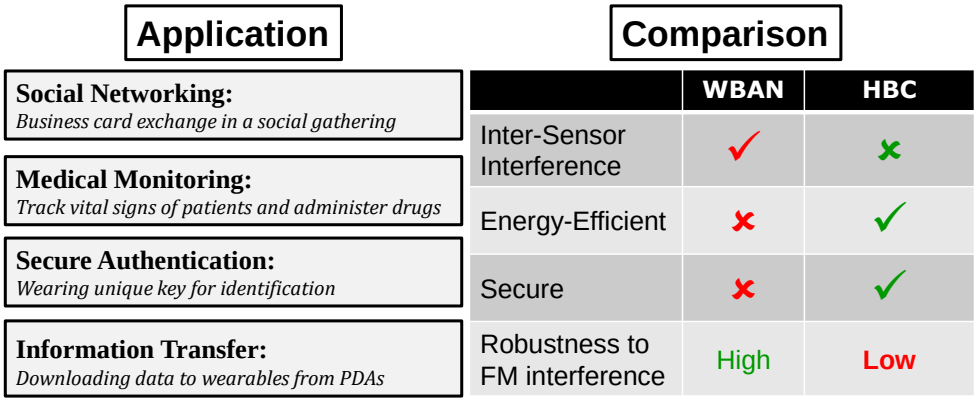


Fig. 1.1. Application of HBC and comparison with WBAN

is limited by the size of the device. Small devices are restricted to have small antennas, which makes the operating frequency higher. A high operating frequency in turn requires higher power for operation. In HBC operation, no antenna is required for signal transmission, as the signal is coupled to the body. Hence, the operating frequency of HBC is not limited by any physical parameter. Hence, systems utilizing HBC can operate at lower frequencies which make them power efficient compared to wireless systems using radio waves, subsequently increasing the lifetime of the devices and systems.

The physical security aspect of HBC comes from the fact that the signal transmission is contained primarily within or in close proximity to the human body. Hence, an attacker cannot snoop any ongoing HBC transmission without either touching or coming really close to the person. In radio wave transmission, this is not possible, as the signal is radiated from the transmitter into the air medium and any malicious attacker who is within the range of the transmission can pick up the transmitted signals. The human body as a communication medium can potentially provide this additional physical layer security which is not present in radio wave communication.

There are a few key challenges involved in designing a HBC based WBAN system. The human body acts as an antenna in a wide frequency range. As a result, any interference present in the environment in this frequency range gets picked up by the

human body. This interferes with any data communication going on within the body creating a bottleneck for HBC.

## 1.2 Different Types of HBC

Human Body Communication (HBC) was first proposed by Zimmerman [1] as a method of communication for devices in Personal Area Networks. Here a battery operated transmitter is used to couple a modulated picoamp displacement current into the human body and transmit it through to the receiver. This kind of HBC technique is termed as Capacitive HBC, since the closed loop circuit in this scenario is formed by a capacitive return path through coupling between the transmitter, receiver ground planes and the surrounding environment. However this results in the signal getting attenuated at the receiver end. Wegmueller et al. [2] proposed Galvanic HBC, where the transmitted signal is applied to the human body between two electrodes connected to the body and picked up at the receiver end through two similar electrodes. However, it has been established that, in Galvanic HBC the signal gets attenuated more for longer distance communication within the body (left arm to right arm / arm to torso). Recently there has been studies about Magnetic Human Body Communication [3], where magnetic fields are used to communicate between devices on the body. However, this requires bulky coils at the transmitter and receiver end to pick up the magnetic field. Hence, the receiver and transmitter device sizes become big and are not suitable for the design of a wearable form factor device. Hence for our demonstration we have used Capacitive HBC as the type of HBC transmission.

## 1.3 HBC applications

The enhanced energy-efficiency and security property of HBC can be utilized in the following applications 1.2:

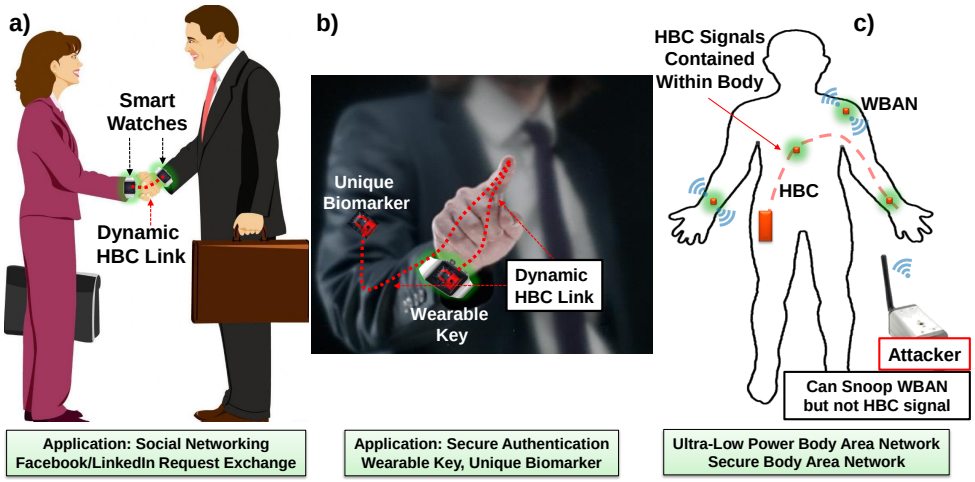


Fig. 1.2. Applications of Human Body Communication (HBC). Dynamic HBC a) Social Networking: Facebook/LinkedIn request exchanged through the human body between smartwatches, during Handshaking in a Meeting/Party b) Secure Authentication: Secure wearable keys on smartwatch or other wearable devices could be used in addition to fingerprint for additional layer of security using the human body to communicate it during touch based authentication c) Static HBC allows ultra-low power body area network (BAN) due to low loss, broadband HBC channel. HBC also implements secure BAN as, unlike WBAN signals, the HBC signals cannot be snooped on by a wireless attacker

- *Social Networking:* With almost everyone having a social and professional digital presence like Facebook or LinkedIn, HBC can be used to exchange social networking requests through smart watches when concerned people shake hands in a gathering.

- *Medical Monitoring:* HBC can be used to aggregate and monitor the vital signs of a patient like pulse rate, blood sugar, blood pressure, ECG etc. from wearable/implantable sensors and administer appropriate dosage of drugs depending upon the captured signatures through remote health monitoring.

- *Authentication:* Apart from the usual authentication of fingerprint or retinal detection, HBC can add an additional layer of unique identification if the user wears a unique key that can be verified when the user touches the sensor.

- *Information Transfer:* Data can be transferred by HBC between Personal Device Assistants (PDA) if users wear a memory device and touch sensors on the PDAs. A user can download the map of a journey to a smartwatch by just touching a PC with fingers.

In this thesis, we characterize the human body channel in the low frequency range to potentially use it as a broadband channel through Electro-quasistatic Human Body Communication. We show that the body can indeed be used as a broadband channel through proper channel engineering. Using the insights built through channel measurements, we design an interference robust receiver IC, which mitigates the interference problem due to the human body antenna effect. We also demonstrate secure , selective HBC for applications such as secure authentication, information transfer through COTS component based HBC devices.

Chapter 2 provides a bio-physical model of electro-quasistatic HBC, validated through measurement results and explains most of the discrepancies found in previous literature. We also discuss about the key techniques required to achieve broadband channel characteristics. The channel loss across different interaction scenarios between devices through HBC has also been explored to illustrate the different channel conditions that can be encountered during HBC.

Chapter 3 discusses the problem of interference in HBC due to the human body antenna effect and provides the theory of an integrating receiver to achieve interference robust broadband HBC.

Chapter 4 describes the detailed design of a Integrating Dual Data Rate receiver based on the theory developed in Chapter 3. The performance of the receiver, fabricated in TSMC 65nm technology, is measured in the presence of different type of interferences.

Chapter 5 provides the details of a COTS implementation of electro-quasistatic HBC for Human Computer Interaction (HCI). Three different applications are demonstrated utilizing the selectivity and security property shown by electro-quasistatic HBC.

Chapter 6 demonstrates secure communication between two devices using Electro-quasistatic Human Body Communication. The effect of posture, environment, inter-person variation on the channel response and the signal leakage out of the body is analyzed to design a prototype demonstrating communication between two wearable devices.

Chapter 7 provides a circuit and FEM simulation based analysis of the safety aspect of HBC by comparing the current, field intensity levels compared to the established safety standards from IEEE, NIOSH and ICNIRP. Chapter 8 provides conclusion, highlighting the key results obtained.

# 2. BIOPHYSICAL MODELING, CHARACTERIZATION AND OPTIMIZATION OF ELECTRO-QUASISTATIC HUMAN BODY COMMUNICATION

Most of the materials in this chapter have been extracted verbatim from the papers:

1. S. Maity, M. He, M. Nath, D. Das, B. Chatterjee, and S. Sen, BioPhysical Modeling, Characterization and Optimization of Electro-Quasistatic Human Body Communication in IEEE Transactions on Biomedical Engineering

2. S. Maity, K. Mojabe, and S. Sen, Characterization of Human Body Forward Path Loss and Variability Effects in Voltage-Mode HBC, IEEE Microwave and Wireless Components Letters, vol. 28, no. 3, pp. 266268, Mar. 2018.

Proper understanding of the human body channel characteristics is necessary in designing efficient HBC transceivers. Previous studies [4–19], which characterizes the body channel has shown wide variation in the measured channel characteristics as shown in fig. 2.1 . This can be attributed to two primary reasons: 1) insufficient ground isolation between the transmitter and the receiver, resulting in lower measured loss; 2) low impedance termination at the receiver end, resulting in higher loss at low frequencies. The devices communicating through HBC have small ground planes and is isolated from each other. So, in case of measurement devices with large ground planes, insufficient ground isolation between transmitter and receiver results in optimistic estimation of the channel loss. Similarly, source resistance at the transmitter end and termination impedance at the receiver end are key factors affecting the channel loss characteristics. This chapter builds a lumped bio-physical capacitive HBC circuit model, which explains the experimental human body channel loss for frequencies up to 1MHz. The signal wavelength at these frequencies (>300 m) are orders of magnitude bigger than the human body size (2 m) and the communication happens in the electro-quasistatic regime. The optimum signaling modality for

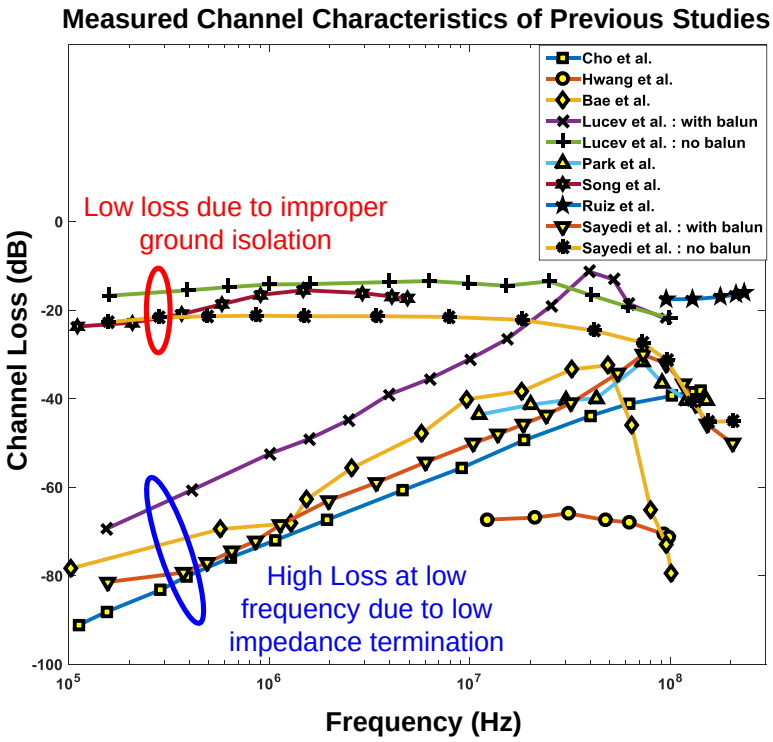


Fig. 2.1. Channel Measurement plots from previous studies, showing wide variance in measured characteristics. Some of the measurements are carried out with transmitter and receiver having insufficient ground isolation. Some other studies achieve isolation through baluns but use Vector Network Analyzer/ Spectrum Analyzer for measurement, which has a low impedance termination, resulting in higher low frequency loss and hence a high pass response.

voltage mode human body communication is also discussed with simulation/ experimental analysis done to understand the effect of each of those factors on the overall channel characteristics and explain some of the discrepancies seen in previous channel measurement studies. Following are the key contributions of this chapter:

- Developed a lumped bio-physical HBC circuit model, for the electro quasi-static regime of operation, which explains the experimental channel loss characteristics up to 1MHz frequency for different excitation and termination. This also

provides a unifying explanation to some of the measurement results shown in earlier studies.

- Developed a miniaturized wearable prototype, which uses time domain sampling, for voltage mode channel measurements to replicate the scenario of an actual wearable to wearable communication.

- Measured the human body channel loss at low frequencies (10KHz1MHz) to characterize it as a broadband communication channel, supporting data rates up to 1 Mbps.

- Analyzed the effect of termination impedance (low vs high impedance, capacitive vs resistive) and source impedance (low vs high impedance) on the overall channel characteristic and provide recommendations for optimum HBC signaling.

## 2.1 Previous Channel Measurement Studies

Several studies [4,6–12] have been carried out to characterize the Capacitive HBC channel loss. However, these studies show a wide variance in the measured channel response. This shows a strong sensitivity of the results on the measurement setup. In this section we discuss about the experimental setup and measurement results of some of those studies.

Cho et al. [4] reported the human body characteristic in the 100KHz-100MHz range to be that of a band-pass filter with loss as high as 90dB at 100KHz. The pass band frequency is greater than 10MHz and the loss at the pass band varies between 35dB to 60dB depending on transmitter, receiver distance and also on the size of the ground electrodes. A battery powered signal generator with a programmable frequency synthesizer is used to transmit signal into the body. A grounded oscilloscope or spectrum analyzer is connected to the receiver electrode to measure the received

signal. So in this case the transmitter and receiver are electrically isolated but the receiver has a strong ground connection.

Lucev et al. [6] uses a network analyzer as both the transmitter and receiver. But the internal ground of the network analyzer acts as a common ground in this scenario. To circumvent this common ground issue, the authors introduce baluns at both the receiver and transmitter end to electrically isolate the two grounds. The channel characteristic without the baluns show a flat band response in the frequency range of 100KHz-100MHz, with a loss of around 20dB. Whereas introducing the baluns show a bandpass characteristic with loss of 80dB around 100KHz and the minimum loss of 20dB around 35MHz. The loss varies depending on the distance between the transmitter and receiver.

Bae et al. [7] also characterize the human body channel in the 100KHz-100MHz range with a battery operated transmitter and an oscilloscope isolated through a balun to observe the signals. The authors report a bandpass characteristic with a peak frequency of 40-60MHz, which varies depending on the distance between the transmitter and receiver electrodes. The channel loss at a particular frequency is also dependent on the distance between the transmitter and receiver, but shows significantly higher variation than those reported in [6].

Hwang et al. [8] uses a battery powered transmitter and an oscilloscope as receiver, synchronized through an optical cable. A differential probe is used at the receiver end to isolate the receiver ground from the oscilloscope ground. Measurement results show that the human body channel shows a flat band response in the 10-100MHz frequency range, with loss of 75dB. Measurements with oscilloscope ground directly connected to the receiver ground show a 6dB change on average loss compared to the non-ground sharing case, but retaining the flat band response. This is contrary to [6], where the introduction of a balun to isolate the receiver ground changed the response from flat band to band pass. Ruiz et al. [9] carry out experiments in the 100MHz-1.5GHz frequency range with a network analyzer to provide and receive signals for different electrode configuration and sizes. The measured channel characteristics show quite

a lot of variation depending on the electrode configuration. But all of them show a low pass response with a minimum loss of around 20dB at lower frequencies for one particular configuration.

Callejon et al. [10] carry out experiments for both galvanic and capacitive HBC and study the effects of channel length, electrode type, different human subjects and different parts of the body, posture of the subject on the channel characteristics. The capacitive coupling measurements are done at 1-100MHz, with input and output both provided by spectrum analyzer and isolated by baluns at both sides. The channel response is bandpass, with peak between 60-70MHz. The channel loss has weak dependence on channel length, with a difference of around 10dB for channel lengths of 15cm and 125cm. Configurations with large ground electrode sizes also showed lesser loss.

Callejon et al. [11] carry out experiments with different kind of transmitter and receiver ground connections in 10KHz-1MHz frequency range to study the effect of experimental setup on measured characteristics of the human body channel. They carry out experiments in 5 different setups: receiver, transmitter ground connected; transmitter ground isolated through a balun keeping the receiver connected to ground; transmitter connected to ground keeping receiver isolated through balun; both receiver and transmitter isolated through balun; battery operated receiver and transmitter with no connection to earth ground. The experimental results show that the results from the battery operated scenario matches closely with the case where only the transmitter is isolated through a balun and the loss characteristic is almost flat over the frequency range with loss of 20dB. This matches closely with the simulation model that has been built in the chapter. Whereas their experiments showed a band pass response, while introducing a balun in the receiver side irrespective of the transmitter being connected to ground or not and this deviates from the simulation results of the model they have developed. From their experiments the authors conclude to discard any measurement setup that introduces baluns at the receiver side. But this kind of setup has been used in [6, 7].

Park et al. [12] characterize the human body channel through a setup containing miniaturized wearable devices. The channel is characterized in the 20-150MHz frequency range. The response shows a peak around 70 MHz with a loss of around -35dB. The overall channel response in this range is almost flat with loss ranging from -42dB to -32dB. The authors provide suggestion of using a miniaturized wearable setup for measuring channel characteristics and show that measurement setup using Vector Network Analyzer (VNA) or Spectrum Analyzer provide optimistic channel loss measurements even with baluns used for isolation. The studies conducted so far either characterize the human body as a bandpass or a lowpass channel with significant variation in the loss magnitude. The goal of this chapter is to explain the sources of discrepancy/ variation in the measurements in literature and provide a unifying explanation and repeatable channel models. We carry out measurements up to the frequency range of 10KHz-1MHz with voltage mode signaling, which will enable characterizing the human body as a channel for broadband communication, supporting data rates up to 1Mbps.

## 2.2 Bio-Physical HBC Circuit Model

### 2.2.1 Electro-quasistatic Transport

The primary focus of this work is on measuring the HBC channel characteristics for the frequency range of up to 1MHz. The propagation wavelength at this frequency range is >300m, which is orders of magnitude longer than possible HBC channel length (a few meters maximum). Also at this frequency range, magnetic fields do not contribute in conduction through the human body allowing electro-quasistatic transport. In case of electro-quasistatic transport the ratio between the approximation error ($E_{error}$) and the developed electric field (E) is provided as:

$$\frac{E_{error}}{E} = 4\pi^2 f^2 \mu_{tissue} \epsilon_{tissue} r^2, E = E_{EQT} + E_{error} \tag{2.1}$$

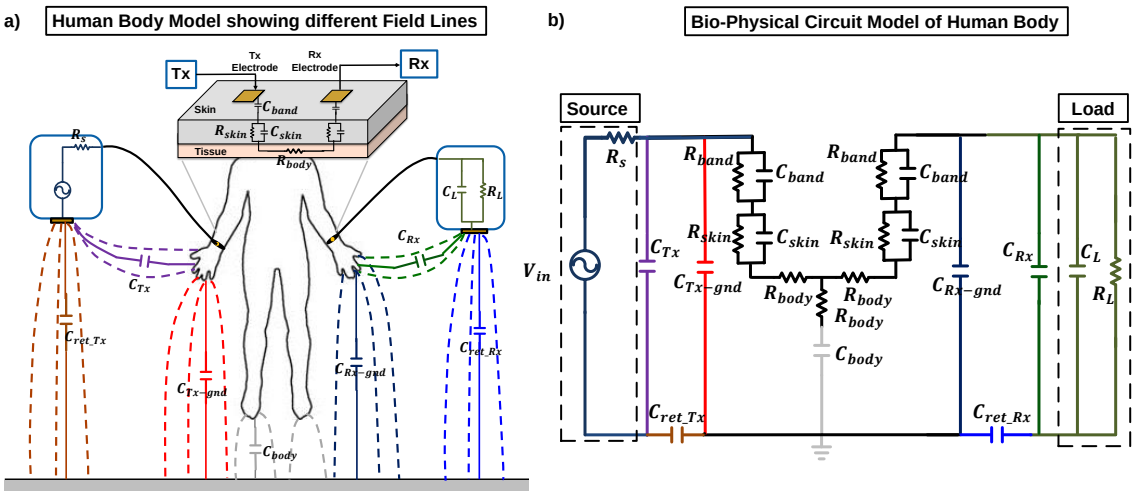


Fig. 2.2. a) Diagram explaining the origin of different resistances and capacitances of the electro-quasistatic HBC model. The parasitic capacitances are formed by coupling between the body, transmitter/receiver ground plane and the earth ground. The internal body resistance and capacitances are shown in the tissue model. b) The HBC circuit model considering all the components as shown in part a.

where $\epsilon_{tissue}$ is the permittivity and $\mu_{tissue}$ is the permeability of subcutaneous tissue, $r$ is the distance of human body communication and is $< 2$ meters, $f$ is the frequency of operation ($< 1$MHz). Now using $\epsilon_{tissue} = 8\epsilon_{air}$ [20],$\mu_{tissue} = \mu_{air}$, $r = 2m$ and $f = 1$MHz, the approximation error

$$\frac{E_{error}}{E} = 0.014 \tag{2.2}$$

Hence in this frequency range of operation the approximation error is small and it is reasonable to assume quasi-static electric field as the dominant mode of signal propagation through the human body. Assuming up to 5% approximation error is allowable then the electro-quasistatic approximation is valid up to 1.89 MHz frequency. So in this frequency range, the signal is primarily contained within the human body. Since skin has higher impedance compared to the underlying low impedance layers such as the dermis, connective tissue,

| Component | Value | Comments |
|---|---|---|
| Source Resistance ($R_s$) | 50Ω | Source impedance of the signal generator |
| Band to Skin Capacitance ($C_{band}$) | 200 pF | The transmitter/receiver electrode is in direct contact with the skin for our experiments, hence the air gap (d) between them is very small (<0.1mm). With an electrode size of $4cm^2$ and $d = 0.01mm$, $C = 354pF$. This capacitance will become prominent when the electrode skin contact is loose. |
| Band to Skin Resistance ($C_{band}$) | 100Ω | Tight contact between skin and electrode will create a resistive path between them with low resistance. |
| Skin Layer Resistance ($C_{band}$) | 10KΩ | The skin impedance varies in the range of 1K-100K depending on skin moisture and other factors [14–16] |
| Skin Layer Capacitance ($C_{band}$) | 90pF | Typical skin layer thickness is 0.2-4mm, hence taking a maximum thickness (d) of 4mm, dielectric constant of 100 [20], skin area (A) of 4 cm2 near the transmitter or receiver, the calculated capacitance is 90pF ($C = 100 * \epsilon_o * A/d$) |
| Tissue Resistance ($R_{body}$) | 200Ω | Subcutaneous tissue resistance is 100Ω-400Ω [14, 17] |
| Feet to ground capacitance ($C_{body}$) | 9pF | Assuming a feet area of 100 cm2 and feet to ground distance of 1cm, calculated capacitance is around 9pF |
| Body to ground capacitance at Transmitter ($C_{Tx-gnd}$) | 75pF | Half of the capacitance value determined from the experiment described in Section III.C |

| Component | Value | Comments |
|---|---|---|
| Body to ground capacitance at Receiver ($C_{Rx-gnd}$) | 75pF | Half of the capacitance value determined from the experiment described in Section III.C |
| Transmitter ground to body capacitance ($C_{Tx}$) | 300fF | Depends on the ground plane size and separation of ground plane from body. Ground plane size of 4 cm2 and separation of 1cm body results in a cap of 354fF |
| Receiver ground to body capacitance ($C_{Rx}$) | 300fF | Calculated in the same way as transmitter to ground capacitance, added as part of load capacitance as value is small compared to the load capacitance |
| Transmitter Ground to earth Capacitance ($C_{ret\_Tx}$) | 1.5pF | Experimentally determined by experiment in Section III.D |
| Receiver Ground to earth Capacitance ($C_{ret\_Rx}$) | 1.5pF | Experimentally determined by experiment in Section III.D |
| Load Capacitance ($C_L$) | 13pF for 10x probe 79pF for 1x probe 1pF for wearable | The load capacitance for the probes are taken from the data sheet. The input capacitance of the wearable device will be lower due to its smaller size. |
| Load Resistance ($R_L$) | 10MΩ for 10x probe 1MΩ for 1x probe 10MΩ for wearable | Load resistance values for the probes are taken from the data sheet. Since the wearable IC is made in CMOS technology, its input impedance is primarily capacitive and hence the input resistance is taken as 10M (high value). |

muscles, fat etc., the signal transmission primarily occurs through those conductive layers. Hence the signal transmission happens through electro quasi-static transport at the frequency range of interest in our measurements. We develop a lumped bio-physical model of electro quasi-static human body communication (EQS-HBC) at this frequency range.

### 2.2.2 Human Body Forward Path Components

In HBC the transmitter couples the signal through a metal electrode onto the skin. The outer most layer of the skin has higher impedance compared to the inner layer of fat, tissue and conductive fluids [11]. So, the signal transmission is primarily through the internal layers of the body. At the receiver end similar electrodes are used to receive the signal. As shown in fig. 2.2 (a), the electrode to skin contact can be modeled with a capacitance ($C_{band}$). A tighter contact will result in higher capacitance and hence lesser impedance. The capacitance value is dependent on the separation and is in the order of 100s of pF if the electrode skin contact distance <0.1mm. The skin impedance is also shown to be in the order of KΩ as found by previous studies [2,21,22]. The internal fat and conductive tissue has impedance in the order of 100s of ohms [21,23]. The source impedance of the transmitter is a few ohms. The load impedance provided is determined by the receiver device. If an oscilloscope is used for measurements, the impedance provided by the probe is a combination of resistance (1MΩ, 10MΩ) and capacitance (13pF, 79pF). These values are used to construct the circuit model of HBC transmission as shown in fig. 2.2 (b). The circuit model is also dependent on the termination and excitation modalities. For example, a single ended excitation model will have one electrode and skin impedance connected to the source, whereas a differential excitation will have two electrode impedances and two skin impedances connected to the source. The values of each of the resistance and capacitances used in the HBC bio-physical model and the parameters considered to get those values are discussed in Table I.

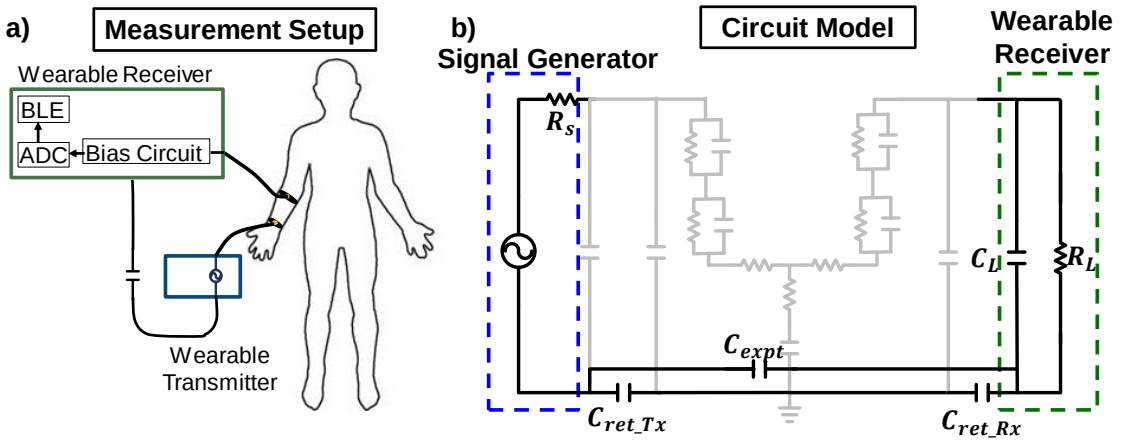


Fig. 2.3. a) Measurement setup used to estimate the return path capacitance between a wearable transmitter and receiver. b) Circuit model of the measurement. The equivalent return cap is $C_g = C_{expt} + \frac{C_{ret\_Tx} * C_{ret\_Rx}}{C_{ret\_Tx} + C_{ret\_Rx}}$ ). Loss measurements with multiple known value capacitances ($C_{expt}$) enable us to find the unknown return path capacitances ($C_{ret\_Tx}, C_{ret\_Rx}$).

### 2.2.3 Return Path Capacitance Estimation experiment

The overall channel loss is strongly dependent on the return path capacitance between the transmitter and the receiver. To estimate the return path capacitance, several known value capacitances ($C_{expt}$) are connected between the transmitter and receiver ground and the loss value measured. The experimental setup and the equivalent circuit model is shown in fig. 2.3. From the circuit model in fig. 2.3 (b), the channel loss can be estimated as $\frac{C_g}{C_L + C_g}$ , which is the capacitive division ratio of the equivalent return path capacitance ($C_g$) and the load capacitance ($C_L$). Now the return path capacitance in presence of the extra experimental capacitance is $C_g = C_{expt} + \frac{C_{ret}}{2}$ , assuming $C_{ret\_Tx} = C_{ret\_Rx} = C_{ret}$. From the loss measurements with different $C_{expt}$, we can now estimate the return path capacitance ($C_{ret}$). The estimated return path capacitance from this experiment is around 1.5pF. We use this

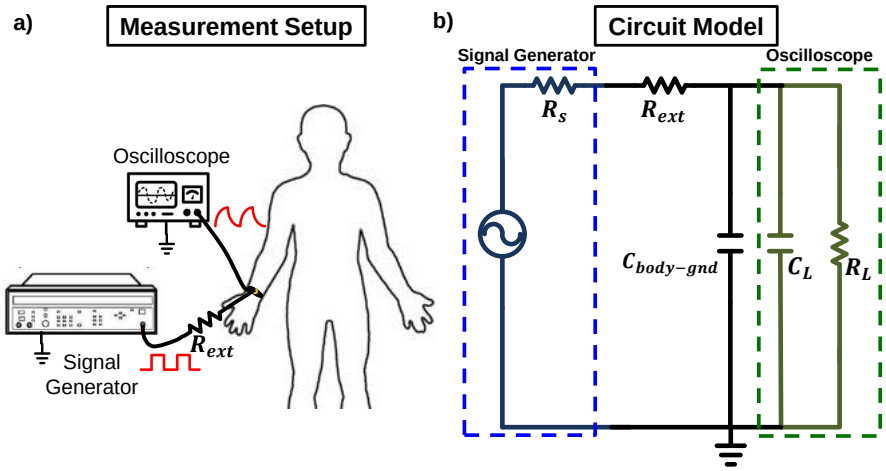


Fig. 2.4. a) Measurement setup used to estimate the capacitance between the body surface and ground. The input signal is applied to the body through a series resistance and observed through a oscilloscope. b) The equivalent circuit diagram of this experiment. The body to ground capacitance will act as an extra parallel capacitance to the oscilloscope load capacitance and hence affect the time constant of the received signal.

as the value of return path capacitance for the simulations of the HBC circuit model as shown in Table I.

### 2.2.4 Skin to Ground capacitance estimation experiment

One of the key components of the proposed HBC circuit model is the capacitance between the human body and the earth ground. The experimental setup shown in fig. 2.4 (a) is used for this measurement purpose. A signal generator is used to provide square wave input and is applied to the body through a series resistance. The series resistance is used to increase the time constant of the received signal at the receiver end. First the time constant of the signal is measured by directly applying it to the oscilloscope. The time constant in this scenario ($\tau_{osc}$) will be dependent on the series resistance and oscilloscope load capacitance, $\tau_{osc} = R_{ext}C_L$. Now, to measure the effect of capacitance between the body and external ground, the signal is applied to

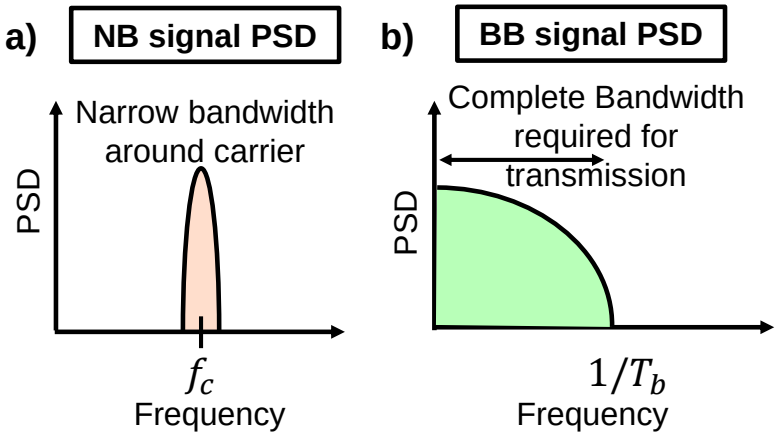


Fig. 2.5. a) PSD of a narrowband signal occupying only a small bandwidth around the carrier frequency, requiring the channel to be characterized around the carrier frequency and not until low frequencies. b) Power Spectral Density (PSD) of a broadband transmitted signal occupying the complete bandwidth from DC up to data rate, motivating the characterization of the human body channel up to low frequencies.

the body and the time constant measurement repeated. The time constant in this scenario ($\tau_{osc-body}$) is dependent on both the oscilloscope load capacitance as well as the body to ground capacitance, $\tau_{osc-body} = R_{ext}(C_{body-gnd} + C_L)$ (fig. 2.4 (b)). Measurement results with two different series resistance shows the body to ground capacitance to be around 150pF. Since this consists of the total capacitance from the body to ground, we model half of the capacitance at the transmitter end and the other half at the receiver end.

## 2.3 Broadband HBC

In this chapter, the HBC channel characterization is carried out in the frequency range of $<$ 1MHz. The goal is to analyze the feasibility of using the body as a wire-like broadband communication channel. A broadband channel with 1MHz bandwidth can enable transmission up to 1Mbps data rate, which is sufficient for most HBC appli-

cations such as physiological health monitoring, remote authentication, exchange of business card / social networking request [24–26]. During transmission, broadband HBC does not require modulation and demodulation, which requires high power circuits. Also, broadband HBC utilizes the complete bandwidth of the body for data transmission. Hence Broadband HBC promises to be more efficient than narrowband HBC in terms of required energy per bit with achievable energy efficiency of up to 6.3pJ/bit [27]. In a narrowband scenario (fig. 2.5 (a)) power can also be transferred for communication and hence the channel transfer characteristics can be determined as the ratio of received and transmitted average power [12]. However, broadband communication (fig. 2.5 (b)) requires the signal to be sent as a voltage corresponding to a 1/0 bit. Hence to characterize the channel for possible usage in broadband HBC we use voltage mode signaling, where voltage signal is applied as input. The received signal is also in voltage domain and is detected through time domain sampling of voltage signal. Due to the potential advantages of Broadband HBC, we characterize the HBC channel until low frequencies (10s of KHz) and compare the results with the simulation results from the developed bio- physical model in the following sections.

## 2.4 Common Ground Measurements: HBC Forward Path Characterization

Recently there has been studies [28] on characterizing the human body forward path channel loss. In this section we discuss about the forward path characterization experiment and compare the measurement results with the results obtained from the bio-physical model to validate the model. For all the measurement and simulation results throughout this chapter, the path loss has been represented with negative values.

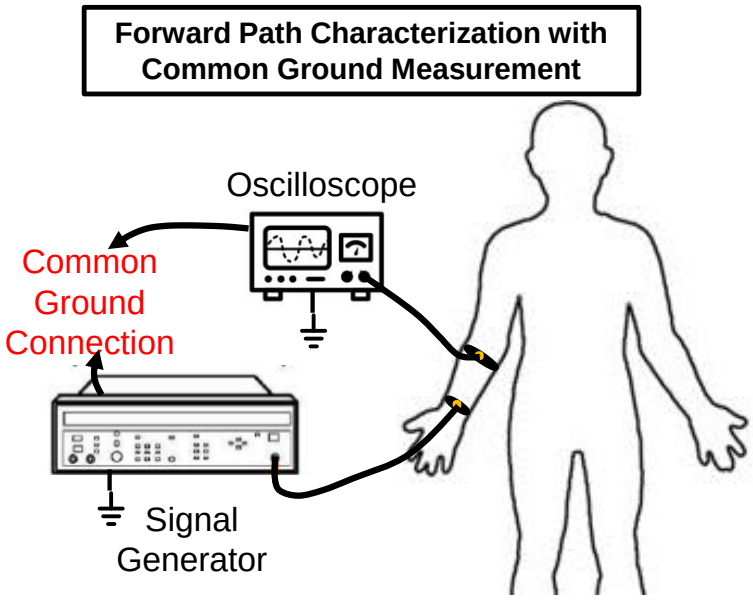


Fig. 2.6. Measurement setup for human body forward path characterization. A signal generator is used as a transmitter and an oscillscope measures the received voltage. The transmitter and receiver grounds are connected to remove the effect of return path capacitance on the measurement and characterize only the forward path.

### 2.4.1 Motivation

The channel loss in HBC has two primary sources: 1) the transmission channel, 2) the return path. To design better interface circuits with the human body channel by minimizing total loss, it is necessary to characterize and decouple the major sources of loss, e.g. if most of the loss is coming from the body or from the capacitive return path. In this section we try to address this issue by doing common ground measurements and hence removing the non-common ground effect. This will enable us to characterize the human body channel forward path and also determine the values of the different circuit elements used to characterize the human body.

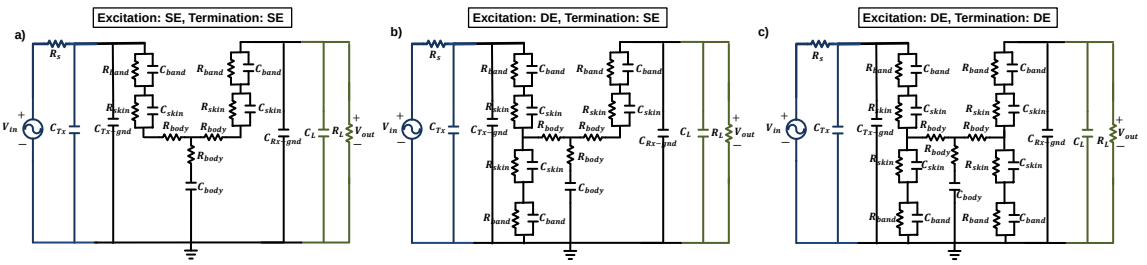


Fig. 2.7. Lumped Circuit Model of the human body for different transmitter receiver electrode configuration for forward path characterization with common ground between transmitter and receiver. Circuit model with: a) Single Ended (SE) excitation and Single Ended (SE) termination, b) Differential Ended (DE) excitation and Single Ended (SE) termination, c) Differential Ended (DE) excitation and Differential Termination. These different excitation/termination modalities help validate the developed circuit model and the component values.

### 2.4.2 Experiment Setup

A BK precision 4055 signal generator is used to provide a sine wave input at the TX and the signal at the RX end is observed in a Tektronix DPO 7104 oscilloscope (fig. 2.6). The oscilloscope and the signal generator grounds, are shorted to eliminate any effect coming from the return path through the power supply. Copper electrodes are used to couple the signal into the body. The frequency of the input sine wave is changed and the attenuation at the receiver end is measured to find the human body channel loss characteristics over different frequencies. Experiments are carried out for both differential (DE) and single ended (SE) excitation at multiple frequencies to find the forward path channel characteristics of the human body. The circuit model for each of these scenarios is shown in fig. 2.7. Voltage mode signaling is used for the experiments, which is provided by a low output impedance transmitter and a high input impedance receiver.

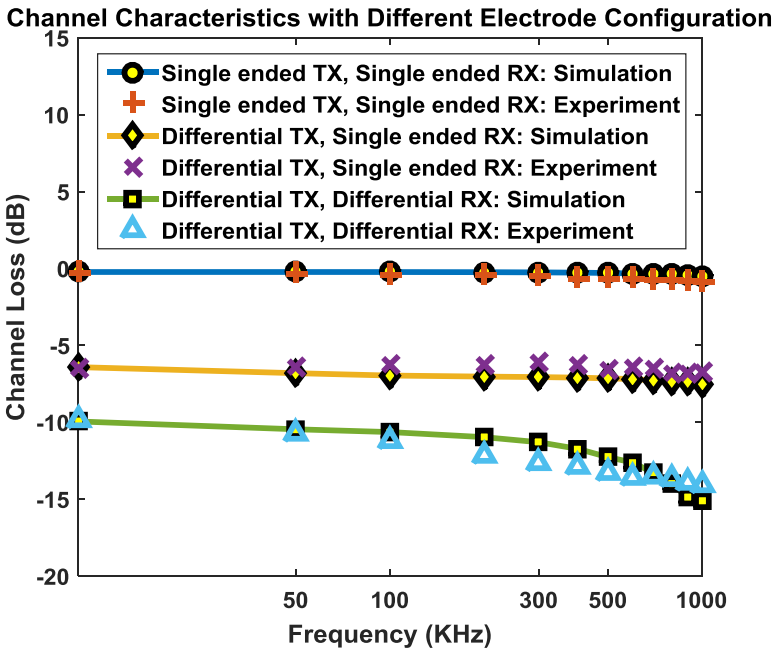


Fig. 2.8. Measurement results showing the characteristics of human body forward path under different excitation, termination modalities. The measured channel loss show close correspondence with the simulated loss from the developed human body circuit model.

### 2.4.3 Measurement Results

Experimental results (fig. 2.8) show that single ended excitation and termination shows minimum loss 0dB. Differential excitation with single ended termination, on the other hand shows a loss of 6dB whereas differential excitation and termination results in 10dB loss. This shows that the forward path channel loss not only depends on the human body channel characteristics but also on the excitation termination modalities. The measured loss characteristics match with the simulation model with the values of circuit components as shown in Table I.

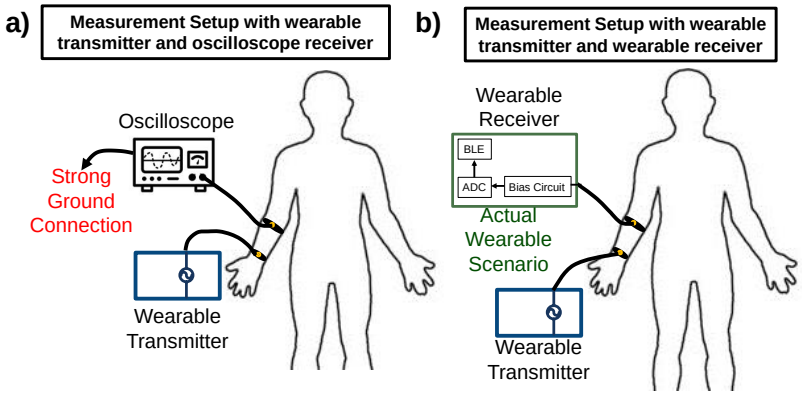


Fig. 2.9. a) Measurement setup using a wearable signal generator as transmitter and oscilloscope as receiver. The oscilloscope is a ground connected instrument and hence do not represent an actual scenario for werable HBC measurement. b) Setup using a wearable transmitter and wearable receiver, consisting of a bias circuit, ADC and bluetooth module. This represents an actual wearable HBC scenario.

### 2.4.4 Conclusion: Channel Loss dominated by Return Path

From the experimental results, with common ground it is clear that forward path channel loss of the human body is small and most of the loss in HBC is due to the non-common ground return path capacitance. Also, excitation termination modality has direct effect on the forward path loss, hence the receiver and transmitter configuration and impedance values have to be chosen properly to minimize the channel loss.

## 2.5 Non Common Ground : Measurement Setup With Capacitive Return Path

This section discusses the measurement set up used for measuring the human body channel loss in a non-common ground scenario and experimentally validate the different component values of the human body model. We use two different type of measurement setup for the channel measurements: (1) An oscilloscope based measurement to provide high impedance capacitive termination for voltage mode channel

measurements, (2) a miniaturized wearable receiver to replicate an actual HBC scenario without any measuring instruments with large ground. Recently [12] has shown a wearable measurement setup for power loss measurement. Here we carry out wearable measurements to 1) perform voltage loss measurements in the low frequency range to characterize the body for time domain broadband communication , 2) validate the developed bio-physical model for wearable scenarios. A battery operated signal generator is used to provide voltage signal as stimulus. The signal is coupled to the body through copper electrodes connected to a band. The measurement setup and the circuit model of the system with oscilloscope and wearable receiver is discussed in the next subsections.

### 2.5.1 Oscilloscope based Setup: Large Ground

To achieve high impedance termination for voltage measurements an oscilloscope is used as the receiver (fig. 2.9 (a)). The transmitter consists of a battery operated miniaturized signal generator. The termination impedance provided by the oscilloscope is dependent on the probe used for measurement. In our experiments we use two different probes to provide capacitive and resistive termination of different values. This helps validating the developed bio-physical HBC circuit model parameters under these scenarios. Since we want a high impedance termination at the receiver end an oscilloscope is used for voltage measurement. fig. 2.10 (a) shows the circuit model with a 10x probe with an equivalent resistance of 10M and capacitance of 13pF. The 1x probe provides an equivalent resistance of 1M and capacitance of 79pF as shown in fig. 2.10 (b). Both the probes provide a high impedance capacitive termination at the receiver end. However, since the oscilloscope is a wall power supply connected device with a large ground plane, the return path capacitance between the transmitter and the receiver will be larger than that of a wearable scenario and result in an optimistic measure of the HBC channel loss. Hence it is required to build a miniaturized receiver device, which will provide a more accurate estimation of the HBC channel loss.

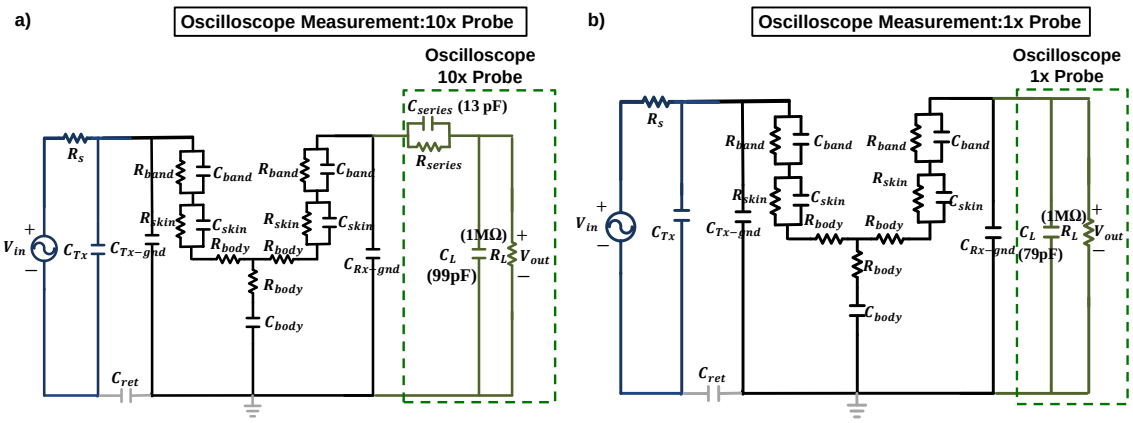


Fig. 2.10. Human body circuit model with an oscilloscope as a load device at the receiver end. a) Oscilloscope with a 10x probe provides an equivalent load of 10M resistance in parallel with a 13pF capacitance. b) A 1x probe at the oscilloscope provides a load with 1M resistance in parallel with 79pF load. The electro-quasistatic HBC model is used to provide loss estimates for both these load scenarios and compared with the experimental measurements.

### 2.5.2 Miniaturized Wearable Prototype based Setup

The oscilloscope measurements discussed in the previous subsection do not emulate an actual wearable scenario due to the presence of a large ground at the receiver end. We use a battery-operated device, which has a small ground plane, at the receiver end to emulate a more realistic HBC scenario (fig. 2.9 (b)). Since our experiments are carried out in voltage mode, the received signal is a voltage waveform and needs to be sampled in time domain for measurement. Hence, we use an ADC at the receiver end to sample, digitize the received waveform and recover the received signal amplitude information. For the miniaturized receiver we use a STM32F103C8 microcontroller, which has 12 bit, 1 MSPS ADC modules. The sampled ADC data is stored in the microcontroller at the receiver end and then transmitted through an HC-06 Bluetooth module. The transmitted data is acquired through a similar HC-06 Bluetooth module connected to the PC and processed in MATLAB to extract the

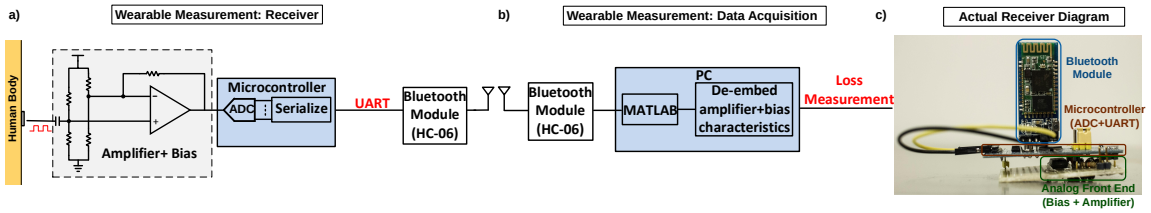


Fig. 2.11. a) Block diagram of the receiver used for wearable measurements. The received signal is amplified with a known gain amplifier and then digitized using an ADC, which sends the bits out through Bluetooth after serializing them. b) Setup to acquire the data sent from the receiver and do the loss measurements. The data transmitted from the wearable receiver is processed in MATLAB after de-embedding the circuit characteristics and plotted to find the channel characteristics with miniaturized wearable transmitter and receiver. c) Actual diagram of the wearable receiver device showing the different components.

received amplitude information. The conceptual block diagram of the receiver and the data acquisition system is shown in fig. 2.9 (a) and fig. 2.9 (b) respectively. fig. 2.9 (c) shows the actual implementation of the miniaturized receiver device.

The maximum frequency signal which can be digitized to recover amplitude information through sampling is limited by the sampling rate of the ADC. With the ADC sampling rate limited to 1MSPS, a 10x oversampling will limit the maximum frequency of operation to 100 KHz. To characterize the channel up to 1MHz with a 1 MSPS ADC, a histogram based approach is used. In this approach, a square wave is used as the input waveform. The signal is sampled randomly and the difference between two consecutive samples is measured. The whole amplitude range is divided into a few smaller bins and the histogram of the difference is computed. For an ideal square wave input, the difference will either be zero or equal to the amplitude of the signal. Hence, the histogram of the difference between two consecutive samples will contain two sharp peaks around 0 and the amplitude of the signal as seen in fig. 2.12. Hence by analyzing the histogram of the sampled signal it is possible to

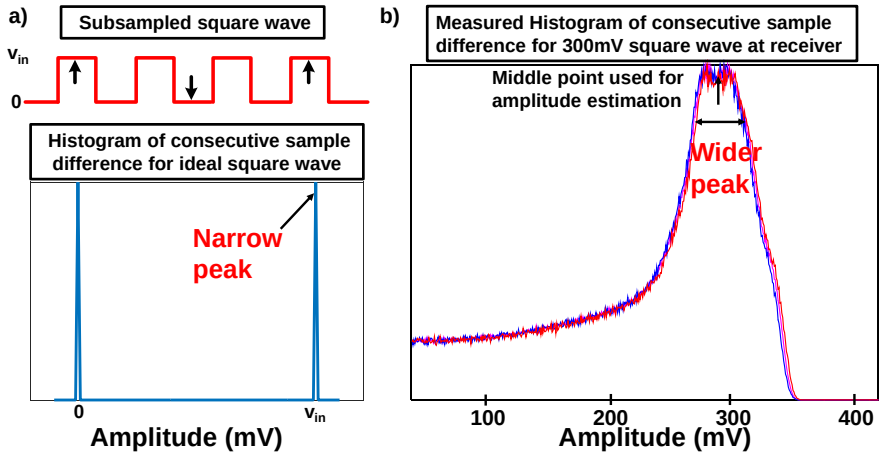


Fig. 2.12. a) Histogram plot of difference between consecutive samples from a sub sampled ideal square wave. b) Actual measured histogram plot for a 300mV received signal through HBC. The plot only shows the peak corresponding to amplitude of the signal. Since the peak shows a wide spread, the mid-point is taken as the amplitude.

estimate its amplitude. Since the sampled voltage can only be on either of the two levels of the square wave, it is not required to reconstruct the signal accurately in time domain to estimate its amplitude. Hence, this approach is not dependent on the sampling rate and will provide accurate results even if the sampling rate is lower than the frequency of the received signal. So even by subsampling the signal it is still possible to find the amplitude information, enabling measurements up to 1MHz with a 1MSPS ADC. In a real scenario, due to presence of noise, the received signal will not be a perfect square wave and the histogram peaks will be spread out. So for our experiments the histogram is taken multiple times and averaged to find the average peak and subsequently the amplitude of the signal.

Since the wearable transmitter and receiver do not have a common ground reference, it is necessary to bias the signal at the receiver end before applying it to the ADC. This requires a resistive bias circuit as shown in fig. 2.9 (a). Also we amplify the biased signal through a known gain amplifier and apply it to the ADC. This only amplifies the received signal but do not amplify the noise in the ADC, which enables

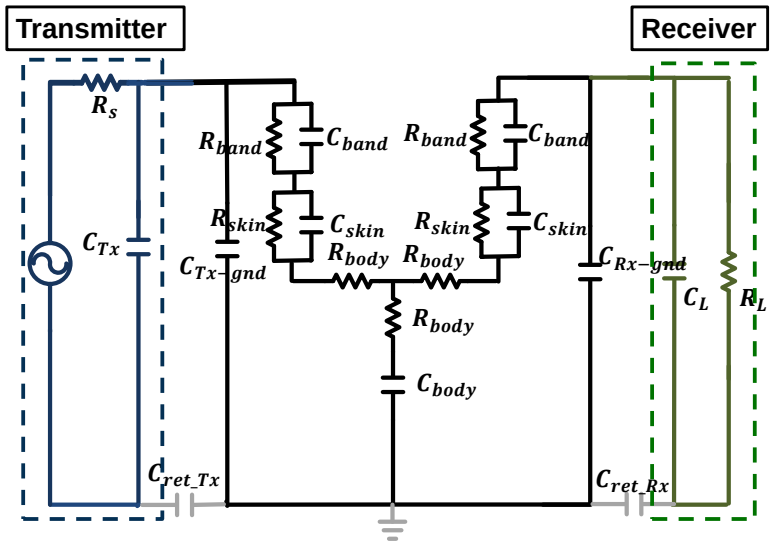


Fig. 2.13. Circuit model for measurement setup with a wearable transmitter and receiver. The load is a parallel combination of a resistance and capacitance corresponding to the input impedance of the wearable receiver.

detecting the received signal correctly. Hence for channel characterization we need to de-embed the amplifier characteristics from the received signal. In this scenario we have an amplifier of gain 12 over the measured frequency range, hence the received signal amplitude is divided by 12 to find the channel loss. Also the bias circuit for the amplifier creates a high pass response which needs to be de-embedded from the measured response to get the actual channel response. Hence the final response is obtained by de-embedding the amplifier and bias circuit response from the measured channel characteristics. The measurement results from these two different experimental setup is discussed in the next section. The equivalent circuit diagram of this setup is shown in fig. 2.13.

## 2.6 Measurements : Broadband Electro-Quasistatic HBC

This section discusses the measurement results through oscilloscope and wearable receiver and compares them with the developed circuit model. The experiments were

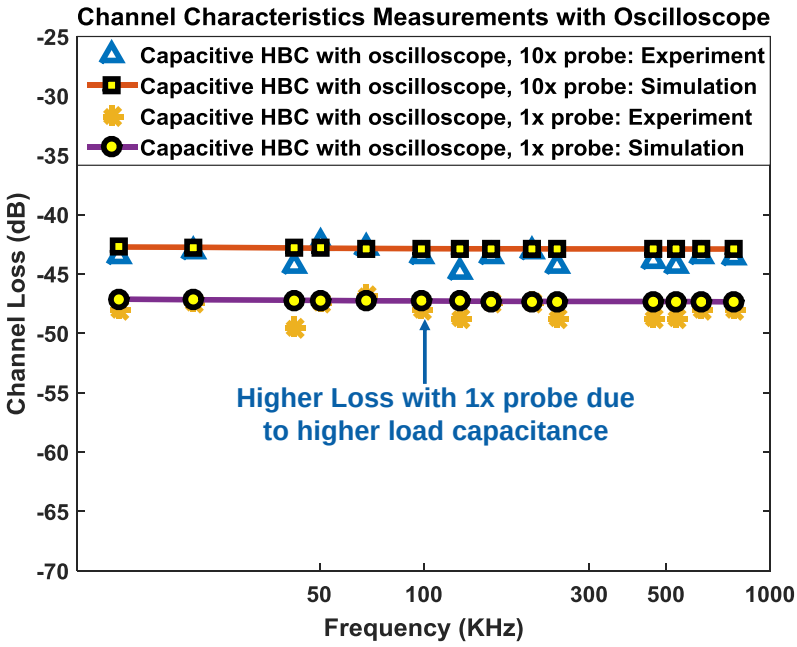


Fig. 2.14. Comparison of oscilloscope measurement results for two different probes with simulation model. Both simulation and measurements, show higher loss for a 1x probe due to its higher load capacitance.

carried out on 4 male subjects over 6 days. The transmitter was placed on the forearm and the receiver is placed on the wrist. The resulting HBC channel length is 20-25 cm.

### 2.6.1 Oscilloscope based Measurement Results

Two different probes are used for oscilloscope measurements providing termination with different capacitances. With a capacitive termination, the channel loss $\frac{C_g}{C_L+C_g}$ is determined by the ratio of return path capacitance ($C_g$) and load capacitance ($C_L$). Hence, the response should be constant over frequency. The measured channel response is indeed flatband, as seen in fig. 2.14. This matches closely with the simulated results from the model. Also, it is expected that a higher termination capacitance should result in a higher loss. As seen from fig. 2.14, the channel loss

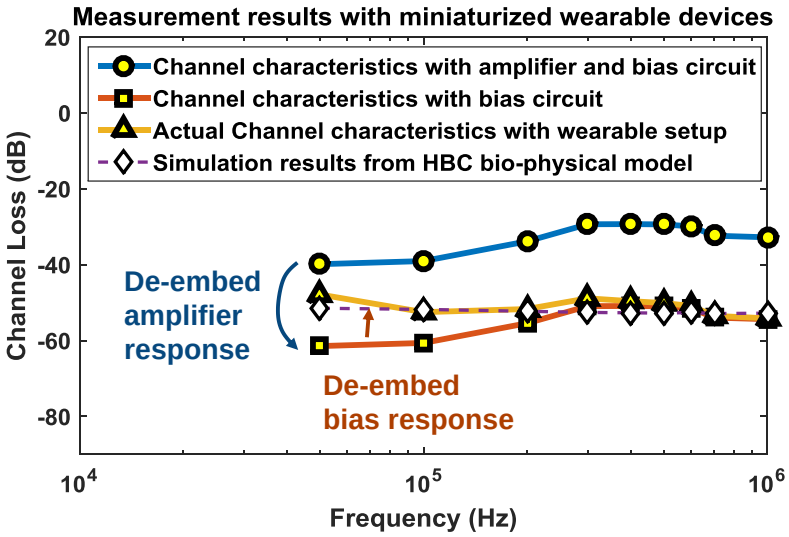


Fig. 2.15. Measurement results using miniaturized wearable prototype. After de-embedding the amplifier characteristics and the bias circuit characteristics from the measured result the channel response is flat-band. This matches closely with the simulation results assuming a 1pF input capacitance of the wearable receiver.

during measurement through a 1x probe (79pF capacitance) is around -47 dB. This is higher than the -43 dB channel loss measured with 10x probe (13pF capacitance). These measurements show that it is indeed possible to have a flat-band channel until low frequencies by utilizing a capacitive termination at the receiver end. This shows the possible utilization of the human body channel as a broadband communication medium.

### 2.6.2 Wearable Prototype based Measurement Results

The wearable measurements require an amplifier and a bias circuit at the receiver end. Since these circuits have their own frequency response, it is necessary to de-embed them from the measured characteristics. The amplifier has a flatband gain of 12 over the frequency range. The bias circuit has a high pass frequency response, which results in an overall high pass channel response. Hence de-embedding the bias

circuit response from the overall response results in a flat band channel response as shown in fig. 2.15. However, the channel loss in a wearable scenario is higher (-49 to -52 dB) than oscilloscope measurements (-43 dB and -47 dB respectively with 10x and 1x probes). This is due the lower return path capacitance in this wearable measurement scenario, as there is no device with big ground. This shows that channel measurements with oscilloscope provides optimistic estimation of the channel loss and hence should be avoided.

## 2.7 Optimum HBC signaling Modality: Key Learnings

From the experimental results in Section III and Section VII it can be seen that the human body channel loss can be minimized by applying proper value and configuration of excitation and termination. In this section we discuss about some of the excitation and termination modalities that should be used for HBC channel measurements in voltage mode.

### 2.7.1 Avoid 50Ω Termination

Most previous studies for HBC channel measurements use a VNA or a Spectrum Analyzer to measure the received signal. Both of these instruments have a 50Ω input impedance and hence they provide a very low impedance termination when used as a receiver. Since the human body channel impedance is of the order of a few KΩs, any voltage loss measurement using a 50Ω termination resistance will result in a high loss. This can be observed from fig. 2.16, where previous studies using VNA show about 20dB loss even when there is no ground isolation. Using a 50Ω termination in the developed HBC circuit model also shows similar loss. To remove the effect of measurement setup on the channel loss, a high impedance termination should be used at the receiver end. Hence any measurements with a Vector Network Analyzer or a Spectrum Analyzer will show a higher channel loss at low frequencies due to its low input impedance and should not be used in voltage mode channel loss measurements.

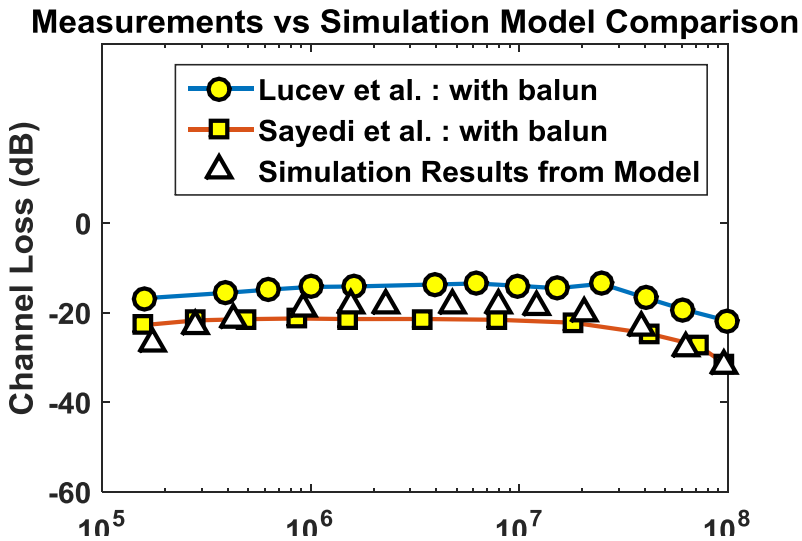


Fig. 2.16. Comparison of simulation and measurement result from previous studies for a 50Ω termination at the load end. The measurements are carried out by simultaneously providing input and measuring the received signal in a VNA without using any balun for isolation, effectively making it a common ground measurement. Simulation results with common ground and 50Ω termination also show similar loss.

### 2.7.2 Desired: High Impedance Termination

As discussed in previous literature and also found from the models in Section III, the human body impedance is in the order of a few Ks. So, voltage measurements with a low input impedance device will result in a higher loss, since most of the voltage drop will happen across the body. Also, the low termination resistance along with the return path capacitance will create a pole in the channel transfer function, resulting in a high pass response. Lower the termination resistance, higher the pole frequency, more the effect on low frequency measurements (fig. 2.17). Majority of the measurements in previous literature [4, 6, 10] has been carried out with VNA or spectrum analyzers, which has 50 input impedance. This results in higher estimation of measured channel loss. A high input impedance measurement device (oscilloscope) provides a more realistic scenario, as it will replicate a CMOS receiver circuit with

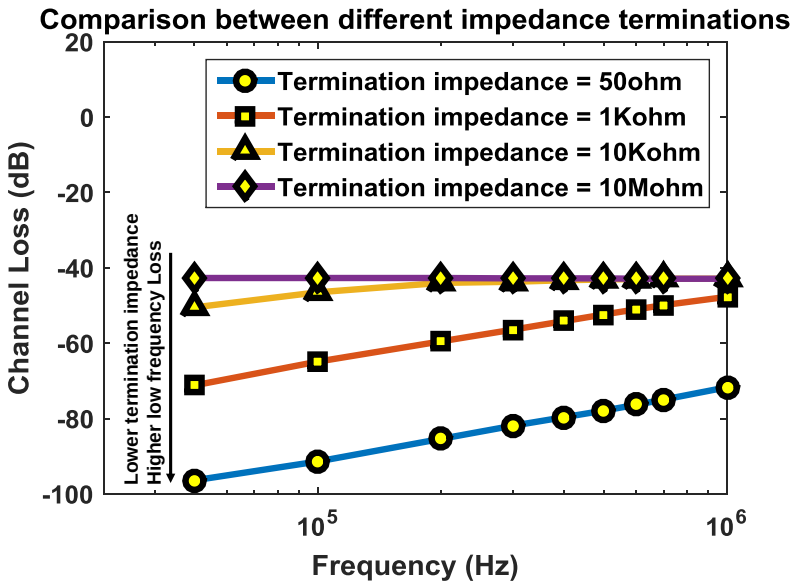


Fig. 2.17. Comparison of channel characteristic for different termination impedance from simulation model. Lower termination impedance results in higher low frequency loss, as well as higher cut-off frequency. Hence, it is necessary to have a high termination impedance receiver to measure channel characteristics at low frequencies.

very high input impedance. So voltage loss measurements should be carried out with high impedance devices, which shows lesser loss than 50 termination measurements.

### 2.7.3 Capacitive Termination: Low frequency loss reduction

The return path in capacitive HBC is formed by the coupling capacitance between the transmitter and receiver. Any resistive termination will result in high loss at lower frequencies, because the high impedance of the capacitor will result in most of the voltage drop happening across it. This results in a high pass response with cut-off frequency determined by the return path capacitance ($C_{ret}$) and termination resistance ($R_{load}$). The cut-off frequency ($\frac{1}{R_{load}C_{ret}}$) is inversely proportional to the load resistance. Hence very low impedance termination (50Ω), as is the case for a spectrum analyzer or VNA, will result in a high cutoff frequency. So the low frequency

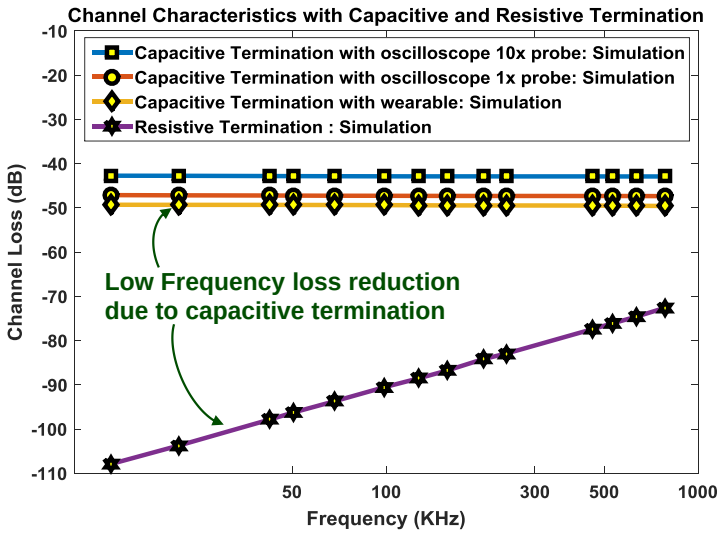


Fig. 2.18. Simulation results showing the effect of capacitive termination on low frequency loss compared to a resistive termination. Capacitive termination results in a flat-band response of the human body channel. This also explains why previous studies using VNA and providing 50 termination impedance, report a high pass channel response.

measurements with 50Ω input impedance measurement devices will result in higher loss. On the other hand, a high impedance receiver 'with capacitive termination will result in a flat-band channel response as the output voltage will be a capacitive division between the return path and termination capacitance. It is possible to achieve up to 50dB loss reduction at low frequencies through capacitive termination, as seen from fig. 2.18. This is also a realistic scenario for CMOS based circuits and systems, where the receiver input capacitance will act as the termination capacitance and hence will enable a flat band channel until low frequencies. This explains the high pass response reported in many of the previous studies [4, 6, 7] and also shows the feasibility of broadband transmission, using the human body as a communication medium.

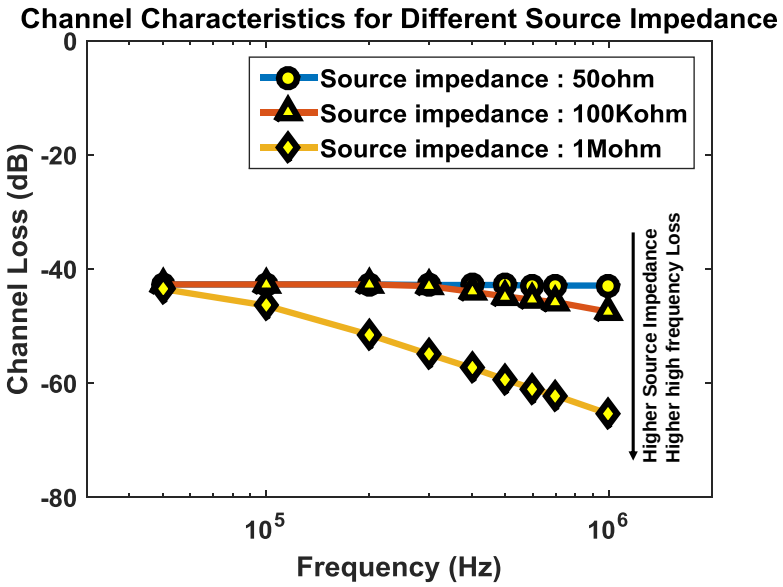


Fig. 2.19. Comparison of simulated channel characteristic for different source impedance. Higher source impedance results in more high frequency loss and lower roll off frequency. So a low source impedance is desired at the transmitter end for voltage mode channel measurements.

### 2.7.4 Voltage-Mode Signaling

Most previous studies use voltage signal as excitation and the channel loss is measured in terms of the ratio of received and transmitted voltage. Since voltage is the measured metric in this scenario, the signaling modality should maximize the received voltage. To that end, the receiver impedance can either be conjugate matched or be as high as possible. Conjugate matching is important for reducing reflections at the receiver end. However, at low frequencies (order of few MHz), the wavelength of the transmitted waves are significantly larger than the communication channel length. Hence it is not necessary to provide conjugate matching at this frequency range. So, the termination impedance has to be large for voltage mode signaling. The source impedance on the other hand has to be minimized to reduce voltage drop across it and maximize the voltage received at the receiver end. As can be seen from fig. 2.19,

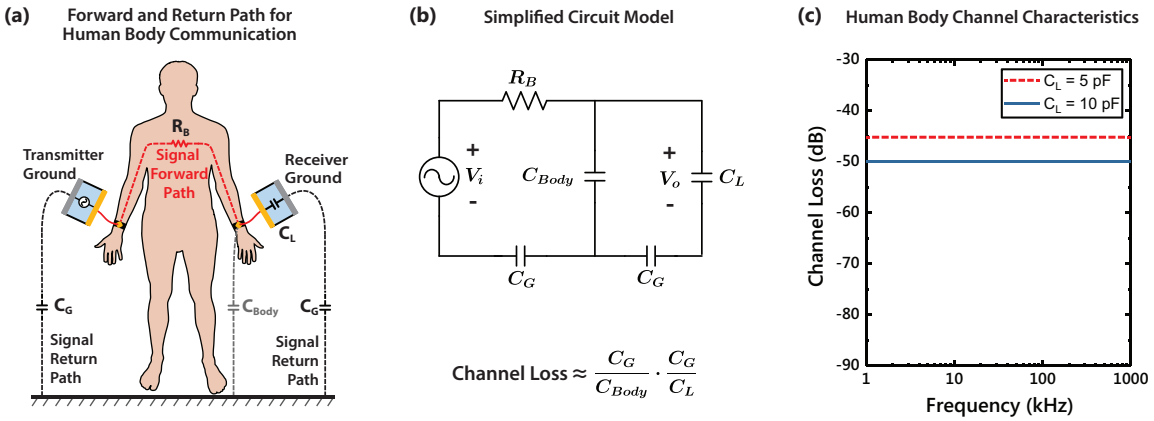


Fig. 2.20. a) Illustration of capacitive HBC, where signal return path between transmitter and receiver is formed by parasitic capacitance between their respective ground plates and earth's ground b) Simplified circuit model for calculating HBC channel loss (b) Frequency response of HBC channel loss, showing constant loss dependent on load capacitance at the receiver and return path capacitance.

as the source impedance increases, the voltage loss increases for higher frequencies. Hence, it is desirable to have a low source impedance for voltage mode signaling.

## 2.8 Theoretical Derivation of Return Path Capacitance

In this section, we calculate an expression for HBC channel loss to motivate the importance of return path capacitance $C_G$ in HBC and then explore an equation based model for variance of $C_G$ with respect to distance of an HBC device with earth ground.

### 2.8.1 Derivation of Channel Loss from Simplified Channel Model

The simplified circuit model for the human body channel characteristics is shown in figure 2.20. The output voltage ($V_o$) and the input voltage ($V_i$) are related to each other as follows (neglecting the forward path body resistance $R_B$):

$$\frac{V_o}{V_i} = \frac{C_G}{C_G + C_{Body} + \dfrac{C_L C_G}{C_L + C_G}} \cdot \frac{C_G}{C_L + C_G} \tag{2.3}$$

Where $C_G$ is the return path capacitance, $C_{Body}$ is the capacitance between the body and the ground, $C_L$ is the load capacitance. The forward path resistance ($R_B$) is neglected in this calculation, as $R_B$ is of the order of $10K\Omega$, whereas the impedance provided by the return path capacitance is greater than $100K\Omega$ for frequencies less than 1 MHz. Further, the return path capacitance ($C_G$) is an order of magnitude smaller than the load capacitance ($C_L$, order of 10 pF) which in turn is an order of magnitude smaller than the body to ground capacitance ($C_{Body}$, >100 pF) [29]. Hence we can make the following simplifications:

$$C_L + C_G \approx C_L, \tag{2.4}$$

$$\frac{C_L C_G}{C_L + C_G} \approx C_G \tag{2.5}$$

and,

$$C_G + C_{Body} + \frac{C_L C_G}{C_L + C_G} \approx C_{Body} \tag{2.6}$$

Substituting equations 2.4, 2.5 and 2.6 in equation 2.3, a simplified expression for the human body communication channel loss ($V_o/V_i$) can be obtained as

$$\frac{V_o}{V_i} \approx \frac{C_G}{C_{Body}} \cdot \frac{C_G}{C_L} \tag{2.7}$$

Equation 2.7 shows that the channel loss for communication between two wearable devices is dependent on ${C_G}^2$. This shows the importance of determining the value of return path capacitance to estimate the HBC channel loss and be able to design optimized HBC systems.

### 2.8.2 Variation of $C_G$ with Distance from Earth Ground

The ground plate of an HBC device, e.g. a smartwatch, can be modelled as a disc to analyze the return path capacitance to the earth's ground. Now if earth's ground

was to be placed infinitely far away from the object, the return path capacitance would simply be the *self-capacitance* of that object, which for a disc of thickness $h$ and radius $a$ can be shown to be [30, 31]:

$$C_{disc} = 8\epsilon_0 a \left[1 + 0.87\left(\frac{h}{2a}\right)^{0.76}\right] \tag{2.8}$$

so that for a thin disc, when $h \ll a$,

$$C_{disc} \approx 8\epsilon_0 a \tag{2.9}$$

For a finite distance from the ground, we start with a spherical conductor for simplicity and obtain an analytical expression using image charge analysis. For this purpose, let us assume a sphere of radius $a$ with a surface potential $V_{sphere}$ (figure 2.21) with it's center at a distance $d$ from an infinite ground plane, i.e. a plane at zero potential.

1. To replace the system by a set of image charges, a charge $q_1$ is placed at the center of the sphere such that $V_{sphere} = q_1/4\pi\epsilon_0 a$. This creates an equipotential at the surface of the sphere.

2. Next, a charge $q_1' = -q_1$ is placed at a distance $d$ below the ground plane. This creates a zero potential plane at the ground surface, but destroys the equipotential at the spherical surface.

3. To recover the spherical equipotential, an image charge of $q_1'$, $q_2 = (aq_1)/2d$ is placed at a distance $a^2/2d$ below the center of the sphere. This recreates the spherical equipotential by canceling the effect of $q_1'$, in turn destroying the zero potential plane at the ground.

4. This process is iterated, resulting into an infinite series of image charges, with the magnitude of the image charges diminishing in each subsequent iteration (Assuming $a < d$, which is trivially true.)

The resulting charge distribution indicates a total charge of $Q = \sum q_i$ charge on the sphere. Writing the charges as a function of $q_1$,

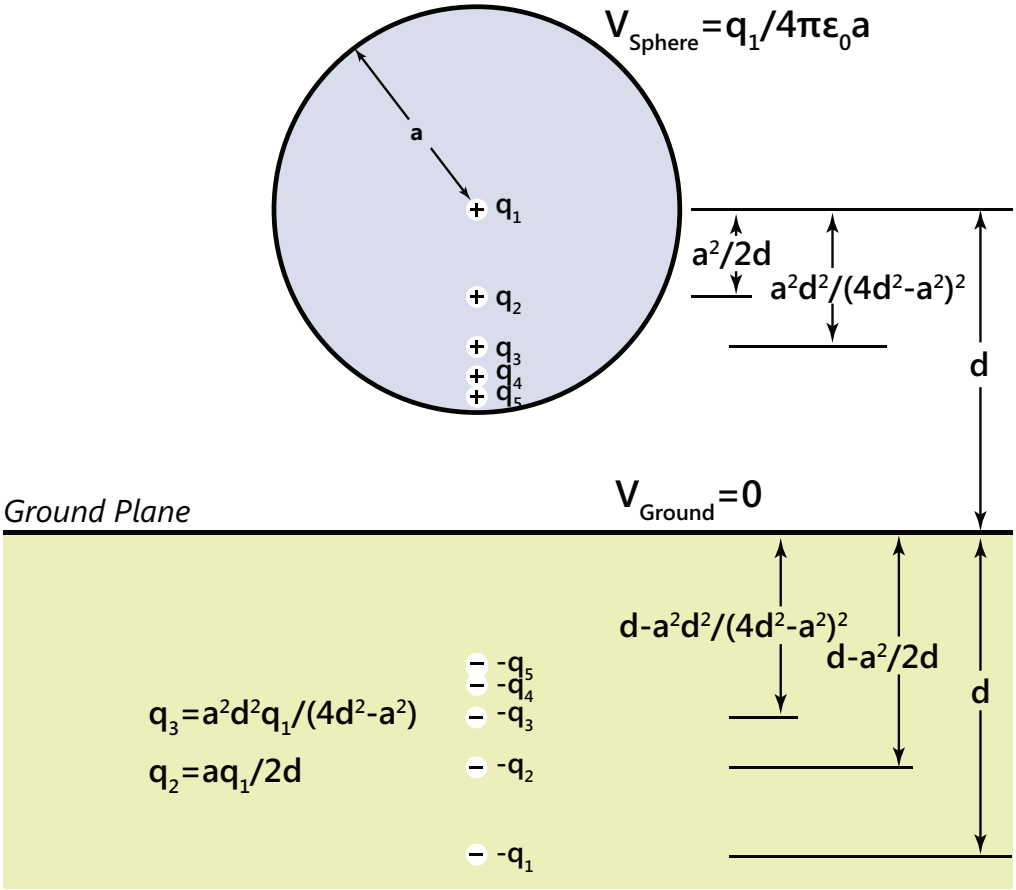


Fig. 2.21. Image charge distribution for a conducting sphere near a ground plane. An infinite sequence of image charges are required to replicate the equipotential at the surface of the sphere along with the zero potential ground plane.

$$Q = q_1 + \frac{aq_1}{2d} + \frac{a^2d^2q_1}{4d^2 - a^2} + ... = C_{sphere}\frac{q_1}{4\pi\epsilon_0 a} \tag{2.10}$$

using $Q = C_{sphere}V_{sphere}$. So, $C_{sphere}$ can be calculated as:

$$C_{sphere} = 4\pi\epsilon_0 a\left(1 + \frac{a}{2d} + \frac{a^2d^2}{4d^2 - a^2} + ...\right) \tag{2.11}$$

When $d \gg a$, this expression reduces to

$$C_{sphere} = 4\pi\epsilon_0 a \tag{2.12}$$

which is the self-capacitance of the sphere. Now the exact closed form solution for the decay of capacitance in the case of a disc may be different, but the trend of decay should be similar to that of a sphere. To demonstrate this, electrostatic FEM based simulations are performed in ANSYS Maxwell to plot the capacitance of a sphere of radius 10 cm and a disc of the same radius and thickness 1 cm with a finite ground plate (to restrict simulation space), as shown in figure **??**. For both the sphere and disc, the simulated capacitances decay to their self capacitances given by equations 2.12 and 2.8 respectively. *The percentage offset from the self-capacitance is less than* 5% *for* $d/a > 10$. So for design purposes, the self-capacitance of the ground plate of a device should provide a good estimate for the return path capacitance, as long as the dimension of the device of interest is small compared to its distance to earth's ground.

## 2.9 Classification of HBC based on interaction scenarios

### 2.9.1 HBC Interaction Scenarios

In HBC, the transmitter couples the signal through an electrode/ a pair of electrodes into the body and it is picked up at the receiver end through electrodes after the signal gets transmitted through the human body. The human body channel can be used as a communication medium for interaction between wearable devices, sensors,

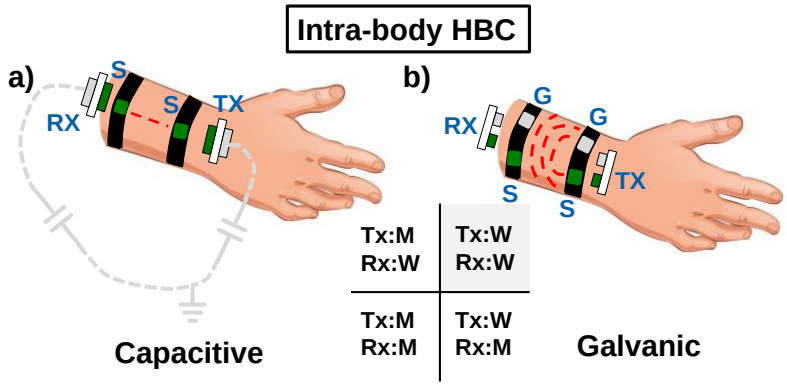


Fig. 2.22. Intra-body HBC between two wearable devices (Tx:Wearable (W),Rx:Wearable (W)). a) Capacitive HBC with single ended(SE) excitation and termination b) Galvanic HBC with differential (DE) excitation and termination

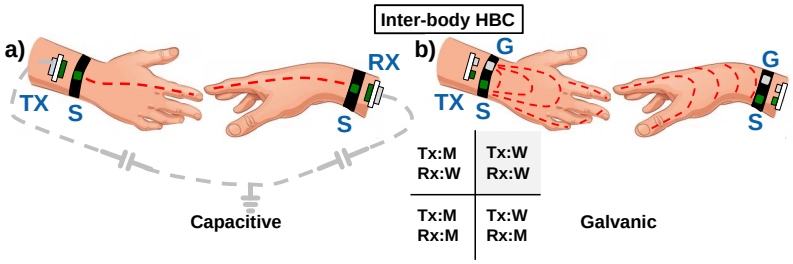


Fig. 2.23. Inter-body HBC enabling communication through dynamic channel formed during handshake. a) Capacitive b) Differential inter-body HBC

as well as between a wearable device and off body electronic devices like printers, personal computers etc. This creates different interaction scenarios as discussed below:

### Intra-body HBC:

Intra-body HBC refers to the communication between devices where the transmitter and receiver reside on the same person (Figure 2.22). Communication between a physiological sensor and a hub device in a wearable health monitoring scenario

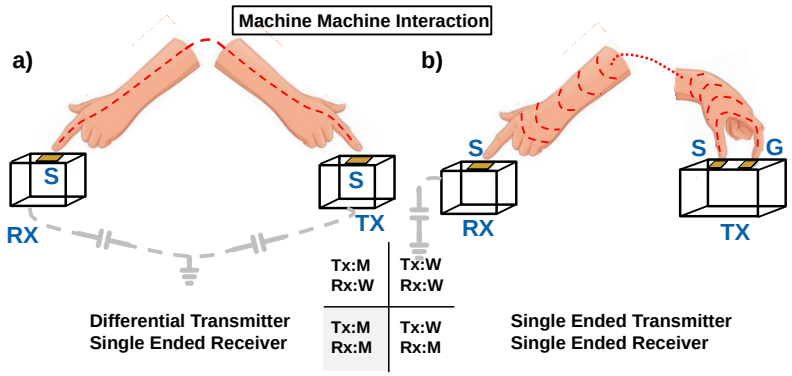


Fig. 2.24. Communication between two off body devices through HBC. a) SE transmitter/ receiver configuration b) DE transmitter with SE receiver.

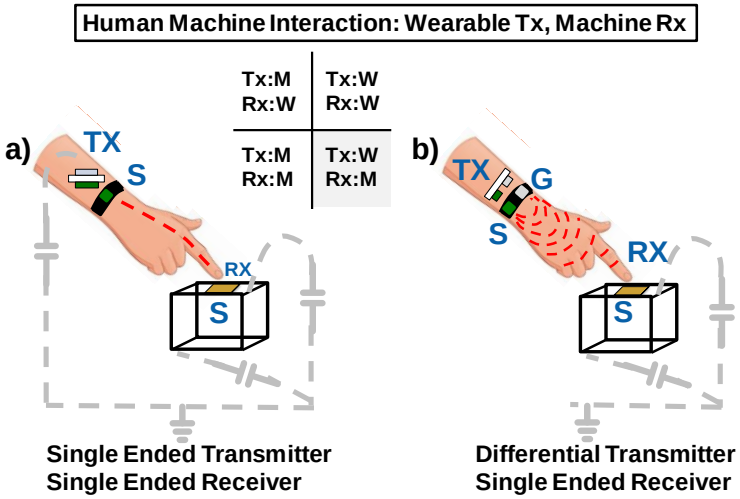


Fig. 2.25. Interaction between a wearable transmitter and an off-body device.a) Single ended excitation provided by the transmitter, b) Differential input provided by the transmitter

or communication between two wearable devices are examples of intra-body HBC. Previous channel measurement studies have primarily focused on characterizing the intra-body HBC channel.

**Inter-Body HBC:**

Inter-body HBC refers to the communication between two devices on separate human beings, where the communication channel is formed dynamically during an interaction between the two persons (Figure 2.23). Data transfer between smartwatches during a handshake between two persons is an example of inter-body HBC [26].

**Human Machine Interaction:**

HBC can enable interaction scenarios where a body worn device can communicate with a battery operated or wall connected (connected to the supply mains) machine (Figure 2.25,2.26). Transfer of images between a computer and a ring worn on the fingers of a person [32], human position tracking, secure authentication through a body worn personal key are two such possible application scenarios.

**Machine-Machine Interaction:**

The human body channel can also be used as a connecting medium between off body devices (Figure 2.24), which maybe wall connected or battery powered. Transfer of an image between a camera and a printer through touch is an example of such an interaction.
The signal transmission path is dependent on the interaction scenario and results in different amount of channel loss as will be seen in the next section.

### 2.9.2 Excitation/Termination configurations

One of the other key factor in determining the channel loss is the signal excitation (at the transmitter end) and channel termination (at the receiver end) configurations. There are two primary excitation/ termination configurations:

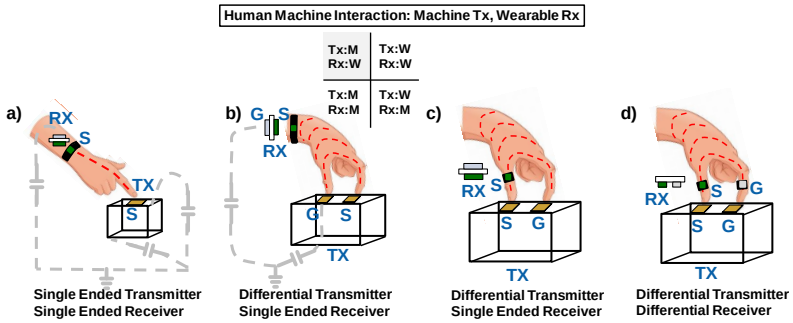


Fig. 2.26. Different interaction scenarios between a body worn wearable as a receiver and an off-body device as a transmitter. a), b) The off-body device acts as the transmitter and the receiver is a wearable device worn on the body. c), d) Differential excitation provided by an off-body device with the receiver worn on the finger.

**Single Ended (SE):**

In single ended excitation (Figure 2.22a, Figure 2.23a, Figure 2.24a, Figure 2.25a, Figure 2.26a) only the signal electrode of the transmitter is connected to the human body. The ground electrode is kept floating and the capacitive coupling between earths ground and the ground electrode creates the return path, which enables signal transmission. Due to the capacitive return path, this is often referred to as capacitive HBC in literature.

**Differential (DE):**

Differential excitation is provided by connecting both the signal and ground electrode of the transmitter to the human body. This forms a closed loop within the body creating an electric field (Figure 2.22b, Figure 2.23b, Figure 2.24b, Figure 2.25b, Figure 2.26b,c,d), which is picked up at the receiver end. If the reception is also differential then the received voltage is the difference in potential between the two receiver electrodes. Differential excitation and termination is commonly referred to as Galvanic HBC [2] in literature.

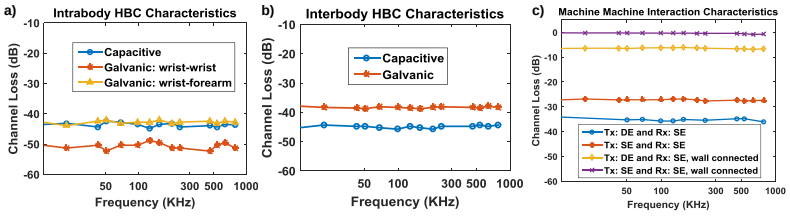


Fig. 2.27. a) Intra-body HBC channel characteristics showing distance dependent loss for galvanic HBC, b) Inter-body HBC characteristics: galvanic HBC has lesser loss in wrist to wrist communication, c) Machine-Machine interaction characteristics: negligible loss for single ended excitation of wall connected devices

## 2.10 Measurement Results

Measurements are carried out to find the channel loss characteristic for the aforementioned interaction scenarios. The wearable devices are built using a Texas Instruments TM4C123G LaunchPad evaluation kit consisting of an ARM Cortex M4 based TM4C123GH6PM microcontroller. The off-body device measurements are done by putting the same device on a table to emulate the larger chassis ground. The transmitter is capable of generating signals in the frequency range of $13.3 - 784$ KHz and the received signal is measured through an oscilloscope.

## 2.11 Intra-body HBC

Intra-body channel characteristics is measured by applying the transmitted signal at the left wrist and measuring the received signal at two locations: left forearm and right wrist. It can be seen from Figure 2.27a, that the galvanic HBC loss is dependent on distance and is almost equal to capacitive HBC loss for short distances (wrist-forearm). As the distance between transmitter and receiver increases the electric field reduces at the receiver end and hence the potential difference picked up by the differential electrodes reduces, hence the channel loss increases with distance. In case of capacitive HBC, the channel loss is primarily determined by the return

path capacitance, which makes it independent of transmitter receiver distance. The capacitive HBC channel characteristics is flat band as the capacitive termination at the receiver creates a capacitive division between the return path capacitance and receiver termination capacitance.

## 2.12 Inter-body HBC

In inter-body channel measurements, the transmitted signal is applied to the wrist of a person and the received signal is measured at the wrist of a second person during a handshake. The galvanic inter-body HBC loss is lesser than the capacitive loss (Figure 2.27b) due to the relatively smaller channel length between the wrists of the two persons.

## 2.13 Human Machine Interaction

The channel characteristics of human-machine interaction are strongly dependent on whether the wearable device is acting as the transmitter or receiver. Measurements with the wearable device acting as the transmitter show maximum loss as shown in Figure 2.28. Figure 2.26a, b shows the scenario, where the off-body machine acts as a transmitter and the received signal is measured at the wrist. Single ended excitation shows lower loss compared to differential excitation in this scenario because of the high return path capacitance due to the larger ground size of the machine. The larger ground size is also the reason for lower loss during human-machine interaction compared to a wearable wearable interaction during intra-body or inter-body HBC. Figure 2.26c, d shows the scenario where the two fingers are placed at the transmitter such that it forms a closed loop and the received signal is picked up between two points within the loop. A differential reception shows minimum channel loss in this scenario. The received voltage in differential reception will increase if the distance between the receivers electrodes increase, because there is a constant electric field

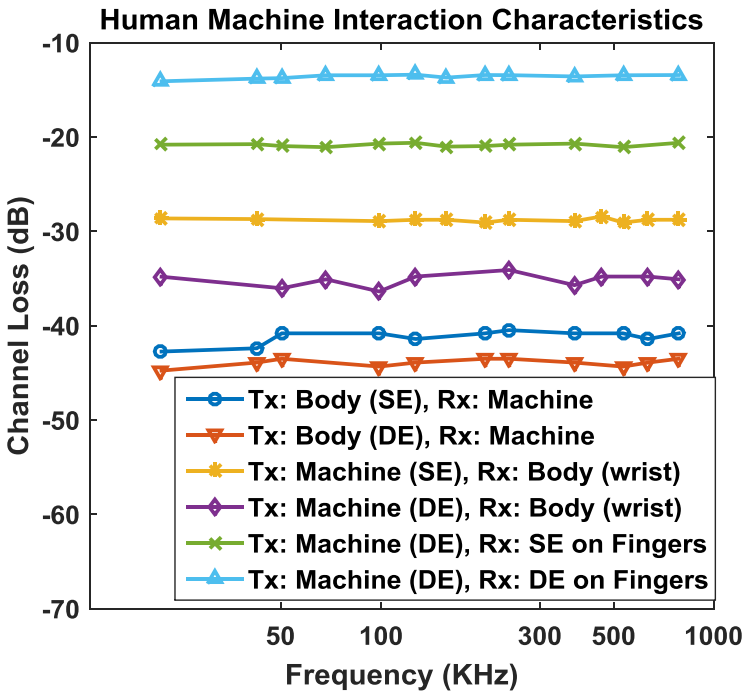


Fig. 2.28. Channel loss characteristics for different human machine interaction scenarios, showing maximum loss with wearable transmitter

between the two electrodes due to the closed path and the potential difference is proportional to the distance between the receiving electrodes.

## 2.14 Machine-Machine Interaction

There are two scenarios considered for channel measurement during a machine-machine interaction: 1) when the machines are battery powered, 2) when they are connected to the electric mains (wall connected). The loss depends on the excitation configuration at the transmitter end with differential excitation showing more loss compared to single ended for both wall connected or battery powered devices.(Figure 2.27c) Also wall connected devices show almost negligible loss as their grounds are connected through the power supply mains.

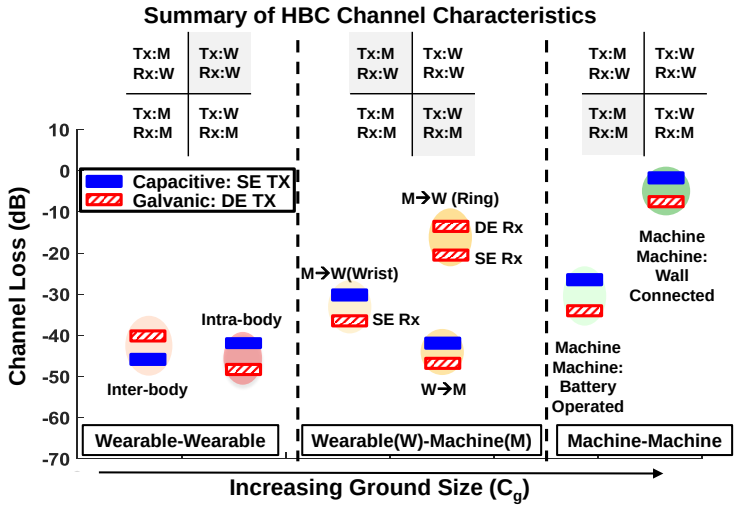


Fig. 2.29. HBC channel measurement summary for different interaction scenarios. Larger ground size results in less loss. SE excitation (capacitive) also has lesser loss compared to DE excitation (Galvanic HBC) unless the channel length is small (wrist-forearm in experiment)

### 2.14.1 Comparison between different Interactions

Figure 2.29 shows a summary of all the measurements. It can be seen that when both the transmitter and receiver are wearable devices the channel loss is maximum due to small ground plane size. The channel loss of human machine interaction, which corresponds to a wearable transmitter, machine receiver (Tx: W, Rx: M) scenario, is lesser compared to wearable interactions but higher than machine-machine interaction. Finally machine machine interaction shows the minimum loss when the devices are powered by the supply mains. Also differential excitation results in higher loss compared to single ended transmission unless the channel length is small or the received signal is picked up from within the closed loop of the transmitter.

## 2.15 Conclusion

This chapter characterizes the human body channel up to 1MHz frequency for capacitive HBC, where the signal transport is in the electro-quasistatic regime pri-

marily through the layers under the skin. A unifying bio-physical model of HBC is developed with component values determined through experiments and previous literature. Common ground measurements with different excitation and termination modalities show that the loss through the human body forward path contributes very little to the overall channel loss and validates the forward path components of the HBC model. Non-common ground experiments with oscilloscope show almost constant loss down to low frequencies (10KHz), highlighting the feasibility of using the human body as a broadband channel. The channel loss shows dependence on the termination impedance varying from -43dB to -47dB for 13pF and 79pF termination respectively. Wearable prototype based measurements in voltage mode with a sampling receiver has almost constant -49dB to -52dB loss across this frequency range, showing the need for actual wearable based measurements for accurate channel loss estimation. Analysis of the developed bio-physical model shows that high termination impedance and low source impedance provides the optimum channel loss and explains some of the high-loss measurements at these low frequencies in previous studies. These results show that the human body can be used as a broadband communication medium, like a *lossy wire*, which can enhance the battery life of small form-factor energy constrained wearable/implantable devices. This can open up applications like remote health monitoring, secure authentication among many others. This chapter also characterizes the human body channel under different possible interaction scenarios in a Body Area Network. Results show that the channel loss is strongly dependent on the excitation modality (differential vs single ended) and the ground sizes of the transmitter and receiver, helping explain wide discrepancies in previous measurements. Larger ground size reduces the channel loss, with supply mains connected (i.e. earth ground) machines showing minimum loss. Differential excitation shows more loss unless channel length is short or the signal is received from within the closed loop of the transmitter.

# 3. THEORY OF INTERFERENCE ROBUST INTEGRATING DUAL DATA RATE RECEIVER

Most of the materials in this chapter have been extracted verbatim from the paper:

1. S. Maity, D. Das, and S. Sen, Adaptive Interference Rejection in Human Body Communication using Variable Duty Cycle Integrating DDR Receiver in in Design, Automation Test in Europe Conference Exhibition (DATE), 2017, 2017, pp. 1763 − 1768.

## 3.1 Interference Robust HBC

The human body acts as a monopole or dipole antenna at frequencies determined by the height of the person. When the human body is not grounded the wavelength is twice the persons height, whereas a grounded body has a wavelength four times the height due to mirror effect. So the resonance frequency of 6ft tall human being is 80MHz or 40MHz depending on whether the body is grounded or not. In actual case due to the lossy nature of the human body the resonance peaking is distributed and the human body behaves like an antenna in the 40-400MHz range. As a result, the human body picks up interference from the omnipresent FM signals (88-108MHz). Fig. 3.1 shows a sample measurement of the FM interference experienced by the human body [33].

The primary challenge of HBC is to transmit data in conditions where SIR is as low as -20 dB. In this chapter we propose the theory of Integrating Dual Data Rate Receiver (I-DDR) to address the problem of signal transmission in presence of large interference.

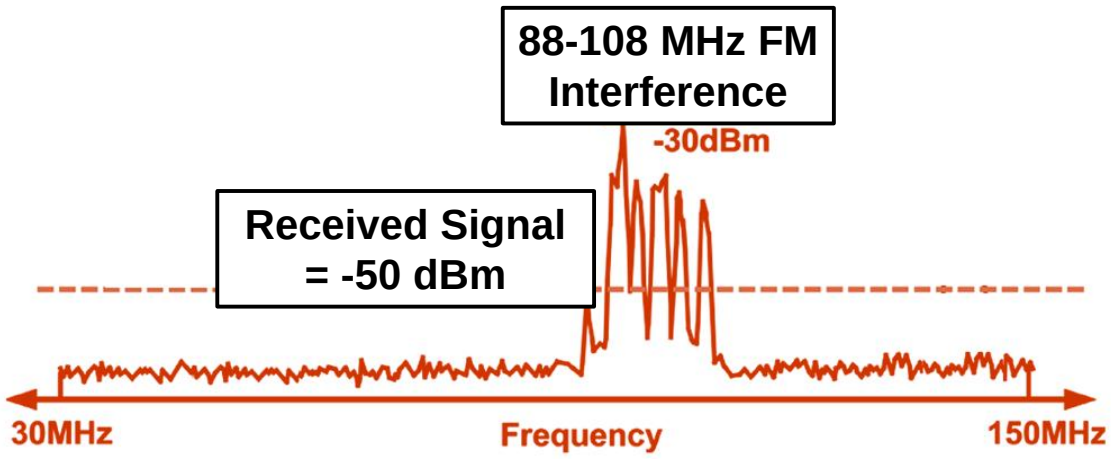


Fig. 3.1. Measured FM interference affecting HBC [1]

## 3.2 Theory of I-DDR Receiver

### 3.2.1 Continuous Wave Interference

The I-DDR receiver takes the integration of the NRZ data + interference over the symbol period ($T_b$) of data and samples it. After each integration period the integrator is reset for one clock cycle requiring two clock phases to sample alternate data bits; leading to a Dual Data Rate (DDR) receiver.

The receiver signal ($S_{RX}$) is a linear superposition of desired NRZ signal ($S_{sig}$) and the undesired interference ($S_{intf}$) of frequency $\omega_i$, and can be expressed as follows:

$$S_{RX} = S_{sig} + S_{intf} \tag{3.1}$$

$$S_{sig}(t) = \pm A_{sig} 0 \leq t \leq T_b \tag{3.2}$$

$$S_{intf}(t) = A_{intf} sin(\omega_i t + \phi) \quad \forall t \tag{3.3}$$

The integration of $S_{RX}$ for a duration of $T_b$, can be written as

$$IS_{RX}(T_b) = IS_{sig}(T_b) + IS_{intf}(T_b) \tag{3.4}$$

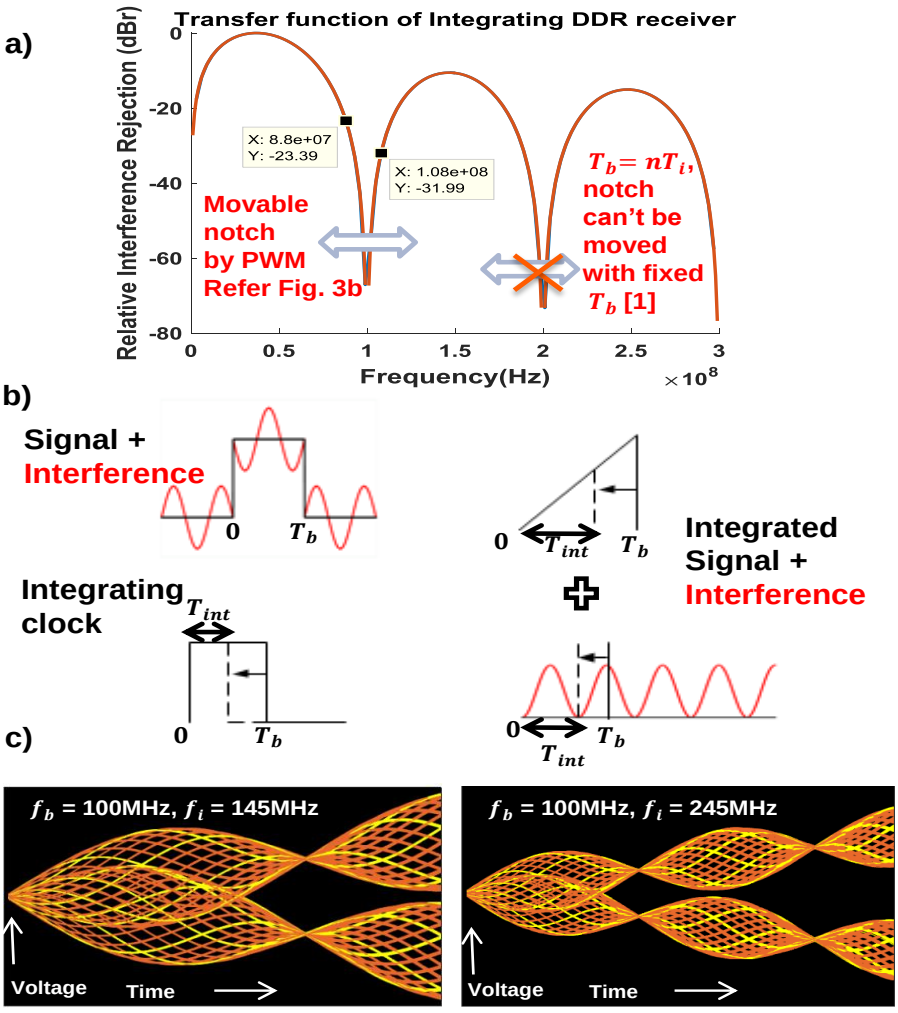


Fig. 3.2. a) Interference suppression for different interferer frequency, for I-DDR receiver ($T_b = nT_i$) [25] b) Movability of notch with clock duty cycle c) Eye diagram showing increase in eye height for particular duty cycles for a particular data and interference frequency combination. These correspond to the optimum duty cycle of operation.

$$IS_{sig}(T_b) = \int_0^{T_b} S_{sig} dt = \pm K_{int} A_{sig} T_b \tag{3.5}$$

Here $K_{int}$=integrator gain

$$IS_{intf}(T_b) = \int_0^{T_b} S_{intf} dt = K_{int} \frac{A_{intf}[cos(\phi) - cos(2\pi \frac{T_b}{T_i} + \phi)]}{\omega_i} \tag{3.6}$$

$$IS_{intf}(T_b) = 0 \; \forall T_b = nT_i; n = positive\ integer \tag{3.7}$$

Hence, for any arbitrary phase of the interference ($\phi$), its contribution to the integrated signal can be nullified by choosing the data bit period as an integral multiple of the interference time period. This shows that the I-DDR receiver can be used as a notch filter to eliminate the FM interference from HBC, as shown in fig. 3.2 (a). In a practical scenario due to jitter it will not always be possible to sample at $t = T_b$; so the contribution from interference will be close to 0.

### 3.2.2 Amplitude Modulated Interference

This section looks into the analysis of I-DDR receiver performance in presence of AM interference. The interference signal ($S_{intf}$) and the integrated interference ($IS_{intf}$) are presented as in 3.8, 3.9 respectively.

$$S_{intf}(t) = A_{intf}sin(\omega_i t+\phi)+\frac{A_{intf}M}{2}[sin((\omega_i+\omega_m)t+\phi+\phi_m)+sin((\omega_i t-\omega_m)t+\phi-\phi_m)]\ \forall t \tag{3.8}$$

$$IS_{intf}(t) = IS_{intf1}(t) - IS_{intf2}(t) 0 \leq t \leq T_b \tag{3.9}$$

$$IS_{intf1}(t) = \frac{K_{int}A_{intf}}{\omega_i}[cos(\omega_i t + \phi)] - \frac{K_{int}A_{intf}M}{2(\omega_i + \omega_m)}cos(\omega_i + \omega_m)t + \phi + \phi_m) \tag{3.10}$$

$$IS_{intf2}(t) = \frac{K_{int}A_{intf}M}{2(\omega_i - \omega_m)}cos(\omega_i - \omega_m)t + \phi - \phi_m) \tag{3.11}$$

$$IS_{intf}(t) = 0 T_b \leq t \leq 2T_b \tag{3.12}$$

$$SIR_{non\_int} = \frac{A_{sig}}{S_{intf}(T_b)} \tag{3.13}$$

AM is used for broadcasting in the medium wave range from 0.5 MHz to 1.7MHz and shortwave range from 5.9 MHz to 26.1 MHz. Since shortwave range is closer to the antenna frequency of human body of around 40 MHz, for our analysis of I-DDR receiver in presence of AM interference, we use a carrier frequency($f_i$ )=20 MHz. The reasonable modulation frequency ($f_m$ ) for such a carrier frequency is less than 5 kHz, so we choose $f_m$=2.5 kHz as an example of a practical scenario. But for better illustration of robustness of I-DDR receiver to AM interference, we also simulate in a scenario with $f_m$=2MHz.

Figure 3.3a shows the dependence of integrated interference ($IS_{intf}$) on the ratio of integration period and interference period ($\frac{t}{T_i}$ ). For any arbitrary carrier phase ($\phi$) or modulating signal phase ($\phi_m$), the integrated interference does not exactly go to 0 for an integration period, which is an integral multiple of the interference period ($T_b = nT_i$). Figure 3.3b shows the relative interference rejection of the I-DDR receiver with frequency in presence of an AM interference with carrier frequency of 20 MHz and modulation frequency of 2 MHz.

Although the maximum rejection notch locations are not exactly at integral multiples of the interference carrier frequency, the relative rejection is $>$ 10dB even for frequencies $\pm$10% away from the interference carrier frequency. Also there is one notch corresponding to each integral multiple of the interference carrier frequency. Figure 3.3c analyzes the relationship of modulation frequency and relative interference rejection for different bit period for a given interference, since it may not be always possible to have accurate sampling at $T_b = nT_i$. A smaller modulation frequency results in smaller residual integrated interference at the sampling instant. Hence, the I-DDR receiver provides better interference rejection in those scenarios. For a practical scenario in the shortwave range, where $f_m = 2.5$kHz and $f_i = 20$MHz, the rejection is greater than 17dB even for a frequency $\pm$10% away from the notch frequency (figure 3.6a). Figure 3.3d shows a comparison of SIR at the sampling instant for non-integrated and integrated signal as the interference frequency is varied. It can be seen that even for the worst case phase, the integrated signal still ensures

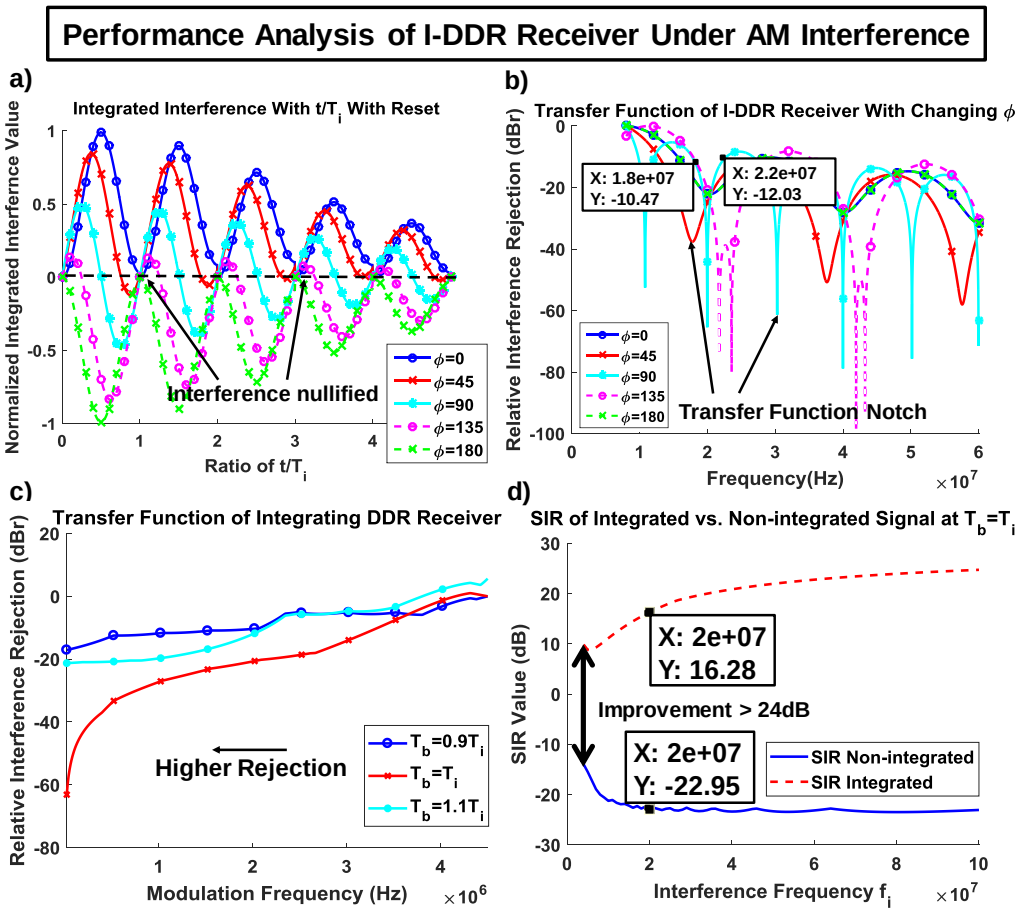


Fig. 3.3. Performance analysis of I-DDR receiver under AM interference ($M = 0.5, f_i, f_b = 20MHz, f_m = 2MHz$). a) Integrated interference ($IS_{intf}$ ) as a function of $\frac{t}{T_i}$ b) Interference suppression as a function of interferer frequency with changing $\phi$ c) Worst case of Interference rejection as a function of $f_m$ with $\pm 10\%$ variation in sampling instant d) SIR of Integrated vs. Non-integrated signal at worst case with varying $f_i$ ($A_{sig} = 1$ mV,$A_{intf} = 10$ mV).

at least 24 dB improvement in integrated SIR for sampling at $T_b = T_i$. However, the relative interference rejection at the sampling instant $T_b = T_i$ is strongly dependent on the phase of the carrier and modulating wave as can be seen from Figure 3.4a. In the special scenario of a modulation phase, $\phi_m = \pi$ the relative interference rejection is high, independent of the carrier phase ($\phi$), which can be attributed to the low residual integrated interference under this condition. The variation of location of the

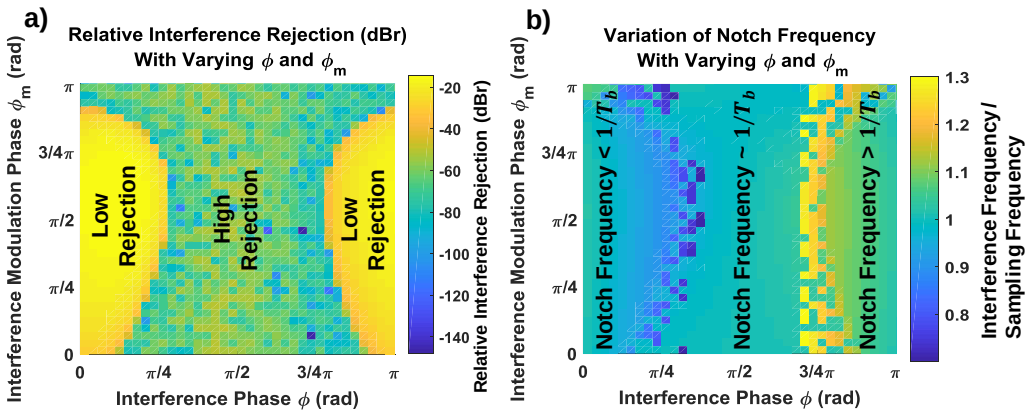


Fig. 3.4. Transfer function notch under AM interference with varying $\phi$ and $\phi_m$ ($f_m = 2$ MHz). a) Transfer function notch value in dB b) Location of notch frequency with respect to data frequency of $\frac{1}{T_b}$.

transfer function notch frequency with modulation and carrier wave phase is shown in Figure 3.4b. The notch is located at the interference frequency for $\phi = \frac{\pi}{2}$, independent to $\phi_m$. The notch frequency is lower than the interference frequency for $\phi < \pi/2$ , whereas it becomes higher for $\phi > \pi/2$. The non-integrated and integrated received eye diagrams are plotted in Figure 3.5a, b respectively. The integrated eye diagram shows clear eye opening enabling correct sampling whereas the non-integrated eye diagram is completely closed. This validates the interference rejection property of the I-DDR receiver in presence of AM interference and the potential SIR improvement achieved from it.

*Key Takeaway*: The presence of AM interference, with high enough modulation frequency, moves the frequency notch away from the data frequency ($f = \frac{1}{T_b}$ ). The position of the notch is dependent on the interference carrier and modulation frequency but provides at least 20dB rejection at $f = 1/T_b$ for all scenarios. For a realistic scenario with shortwave AM, the movement of the notch is minimal due to low modulation frequency.

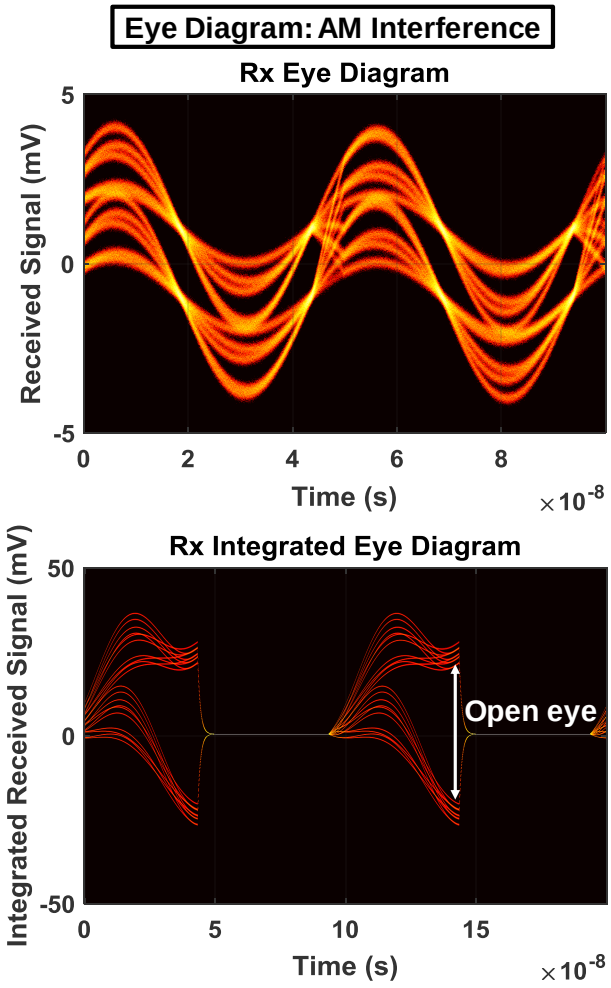


Fig. 3.5. Eye diagram comparison with and without integration ($A_{sig}$ = 1 mV,$A_{intf}$ = 3 mV,$K_{intf}$ = 10) a) Non-integrated eye diagram in presence of AM interference b) Integrated eye diagram in presence of same interference.

### 3.2.3 Frequency Modulated Interference

The performance of I-DDR receiver in presence of FM interference is analyzed in this section. The FM interference is approximated using Bessel function ($J_k$) as in 3.14. For existing FM bands of 88-110MHz, the channel bandwidth (BW) is 200 kHz and the maximum frequency deviation ($\Delta f$) is 75 kHz, which translates to a modulation index (B) of 3. However, we also simulate using a FM signal with high

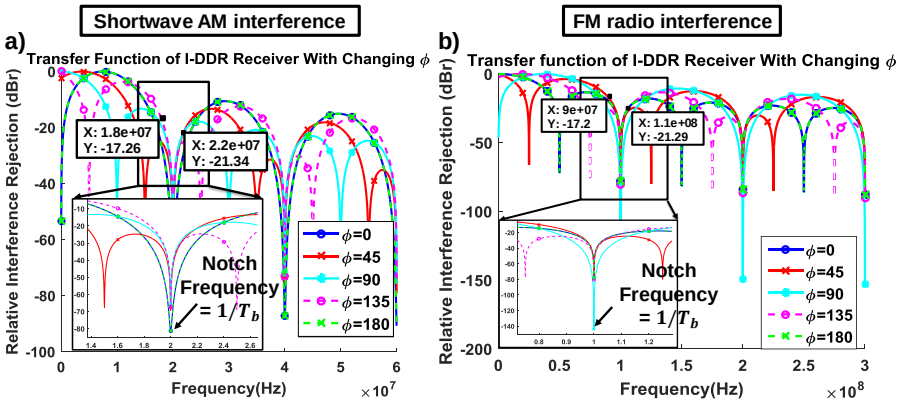


Fig. 3.6. I-DDR receiver transfer function under realistic scenario forAM and FM interference a) AM: $f_i = 20$ MHz, $f_m = 2.5$ kHz b) FM: $f_i = 100$ MHz,$f_m = 25$ kHz. The transfer function notch frequency stays at $\frac{1}{T_b}$, similar to continuous wave scenario.

modulation frequency of $f_m = 10$MHz for analyzing the interference robustness of the I-DDR receiver. The modulation index B is chosen as 0.5 in this scenario to compare the performance of I-DDR receiver in presence of AM and FM interference of same modulation index. The integrated interference and SIR with and without integration is as shown in 3.15. For all our simulations of FM interference, we choose to use the first 7 terms (k=0,±1,,±6) of the Bessel expansion.

$$S_{intf}(t) = A_{intf} cos(\omega_i t + B sin(\omega_m t) + \phi) \; \forall t \tag{3.14}$$

$$S_{intf}(t) = \sum_{K=-\infty}^{\infty} J_k(B) cos((\phi_i + k\phi_m)t + \phi) \forall t \tag{3.15}$$

$$IS_{intf} = \int_0^t S_{intf} = K_{int} A_{intf} \sum_{K=-\infty}^{\infty} J_k(B) \frac{cos((\phi_i + k\phi_m)t + \phi)}{\omega_i + k\omega_m} \tag{3.16}$$

$$IS_{intf} = \int_0^t S_{intf} = K_{int} A_{intf} \sum_{K=-\infty}^{\infty} J_k(B) \frac{cos((\phi_i + k\phi_m)t + \phi)}{\omega_i + k\omega_m} \tag{3.17}$$

$$IS_{intf}(T_b) = \int_0^t S_{intf} = K_{int}A_{intf} \sum_{K=-\infty}^{\infty} J_k(B) \frac{cos((\phi_i + k\phi_m)T_b + \phi) - sin(\phi)}{\omega_i + k\omega_m} \ \forall T_b = nT_i \tag{3.18}$$

Figure 3.7a shows that under FM interference also the integrated interference is nearly 0 for any  if the bit period is chosen as $T_b = nT_i$. Figure 3.7b shows that the relative rejection of the integrated and sampled interference is always greater than 19dB in the FM radio frequency band of 88-110 MHz even if the modulation frequency ($f_m$) is taken as 10 MHz. The relative interference rejection reduces as the FM modulation frequency increases as can be seen in Figure Figure 3.7c. This also shows that, even with $\pm$10% sampling error due to jitter and non-idealities, $>$ 11dB interference suppression can be achieved for modulation frequencies up to 10 MHz. Figure Figure 3.7d shows the SIR comparison between integrated and non-integrated receiver with sampling at $T_b = T_i$. There is a 22dB improvement in SIR achievable through integration in presence of FM interference. In a practical scenario with small modulation frequency (25 KHz), there exists a notch in the I-DDR transfer function for frequencies which are an integral multiple of the interference frequency, independent of the phase of the interference signal (Figure 3.6b). For higher modulation frequency (10 MHz) on the other hand, the notch frequency with the highest rejection is dependent on the initial phase of the interference and can be $>$ 10% away from the interference carrier frequency ($f_i$) as can be seen in Figure 3.8b. Figure 3.6a shows the interference rejection of I-DDR receiver at the interference carrier frequency with varying carrier phase of the FM interference. It demonstrates that the carrier phase doesnt have much effect on the relative interference rejection and ¿60dB interference rejection can be achieved at interference frequency for any relative phase difference between the data and interference. Similar to AM interference the integrated eye diagram shows clear eye opening in presence of FM interference (3.9b) , whereas the non-integrated eye is almost completely closed (3.9a).

*Key Takeaway:* In presence of FM interference with high modulation frequency, the transfer function notch of the I-DDR receiver does move away from the data

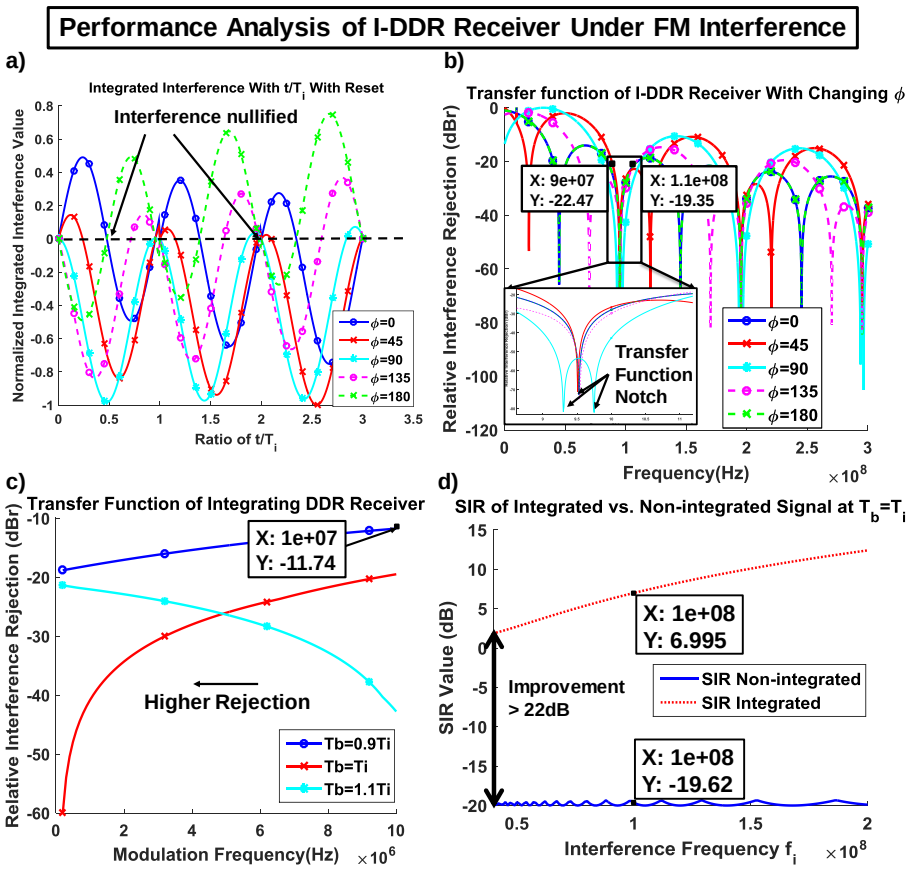


Fig. 3.7. Performance analysis of I-DDR receiver under FM interference ($f_i$ = 100 MHz, $f_m$ = 10 MHz,$B = 0.5, N = 7$) a) Integrated interference ($IS_{intf}$ )as a function of $\frac{t}{T_i}$ with reset b) Interference suppression as a function of interferer frequency with changing c)Worst case Interference rejection as a function of modulation frequency in presence of ±10% sampling mismatch. d) Worst case SIR of Integrated vs. Non-integrated signal with varying $f_i$ ($A_{sig}$ = 1 mV, $A_{intf}$ = 10 mV).

frequency ($f = \frac{1}{T_b}$ ). However there is at least one notch within ±5%of the data frequency (Figure 3.7b). This shift is considerably lesser than AM interference which can show up to ±30% shift in notch frequency (Figure 3.3b, Figure 3.4b). Since AM results in varying amplitude of the interference and the residual of integration is affected more by amplitude of interference than its frequency variation (as in FM

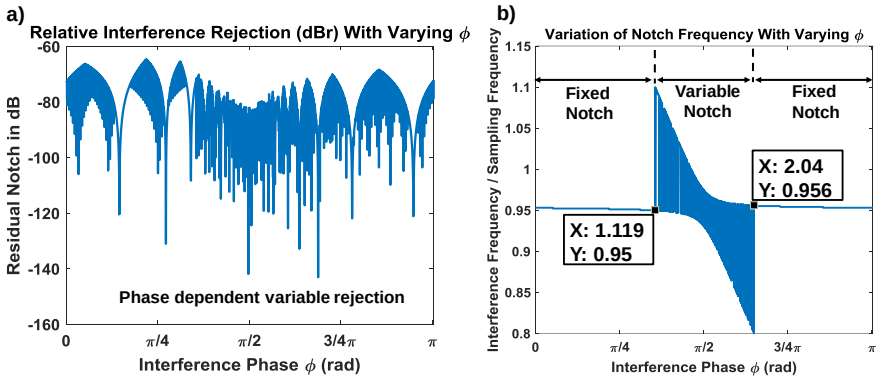


Fig. 3.8. Residual notch under FM interference with varying $\phi$ and $\phi m$ ($f_i = 100$ MHz, $f_m = 10$ MHz,$B = 0.5, N = 7$) a) Residual value in dB b) location of maximum rejection notch as a ratio of interference frequency ($f_i$) and sampling frequency ($f_b$).

interference), the movement of notch away from the data frequency is more in case of AM interference.

## 3.3 Discussion

### 3.3.1 Experimental Method

The I-DDR principle is validated using actual HBC signals transferred through the body. The HBC channel loss shows day to day and person to person variation. Hence, HBC channel loss measurement studies require multiple experiments to be run over multiple subjects on multiple days to measure the average and variation of channel loss and provide statistical significance to the results. However, for our experiments HBC signals are used only to capture the effect of channel loss on the transmitted signal and the day to day channel loss variation is not critical for the validity of the I-DDR principle. Hence, the experiments are not carried out on multiple subjects and is carried over three different measurements on the same person.

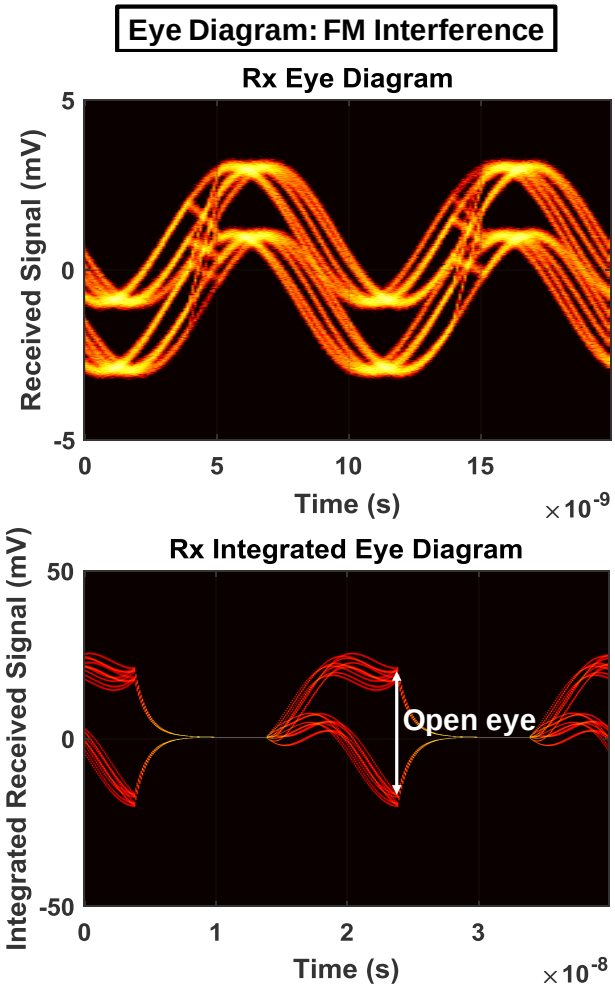


Fig. 3.9. Eye diagram comparison with and without integration ($A_{sig}$ = 1 mV, $A_{intf}$ = 3 mV,$K_{intf}$ = 10) a) Non-integrated eye diagram in presence of FM interference b) Integrated eye diagram in presence of same interference.

### 3.3.2 Clock-Data Phase Alignment: Clock Data Recovery

The output of the integration operation at the front-end is dependent on the phase relation between the integrator clock and data. Since the integration operation is an accumulation of the voltage level over time, any relative phase mismatch between integrator clock and data will directly reflect in the integrated voltage amplitude. The integrator output is maximized when the integration operation starts at the begin-

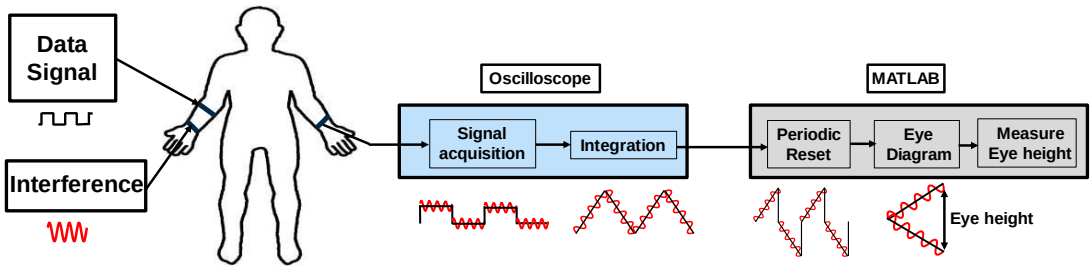


Fig. 3.10. Measurement setup diagram showing interference being injected along with the data signal and the combined signal being received at the oscilloscope, which is post processed according to the I-DDR principle to create the received eye diagram.

ning of the data period and continues over the complete data period. This requires appropriate phase and frequency relation between the data and the integrating clock. This can be achieved through a Clock Data Recovery (CDR) loop commonly used in broadband wireline receivers. In a traditional CDR loop, the sampling clock is aligned with the middle of the data period. However, in the current scenario of the integrating receiver, the sampling clock is aligned with the beginning of the data period. The CDR loop utilizes a phase frequency detector to find the phase mismatch between clock and data and convert it to a voltage, which is then utilized to control the frequency of a Voltage Controlled Oscillator (VCO). The VCO frequency is controlled to enable phase alignment between the clock and the data by moving the clock phase. Alternatively a phase interpolator can also be used to move the phase of the integrating clock to align with the beginning of the data period. A detailed analysis of clock data phase recovery through an Integrating Mueller-Muller CDR for the I-DDR receiver is presented in.

## 3.4 Measurements: Validation of I-DDR principle

### 3.4.1 COTS Component based Measurements

Figure 3.10 shows the conceptual diagram of the measurement set up and is used to verify the interference robustness of the proposed I-DDR receiver. Data and interference are injected into the body through two separate electrodes. A TIVA-C 123GXL microcontroller board is used to apply a Pseudo Random Bit Sequence (PRBS) at a data rate of 1Mbps. The PRBS bit sequence is coupled to the body through a copper electrode connected to a band. The electrodes are custom made and have a size of 2cmX2cm. The transmitter transmits a voltage of 1V. This emulates the voltage transmission from a custom Integrated Circuit fabricated in TSMC 65nm technology, which typically has a supply voltage around 1V. A battery operated signal generator is used to apply interferences of different amplitude and frequency. The interference is coupled to the body through a separate band containing an electrode. Although in an actual HBC scenario the interference will be picked up due to the human body antenna effect, we use a third electrode to inject an interference with known parameters. The response of the I-DDR receiver is independent of the coupling mechanism. Hence, introducing the interference through a third electrode in a controlled manner will help us to quantitatively characterize the interference rejection capability of the I-DDR principle. The received signal was captured in an oscilloscope through a similar band. To emulate the scenario of actual HBC between wearable devices, battery used to apply interferences of different amplitude and frequency. The interference is coupled to the body through a separate band containing an electrode. The received signal is captured through an oscilloscope and integrated. Using a large power supply connected device to capture signals does not completely reflect an actual HBC scenario for communication between two wearable devices and can affect the HBC channel loss, as previously reported in [6], [12], [29], [10]. Previous studies [12], [29] report up to 9 dB reduction in channel loss due to the introduction of ground connected instruments in the measurement setup. To take care of the extra loss, the

integrated signal fed from the oscilloscope was attenuated, while applying to MATLAB for processing. The attenuated signal is processed in MATLAB through periodic reset, according to the working principle of the I-DDR receiver. Subsequently the eye diagram is plotted and the eye height is measured, as a measure of the interference rejection property of the receiver. The I-DDR operation of integration with periodic reset is achieved through integrating in the oscilloscope and achieving the periodic reset operation by processing the integrated signal from oscilloscope in MATLAB. Although this setup doesnt contain the circuit-level non-idealities of a hardware implementation of the integrator, it enables validating the applicability of the I-DDR principle on signals transmitted through the body.

Figure 3.11 shows the eye diagrams obtained from the measured signals while applying CW, AM and FM interference corresponding to two different SIR values. Due to the limitation of the signal generator we could not reach 100Mbps data rate or apply an interference signal of 100MHz. But we have taken the data rate and interference in such a way that the symbol duration remains an integral multiple of the interference time period and the theory of the I-DDR receiver can be validated. Figure 3.11a-3.11d correspond to the case of CW interference of 1MHz with $SIR = -21$dB. Figure 3.11a shows the simulated eye diagram of the Rx NRZ signal, Figure 3.11b shows the eye diagram for the measured received signal under the same condition. Figure 3.11c, d shows the integrated eye diagram from simulation and from measurement. The eye height of the measured and simulated eye diagrams shows that the integrated eye height is more than the normal Rx eye. Figure 3.11e-3.11h shows the simulated and measured eye diagrams for CW interference of $SIR = -24.5$ dB. In both cases the integrated eye shows larger opening than the Rx eye. Figure 3.11i-3.11p correspond to the measured and simulated Rx and integrated eye diagram for AM interference of two different SIR. The frequency of the carrier signal is 500 KHz and the modulating signal is a sine wave of 18 KHz with modulation index 1. Figure 3.11q-3.11x corresponds to the measured and simulated eye diagram for FM interference corresponding to two different SIR conditions. The frequency of the carrier

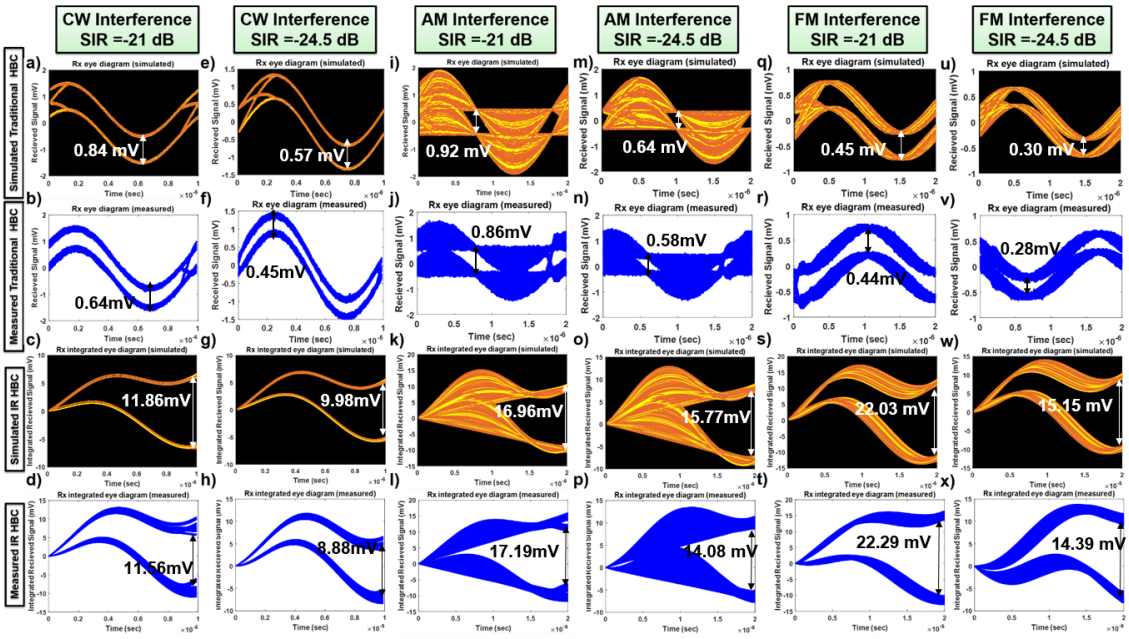


Fig. 3.11. Comparison results between simulated and measured eye diagram for HBC signaling under different interference conditions ($K_{intf}$ = 10). NRZ signal + CW interference with SIR=-21dB a) Simulated Rx eye diagram b) Measured Rx eye diagram c) Simulated eye diagram of integrated Rx signal d) Measured eye diagram of integrated Rx signal. e)-h) Similar plots as a)-d) for NRZ signal + CW interference of SIR = −24.5dB. i)-l) Similar plots for NRZ signal + AM interference with SIR = −21dB, modulating carrier frequency of 18KHz with modulation index 1. m)-p) Similar eye diagrams corresponding to NRZ signal + AM interference with SIR = −24.5dB. q)-t) Eye diagrams for NRZ signal + FM interference with SIR = −21dB, modulating frequency 18KHz and frequency deviation 5 KHz. Integrated eye is significantly less affected compared to the NRZ eye. u)-x) Similar eye diagrams for NRZ signal + FM interference with SIR = −24.5dB. In all the different conditions the simulated and measured eye diagram shows close correspondence. The integrated eye shows higher opening than the normal eye under CW, AM, FM interference condition proving the efficacy of the I-DDR receiver principle.

signal is 500 KHz and the maximum frequency deviation is 5 KHz with a modulating carrier frequency of 18 KHz. In all the cases the measured and the simulated eye heights match closely. Also the eye height measurements show that even with

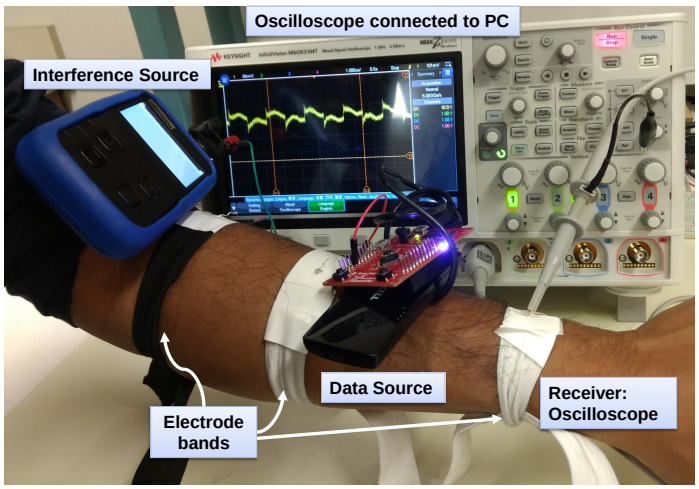


Fig. 3.12. Actual measurement setup picture. The microcontroller board and signal generator is used to provide signal and interference through two separate electrodes. The received signal is captured in an oscilloscope and processed according to the I-DDR principle using MATLAB.

injected interference the I-DDR receiver performs better than a normal receiver and the eye diagrams show significant eye opening. 3.12 shows an actual picture of the setup used for measurements.

### 3.5 Limitations of the I-DDR reciever

The I-DDR receiver can provide high rejection only if the data symbol period is an integral multiple of interference period. In fig. 3.2 (a) the null frequencies are at $\frac{1}{T_b}$, $\frac{2}{T_b}$, , $\frac{N}{T_b}$; which shows to achieve maximum rejection the data rate is constrained by the interference. Also if there is a change in the interference frequency the receiver will not be able to nullify it while receiving data at a symbol duration decided by the transmitter for nullifying some other frequency. In this work we propose an I-DDR receiver which can be tuned to reject any interference of no particular relation to the data frequency. The proposed receiver can also automatically adapt to reject a new frequency if there is any change in the interference.

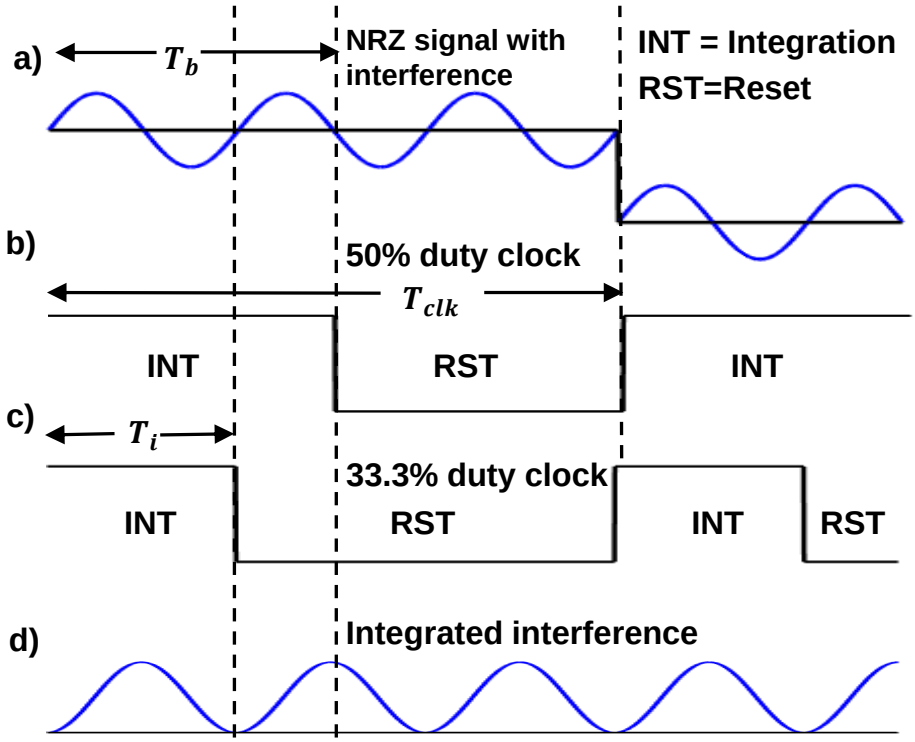


Fig. 3.13. Working principle of the PWM based DDR receiver a) The data signal with the sinusoidal interference superimposed, with $T_b = 1.5T_i$ b) Clock waveform of 50% duty cycle with the integration period equal to the symbol duration c) Clock waveform with 33.3% duty cycle d) Integrated interference with time, which is close to 0 for d=33.3%, not d=50%. Thus d=33.3% clock provides maximum interference rejection

## 3.6 Dynamically Adaptive I-DDR receiver: Variable Notch by PWM

In the I-DDR receiver proposed in [25], the integrating clock duty cycle is fixed at 50% with the integration phase equal to the symbol duration. Here the duty cycle of the clock i.e. the duration of the integration phase is varied to integrate the interference over any time duration $T_{int}$. The integrated signal and interference is as follows:

$$IS_{sig}(T_{int}) = \int_0^{T_{int}} S_{sig}dt = \pm K_{int}A_{sig}T_{int} \tag{3.19}$$

$$IS_{intf}(T_{int}) = \int_0^{T_{int}} S_{intf}dt = K_{int}\frac{A_{intf}[cos(\phi) - cos(2\pi\frac{T_{int}}{T_i} + \phi)]}{\omega_i} \tag{3.20}$$

Lets say duration $T_{int}$ corresponds to duty cycle $d = \frac{T_{int}}{T_{clk}} = \frac{T_{int}}{2T_b}$ and $T_b = kT_i$ , where k can be a non-integer also

$$IS_{intf}(T_{int}) = K_{int}\frac{A_{intf}[cos(\phi) - cos(4\pi\frac{dkT_i}{T_i} + \phi)]}{\omega_i} \tag{3.21}$$

$$IS_{intf}(T_{int}) = K_{int}\frac{A_{intf}[cos(\phi) - cos(2\pi(2dk) + \phi)]}{\omega_i} \tag{3.22}$$

$$IS_{intf}(T_{int}) = 0 \; \forall dk = \frac{n}{2}; n = positive\ integer \tag{3.23}$$

The following result shows that for any arbitrary combination of data rate and interference frequency maximum interference rejection can be achieved by choosing clock duty cycle (d) as:

$$d = \frac{1}{2k}, \frac{2}{2k}, ..., \frac{N}{2k} \;\; s.t. \;\; d \leq \frac{1}{2}; \;\; k = \frac{T_b}{T_i} \tag{3.24}$$

As exemplified by the previous equation, the key idea of the proposed receiver is to vary the duty cycle of the integrating clock and achieve maximum rejection for any arbitrary frequency (fig. 3.2 (b)). This can be achieved by doing a Pulse Width Modulation (PWM) of the integrating clock. Fig. 3.13 depicts a case where $T_b = 1.5T_i$ and as can be seen from the figure the interference integration over the symbol duration is non-zero (fig. 3.13 (d)), which is sampled through a 50% duty cycle clock. Whereas for a clock of duty cycle 33.3% the interference contribution at the sampling points will be 0, as can be seen from the plot of the integrated interference.

For a particular ratio between the symbol and interference frequency there may be multiple points where $IS_{intf}(t) = 0$ , resulting in high interference rejection. But $IS_{sig}(t)$ is an increasing function of $T_{int}$, so the point closest to the end of the symbol period where $IS_{intf}(t) = 0$ will have the maximum ratio of $\frac{IS_{sig}(t)}{IS_{intf}(t)}$ (i.e. SIR) leading to best possible interference rejection. Fig. 3.14 (a) shows that the relative interference rejection increases at the null points closer to the symbol period. This information is taken into account in deciding the start and stop points of the training algorithm for the receiver to lock to the best possible duty cycle.

One downside of reducing the integration period is the degradation of the SNR compared to the case where the integration is for the whole symbol duration as in the

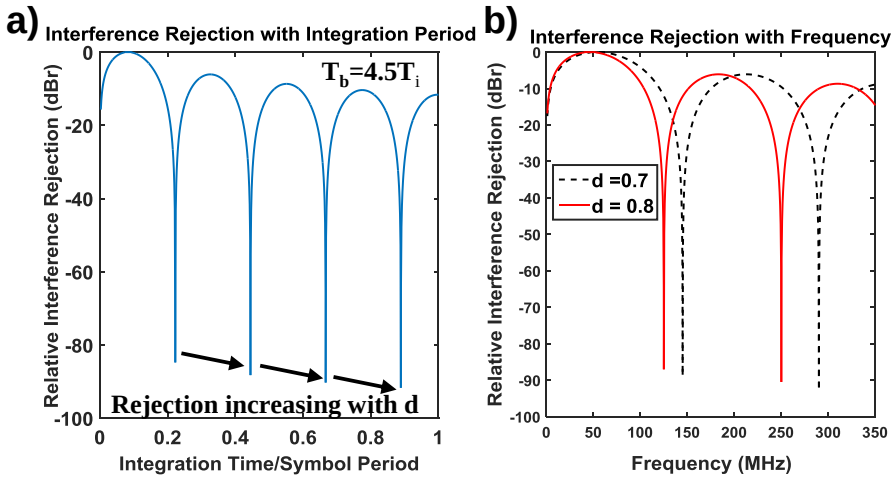


Fig. 3.14. a) Interference suppression as a function of varying integration period, symbol frequency =100MHz, Interference frequency = 450MHz b) Change in null frequencies with duty cycle, symbol frequency =100MHz

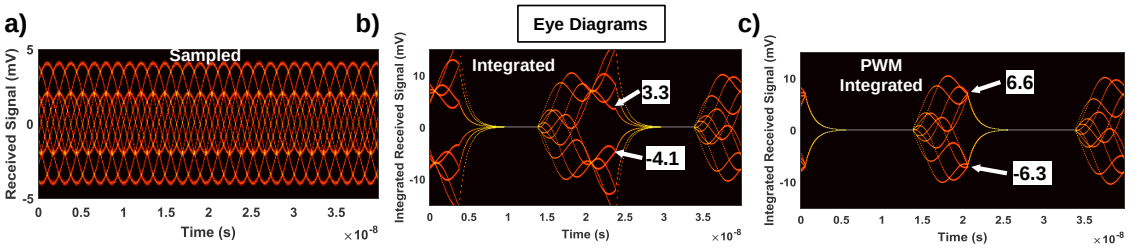


Fig. 3.15. Data frequency = 100MHz, Interference Frequency = 145MHz, SIR = -24.5dB a) Normal Rx eye diagram b) Integrated Rx eye diagram with integration period equal to symbol duration as in I-DDR receiver [25] c) Integrated Rx eye diagram in PWM I-DDR receiver with duty cycle of 0.34 to provide maximum interference rejection. This eye diagram shows significantly more eye opening compared to that of b)

I-DDR receiver in [25]. But since HBC is generally SIR limited than SNR limited, this reduction in SNR does not strongly affect the overall system performance. Moreover, the PWM integrated signals still have better SNR than non-integrating systems.

### 3.7 Results: Comparison of eye diagrams

Fig. 3.15 shows the comparison of the NRZ eye diagram for a normal receiver, I-DDR receiver with and without PWM capability. The interference frequency and data frequency is taken such that $T_b = 1.45T_i$ with SIR of -24.5dB. Fig. 3.15 (a) shows that the NRZ eye is completely closed. Fig. 3.15 (b) is for the I-DDR receiver without PWM capability showing an eye opening of 7.4mV, less than that of the receiver with PWM capability, operating at optimum duty cycle, having 12.9mV opening as shown in Fig. 3.15 (c).

# 4. DESIGN OF INTERFERENCE-ROBUST HUMAN BODY COMMUNICATION TRANSCEIVER USING TIME DOMAIN SIGNAL-INTERFERENCE SEPARATION

Some part of the materials in this chapter have been extracted verbatim from the paper: S. Maity, B. Chatterjee, G. Chang, and S. Sen, A 6.3pJ/b 30Mbps -30dB SIR-tolerant broadband interference-robust human body communication transceiver using time domain signal-interference separation, in 2018 IEEE Custom Integrated Circuits Conference (CICC), 2018

## 4.1 Related Work

Previous state of the art HBC transceivers primarily employ narrowband techniques for data transmission by utilizing channels free of interference, as shown in fig. 4.1 (a). H. Cho et al. [34] presents a dual-wideband full-duplex HBC transceiver which works on two frequency bands of 40MHz bandwidth centered around 40MHz and 160MHz. The FM interference problem is solved by choosing the operating frequency band of the transceiver away from the FM frequency band. The proposed transceiver achieves 79pJ/bit receiver energy efficiency and 32.5pJ/bit transmitter energy efficiency at 80Mbps data rate. Lee et al. [35] proposed a wideband HBC transceiver which enables 60Mb/s data rate using 3-level Walsh coding. The proposed receiver uses broadband HBC transmission and can achieve interference robust operation only in robust mode with a separate band-stop filter but not operating at the maximum data rate. N. Cho et al. [33] presents a 4 channel frequency hopping scheme in the 30-120 MHz frequency band for communication through FSK with an adaptive data rate from 60kbps-10Mbps. The channel conditions are dynamically

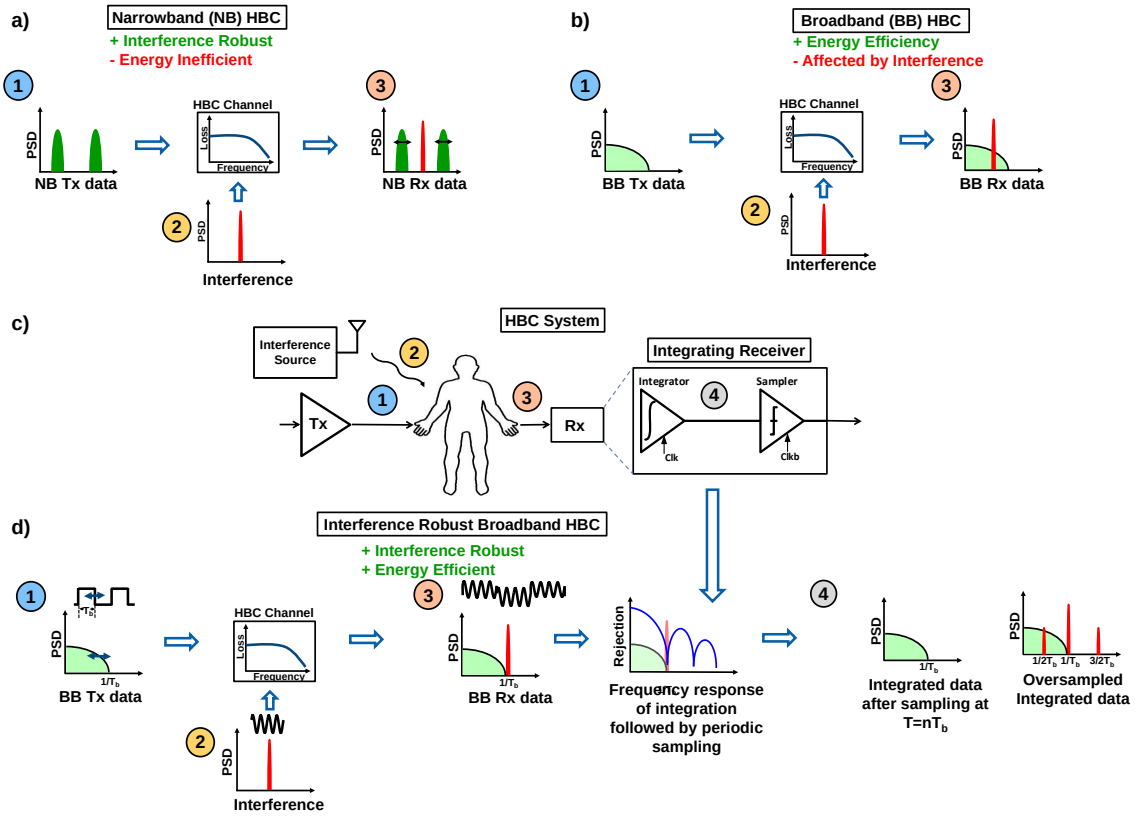


Fig. 4.1. a) Frequency spectrum of narrowband data, narrowband interference showing its effect on narrowband HBC b) Frequency spectrum of broadband data, narrowband interference showing the effect of interference in Broadband HBC. c) System Level diagram of Human Body Communication showing how interference gets added to transmitted data through the human body. d) If we adjust the data bit period to match the null of the frequency response of the data with the interference frequency and then pass it through an integrative receiver with a notch around the interference frequency the complete data can be recovered. This will enable interference robust Broadband HBC which is more energy efficient than Narrowband HBC.

monitored to send the data through a clean channel, free of interference. The proposed receiver achieves an energy efficiency of 370pJ/bit. Bae et al. [36] proposes a double FSK modulation based transceiver in 180nm technology utilizing Contact

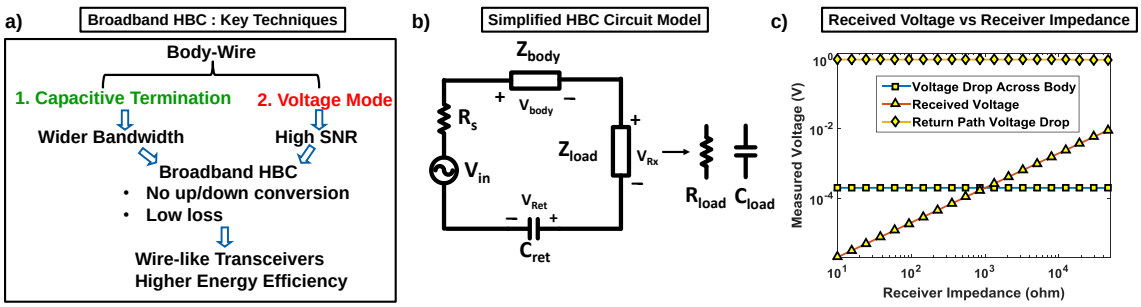


Fig. 4.2. a) Key techniques enabling broadband HBC leading to higher energy efficiency. b) Simplified HBC circuit model showing the body impedance, receiver impedance and return path capacitance, c) Voltage drop across different components of the model for a 1V transmitted voltage at the transmitter end.

Impedance Sensing (CIS) and Resonance Matching (RM) to enhance body channel quality and achieve an energy efficiency of 240pJ/bit. Saadeh et al. [37] proposes a pseudo orthogonal frequency division multiplexing (P-OFDM) based transceiver with contact impedance monitoring and compensation at both the receiver and transmitter end. The digital logic blocks for signal processing are also designed to minimize gate count and power consumption, achieving a receiver and transmitter power consumption of 1.1mW and 0.87mW respectively for a data rate of 2Mbps. In this work we implement broadband HBC by utilizing the human body as a wire-like channel (fig. 4.1 (b)) using an integrating receiver (fig. 4.1 (c)) for interference robust operation (fig. 4.1 (d)). It is interesting to note that oversampling of the integrated waveform does not provide interference rejection. Sampling of the integrated waveform only at a proper rate provides interference rejection.

## 4.2 Key Techniques: Broadband Capacitive Voltage Mode HBC

In this design, we utilize the human body as a broadband communication channel. To that end, certain system level design choices has to be followed. The two key

techniques for enabling broadband HBC (fig. 4.2 (a)) are: a) capacitive termination at the receiver end, b) voltage mode transmitter and receiver operation [24], [26].

### 4.2.1 Capacitive Termination

In capacitive HBC the return path between the transmitter and the receiver is formed through a capacitance. The channel loss is primarily determined by the impedance at the load end and the return path capacitance. From the simplified HBC circuit diagram in fig. 4.2 (b), considering a resistive load, with load impedance and return path impedance considerably higher than the forward path components, the channel loss is obtained as:

$$\frac{V_{out}}{V_{in}} = \frac{s}{s + \frac{1}{R_{load}C_{ret}}} \tag{4.1}$$

Hence, any resistive termination at the receiver end will result in the creation of a pole formed through the load resistance and the return path capacitance ($R_{load}C_{ret}$). The pole frequency depends on the value of the resistive termination and will result in higher loss at low frequencies. Hence, the human body cannot be used as a broadband channel with resistive termination at the receiver end. Several previous studies [4], [8], [7], [9], [5], [13] have used low resistance termination at the receiver for channel measurements. On the other hand, with a capacitive termination at the receiver end, the channel loss can be expressed as:

$$\frac{V_{out}}{V_{in}} = \frac{\frac{1}{sC_{ret}}}{\frac{1}{sC_{load}} + \frac{1}{sC_{ret}}} = \frac{C_{load}}{C_{load} + C_{ret}} \tag{4.2}$$

The channel loss is primarily determined by the ratio of load capacitance and return path capacitance, which is constant over different frequencies. Hence, through capacitive termination at the receiver end, the human body can be used as a broadband channel, which passes all frequencies equally. Hence, the receiver needs to be designed such that the input impedance is primarily capacitive.

### 4.2.2 Voltage Mode Operation

In voltage mode operation, the system is designed to optimize voltage transmission from the transmitter to the receiver end. To optimize voltage mode operation the transmitter requires low source impedance and the receiver termination impedance is required to be high. The overall HBC channel loss from the simplified model, considering all the forward path components, is:

$$\frac{V_{out}}{V_{in}} = \frac{Z_{load}}{R_s + Z_{body} + Z_{load} + \frac{1}{sC_{ret}}} \tag{4.3}$$

Where $Z_{load} = R_{load}$ for resistive termination and $Z_{load} = \frac{1}{sC_{load}}$ for capacitive termination. From equation (4.3) it is evident that the overall channel loss will increase if $Z_{body} > Z_{load}$. Hence the termination impedance has to be higher than the body impedance, which is in the range of a few Ks. Fig. 4.2 (c) also shows that as termination impedance increases, the fraction of voltage drop across it increases and will result in a lower overall loss at the system level. Similarly, a low source impedance at the transmitter end will result in most of the signal being applied at the system and minimize system loss. Hence at the transmitter end, low impedance buffers are used to drive the signal into the human body.

### 4.2.3 Effect: Improved Channel Capacity

The technique of capacitive termination helps us extend the bandwidth of the human body channel. Similarly, voltage mode excitation helps in reducing the overall channel loss and maximizes the received signal amplitude due to the high receiver impedance. Hence, from equation (4.3) it is evident that the signal power is proportional to the square of the termination impedance at the receiver $P_{signal} \propto R_{load}^2$.

The noise power for a CMOS receiver with input impedance R is obtained as $P_{noise} = 4KTR$. Hence, the noise power is proportional to the input impedance ($P_{noise} \propto R$). So, the signal to noise ratio is proportional to the termination impedance

($\frac{P_{signal}}{P_{noise}} \propto R_{load}$). Hence, having a higher termination impedance at the receiver end increases the overall SNR of the system.

The channel capacity of a system is dependent on the available bandwidth and SNR of the system. According to Shanons channel capacity theorem the data rate of a channel is related to its bandwidth ($B$) and SNR as follows:

$$C = B * \log_2(1 + SNR) \tag{4.4}$$

Hence, following these two techniques it is possible to extend the channel capacity of the system by increasing its bandwidth and SNR. The energy efficiency of the system is also significantly increased, since the whole channel bandwidth is now utilized for data transmission and there is no overhead of frequency up-conversion and down-conversion in the transceiver.

Termination with a high impedance at the receiver end results in an impedance mismatch, which can potentially result in reflections. However, the wavelength at these frequencies (10s of MHz) are significantly larger than the circuit dimensions, resulting in no reflections and alleviates the need for matching. Hence, it is possible to have a high impedance voltage mode receiver in the current scenario. Also, as explained earlier, having a capacitive termination results in extension of the channel bandwidth. Hence, the high impedance termination at the receiver end is made capacitive. A MOS input provides a capacitive impedance, which can be utilized as the termination impedance at the receiver end. The capacitance of the ESD diodes connected to the input of the receiver will also determine the capacitance seen at the receiver end.

However, using the body as a communication medium for data transmission introduces the challenge of achieving interference robust operation without the provision of selectively choosing a narrow band of frequency for transmission/ reception, through filtering. The rest of the chapter discusses the design of an integrating receiver , which utilizes these two techniques along with TD-SIS (fig. 4.2) to achieve the goal of broadband interference robust operation.

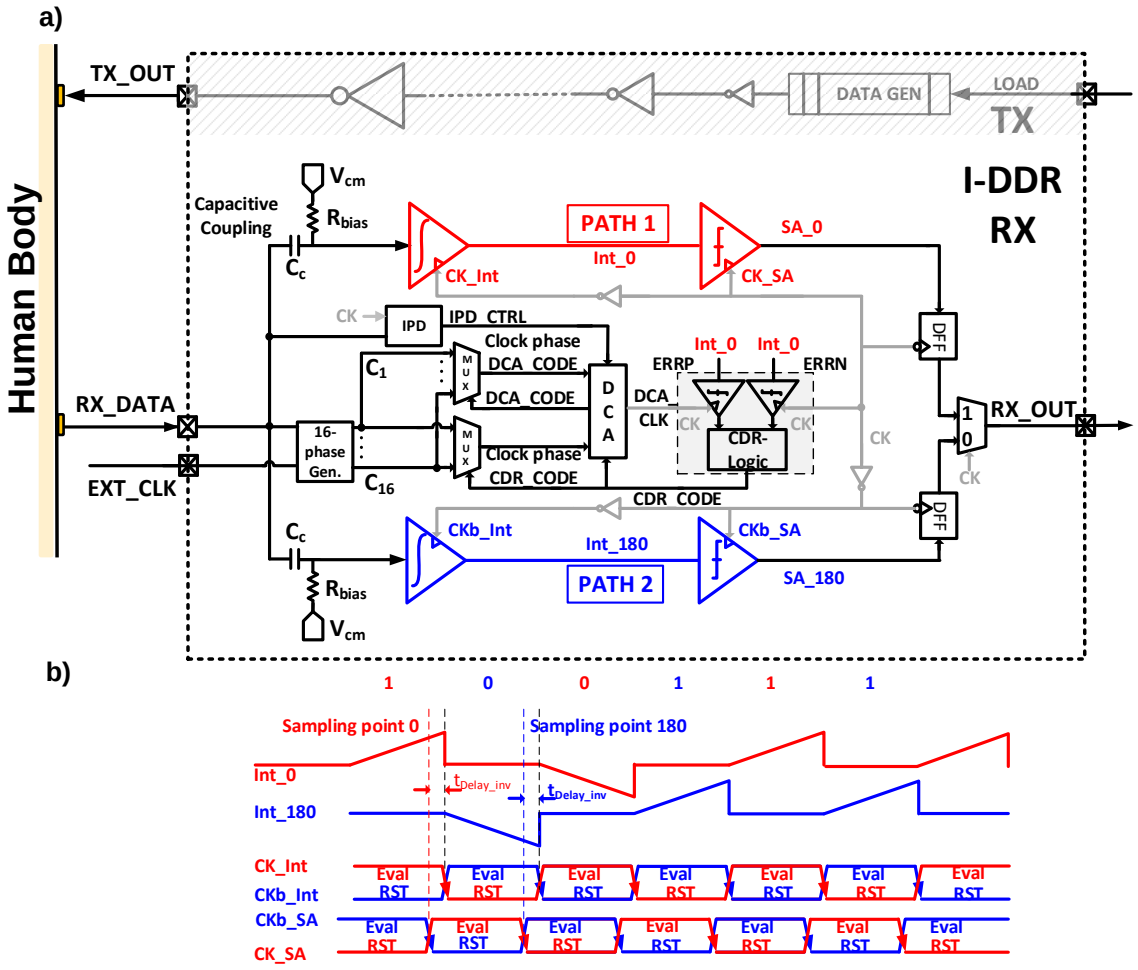


Fig. 4.3. a) System level block diagram of the Integrating DDR transceiver. The receiver front has two paths to process alternate bits, making it a DDR receiver. Each path consists of a mixed signal integrator and sampler which uses TD-SIS technique for interference suppression. The CDR, DCA, IPD blocks are used to generate clock of appropriate frequency and phase for the receiver front end. The transmitter consists of a data generator followed by a string of buffers to drive the signal into the body. b) System Level waveforms showing alternate Reset and Evaluate phases of the two paths.

## 4.3 Transceiver Design: I-DDR Rx Design

The Bodywire transmitter couples the signal into the body through a metal electrode. Multistage buffers are used to drive the broadband full scale voltage signal

into the body. The signal is transmitted through the body and picked up at the receiver end through similar metal electrodes. The signal is capacitively coupled to the receiver, which is biased in voltage mode. The interference coupled received data is integrated and sampled according to the theory of I-DDR receiver as discussed in subsection V.B. Both the integrator and sampler are mixed signal circuits, which require a reset phase in its operation. Hence, two parallel paths enable processing of a data bit per phase of the clock and enable DDR operation. Fig. 4.3 (a) shows the block diagram of the complete BodyWire transciever system. Fig. 4.3 (b) shows the DDR operation with alternate reset and evaluate phase of the integrator and sampler. The two paths work on out of phase clocks to ensure only one of them is evaluating at a given instant. The clock to the integrator also needs to be an inverted, delayed version of the sampler clock for the sampler to sample the appropriate integrated voltage. Mixed signal integration followed by sampling, at the receiver front-end [27] provides the notch filter response necessary for Time Domain Signal Interference Separation (TD-SIS) and enable interference robust broadband HBC. The incoming broadband data and the integrator clock need to be phase aligned to maximize the integrator output. This is achieved through the Clock Data Recovery (CDR) loop. The CDR loop utilizes multiple clock phases from the 16 phase generator to phase align the integrating clock with data. The Duty Cycle Adaptation (DCA) block uses the CDR phase information to enable duty cycle adjustment of the integrating clock and achieve variable frequency interference rejection. The sampled value from the sampler in each path is stored in a flip-flop and then multiplexed to get the final output. We go into the detailed implementation of each of these blocks in the following subsections.

### 4.3.1 Integrator

For the integration operation, a mixed signal clocked integrator is implemented (fig. 4.4 (a)). The integrator consists of a differential NMOS input stage which drives

two PMOS load switches. The clock input is provided to the PMOS load switches. The integrator has two phases of operation: a) Evaluation, b) Reset. During the negative half cycle of the clock, the PMOS switches are turned ON and both the integrator outputs are pre-charged to VDD. During the positive half cycle of the clock period, the PMOS switches turn-off and the parasitic drain capacitances at the output node starts to discharge through the drain current drawn by the input stages. The rate of discharge of the output nodes is dependent on the current being drawn on that particular branch, which is in turn is dependent on the input voltage applied to the input NMOS stages. The difference of input voltage creates a difference in the discharging current, which translates to a difference in output voltage through integration operation at the output node capacitance. For a small signal input difference of $\Delta v_{in}$, the difference in small signal current ($\Delta v_{out}$) flowing through the two branches of the integrator is ($g_m$= transconductance of input NMOS)

$$\Delta i_{out} = g_m \Delta v_{in} \tag{4.5}$$

This difference in discharge current creates a difference in output voltage due to different discharge rates of the parasitic capacitors. Assuming a capacitance of $C_drain$ at the output nodes of the integrator, the difference in output voltage achieved through the discharge current difference is provided by:

$$\Delta v_{out} = \frac{1}{C_{drain}} \int_0^{T_{int}} g_m \Delta v_{in} dt = \frac{g_m}{C_{drain}} \Delta v_{in} T_{int} \tag{4.6}$$

It can be seen from equation (4.6) that the differential output voltage is indeed an integrated version of the differential input voltage applied to the integrator.

### 4.3.2 Sampler

A mixed signal regenerative feedback based sampler (fig. 4.4 (b)) is used for sampling the output of the integrator. The sampler consists of a differential NMOS input stage, which steers current between the two branches of the sampler depending

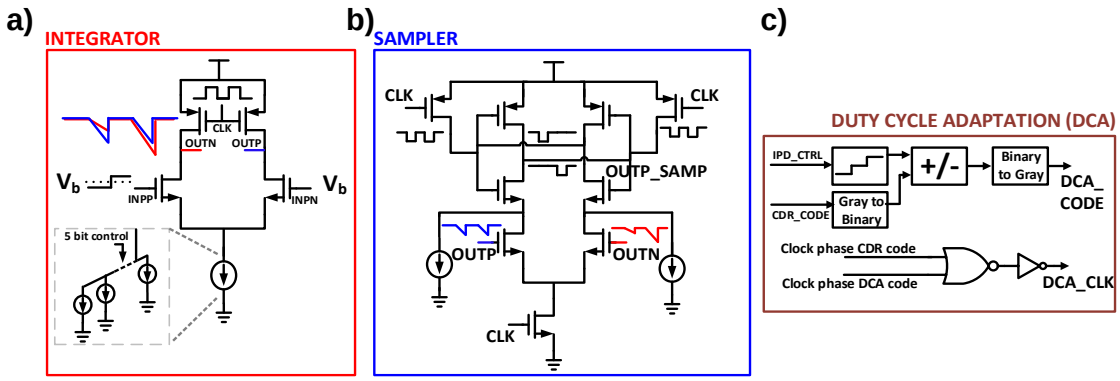


Fig. 4.4. a) Circuit level implementation of the mixed signal integrator with NMOS input stage and PMOS pre-charge switches. b) Regenerative latch based mixed signal sampler c) Duty cycle adaptation block to adjust the duty cycle of the integrating clock to enable variable frequency interference rejection.

on the applied input values. A back to back inverter based regenerative feedback latch is used to perform the sampling operation. During the negative half of the clock period, both the inverter outputs are pre-charged to VDD through the pre-charge switches. During the positive half cycle, both the inverter output nodes start to discharge through the input NMOS stage branches. The input voltage applied to the branch input determines the branch current, which in turn determines the discharge rate of the output node. The branch output with the lower discharge rate eventually gets charged back to VDD through the regenerative action of the back to back inverter based latch. Due to the same action the other output node gets eventually discharged to 0. Hence the sampling operation is performed through current steering by the input stages and regenerative feedback action of an inverter based latch. It is possible to create offsets in the sampler by steering current away from the branches or sinking current into the branches through a parallel path. The direction of offset voltage and its value can be controlled by changing the amount of current being sourced or sinked from the discharge branches.

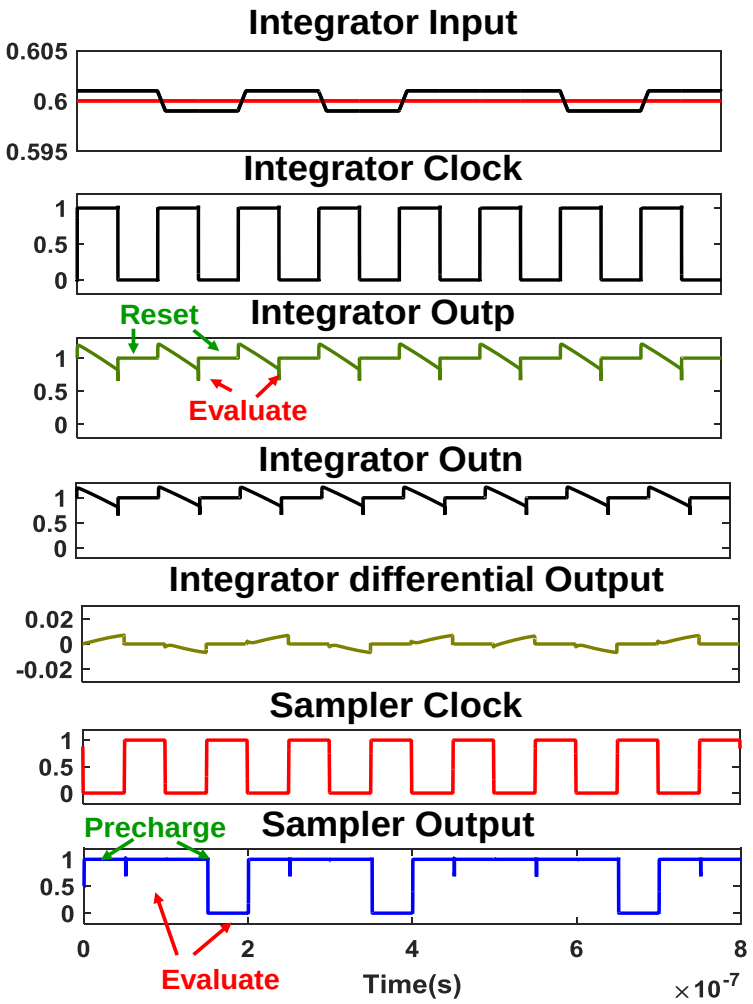


Fig. 4.5. Simulation waveforms from one path of the integrating front-end. The differential output from the integrator is a positive or negative ramp depending on the input bit during the evaluation period. The integration and sampler clocks are almost 180 degree out of phase and have the appropriate delay between them to ensure that the integrator output is sampled at the end of the evaluate period. The sampler output also goes through alternate pre-charge and evaluate phase.

### 4.3.3 Clocking Relation between Integrator and Sampler

To ensure proper operation of the integrating front-end, appropriate clock phase relationship has to be maintained between the integrator and sampler. From the basic

**Mueller-Muller CDR : Integrating Front-end**

| D(n-1) | D(n) | E(n-1) | E(n) | Error Information |
|---|---|---|---|---|
| 0 | 1 | 0 | 1 | LATE |
| 1 | 0 | 0 | 1 | LATE |
| 0 | 1 | 1 | 0 | EARLY |
| 1 | 0 | 1 | 0 | EARLY |

$$\boldsymbol{Errp = 1\ if\ v > +V_{ref}, 0\ if\ v < +V_{ref}}$$
$$\boldsymbol{Errn = 1\ if\ v < -V_{ref}, 0\ if\ v > -V_{ref}}$$
$$\boldsymbol{E(n) = Errp(n) \oplus Errn(n)}$$
$$\boldsymbol{D(n) = current\ data\ bit, D(n-1) = previous\ data\ bit}$$

Fig. 4.6. Truth table of Mueller-Muller Baud Rate CDR for an integrating front-end. Errp and Errn are the error information generated from the two error samplers. The final clock-data phase information can be extracted from two consecutive error and data bit information.

operation of the integrator and sampler, it is evident that both of them operate only during the positive half cycle of the clock and are reset during the other half. However, the sampler has to sample the integrator output only after the completion of the integration period. So the integrator and sampler should have alternate EVALUATE phases, which requires them to have out of phase clocks. Also it is necessary that the sampler samples the integrator output just before the completion of the integration period, as shown in fig. 4.3 (b). To ensure this, the sampler clock needs to be inverted, delayed and applied to the integrator. The simulated waveforms of one path of the front-end is shown in fig. 4.5, showing alternate Reset and Evaluate phases of the integrator, sampler and also the time delay between the inversion of the sampler and integrating clock to ensure sampling at the end of the integration period.

### 4.3.4 Clock Data Recovery

The integration operation has to start at the beginning of the data bit period to maximize the integrated output voltage and subsequently the eye opening at the

receiver end. So it is necessary to continuously maintain a proper phase relation between the data and the integrating clock. This is similar to a wire-line receiver, where the clock phase needs to sample the incoming data bit in the middle to ensure sampling at a point with maximum eye opening. This is typically done through a Clock Data Recovery (CDR) circuit. A Mueller-Muller (MM) [38] baud rate CDR is used in this particular design to maintain appropriate phase relation between the data and integrating clock. Due to the integrating nature of the front-end, the CDR operation for the I-DDR receiver is different from a traditional wire-line receiver. In the integrating scenario the CDR needs to maintain a 0° phase difference between the clock and the data, so that the integration starts at the beginning of the data period. In a wire-line receiver the sampling clock period has to be at the middle of the data bit, resulting in an 180° phase difference. Also, in the I-DDR receiver, any phase mismatch gets directly and proportionally translated to a reduction in voltage margin due to the integration operation, emphasizing the requirement of a CDR circuit.

The MM-CDR requires only one data sample per clock period for CDR operation, hence not requiring an oversampled clock. Two additional error samplers are required to provide necessary error information for the CDR operation. The output of these two error samplers and the data output is used to generate Early/Late information, which provides phase mismatch information between the data and the clock. The truth table for the MM-CDR is shown in fig. 4.6, which is same as that of a non-integrating receiver. The CDR early/late information is used to either advance or delay the integrating clock to maintain proper phase relation with incoming data.

### 4.3.5 Duty Cycle Adaptation

Duty cycle adaptation is required to achieve variable frequency interference rejection by changing the integration duration while keeping the data rate fixed. Through duty cycle adjustment, the goal is to achieve interference rejection of frequencies which are a non-integral multiple of the data rate. Hence, the integration duration

has to be reduced compared to a 50% duty cycle clock in order to achieve variable frequency interference rejection. Logical OR operation between different generated clock phases can be used to create non 50% duty cycled clock. The generated clock is directly applied to the sampler, which is then inverted and applied to the integrator as has been discussed in subsection VI.C. The logical OR operation between multiple clock phases (fig. 4.4 (c)) will create a resultant clock which has a duty cycle >50%. This clock, when inverted and applied to the integrator, creates the necessary <50% duty cycled clock. The appropriate clock phases required for the OR operation is determined by the CDR and through external scan control. This can also be achieved through automatic detection of the interference period through an Interference Period Detector (IPD) and subsequently adjusting the duty cycle of the integrating clock to match the time period. The interference is amplified to generate a square wave of corresponding frequency and the integration duration is adjusted by comparing the ON time of the clock and interference through time to voltage conversion.

### 4.3.6 Interference Period Detector

The Interference Period Detector (IPD) is used to compare the frequency of the interference signal and the integration clock period. Through this estimation, the difference in time period of the interference and the integration clock duration can be determined. This is achieved by converting the time duration information of the clock and interference into voltage domain and comparing them to adjust the duty cycle of the integrating clock. The sinusoidal interference is converted to a square wave by amplifying it through a self-biased inverter stage. The clock and interference signal is applied to control the gate voltage of a PMOS switch whose drain is connected to a current source. During the negative half cycle of the input signal, the capacitor gets pre-charged to VDD. When the control signal is 1, the PMOS switch turns OFF and the output node capacitance discharges through the constant current source. This creates an integrating effect at the output, where the

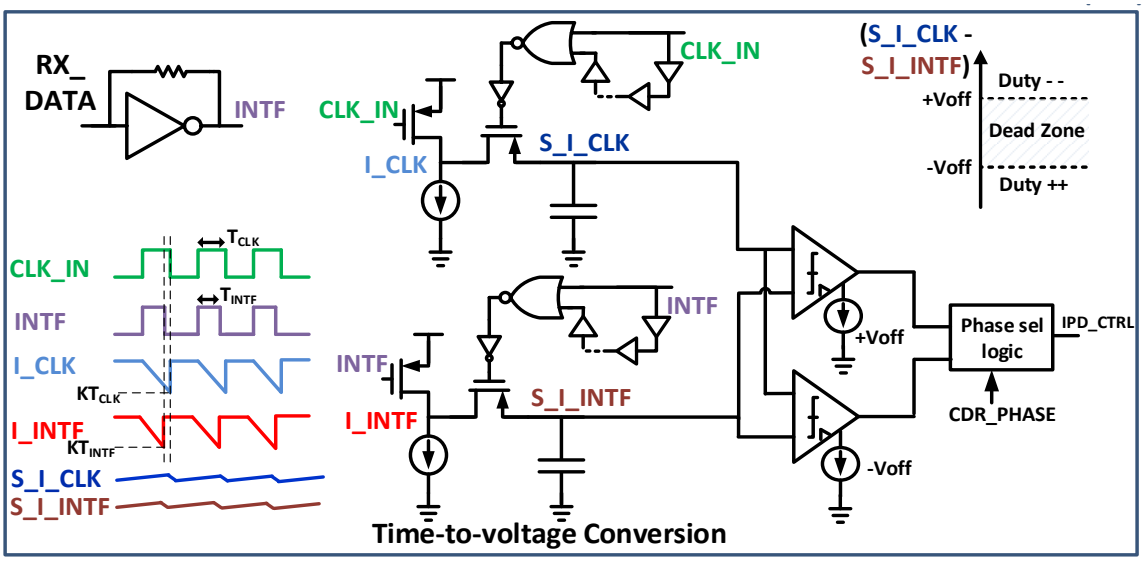


Fig. 4.7. Interference Period Detector (IPD) used to compare the frequency of the interference with the clock frequency. The on-time duration of the interference and the clock is converted to voltage and compared through a comparator to generate the timing mismatch information, which can then be fed back to the duty cycle adjustment block to control the integrating clock duty cycle. This will enable a closed loop operation of interference frequency detection and duty cycle adjustment for adaptive interference rejection.

output voltage is an integrated version of the discharge current. The final value of output voltage after discharging is determined by the duration of the OFF period of the PMOS switch. The amplified square wave interference signal and the clock signal are applied to two such current source switch combination. Since the amount of discharge is dependent on the capacitance at the output node and the current source value, it is important to match them closely so that the output voltage is same for the same duration of discharge for both the clock and interference. Fig. 4.7 shows the complete circuit diagram of the IPD block.

The peak value of the discharged voltage contains the time domain information of the interference and clock signal. Hence, the peak value of the discharge voltage

has to be extracted and compared to determine the timing mismatch between the two signals. The peak value is extracted by sampling the discharged voltage instantaneously on a lager capacitance through a switch. The logic driving the switch should turn it ON for a short duration just before the end of the discharge period. The sampled, peak discharge values are compared through two comparators having equal and opposite offset introduced into them. If the absolute value of voltage difference is more than the introduced offset value then the phase selection logic adjusts the select signals to update the duty cycle of the clock. The offsets are applied to introduce a dead-zone in the duty cycle correction logic, so that the clock duty cycle does not keep on updating continuously if there is mismatch in the duration of the interference and clock period. Conversion of time domain information to voltage domain, followed by precise sampling of the converted voltage and comparison between clock and interference converted voltages, enables duty cycle adaptation of the integrating clock according to the interference frequency.

### 4.3.7 Transmitter Design

In broadband HBC the signal is transmitted as 1/0 bits and do not require any modulation at the transmitter end. This simplifies the design of the transmitter as there is no requirement for frequency up-conversion. As discussed earlier, since we are doing voltage mode HBC, the output impedance of the transmitter also needs to be minimized to maximize signal transmission. Keeping these design constraints in mind, the transmitter consists of a chain of inverters, which drives the data signal into the transmitter electrode coupled to the body.

The data can be generated by two methods: a) externally loading into the registers of the transmitter, b) programmable PRBS generator which can generate PRBS sequences of different length. The maximum supported data rate for this receiver is 30Mbps, which is less than the bandwidth of the human body (close to

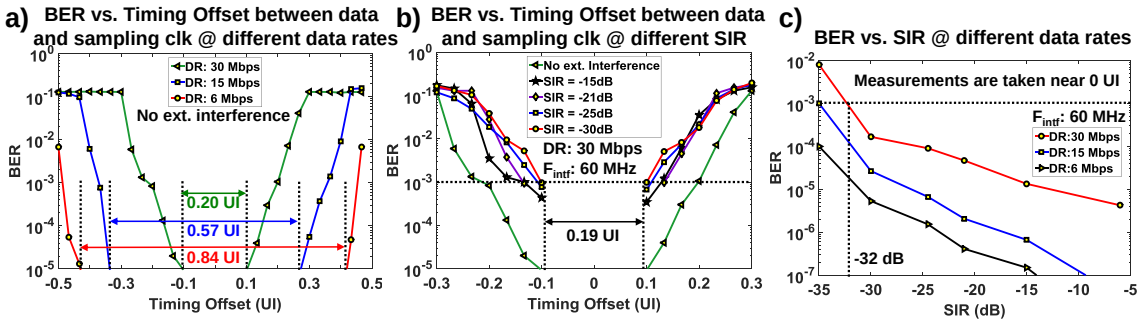


Fig. 4.8. a) Plot showing BER vs Timing offset between data and clock (bathtub curve) for different data rates without the presence of any interference. Lower data rates show higher timing offset tolerance. b) Measured bathtub curve in the presence of 60MHz Continuous Wave (CW) interference for a data rate of 30Mbps. The receiver shows -30dB SIR tolerance with 0.19UI opening (BER level $10^{-3}$). c) BER vs SIR measurement for different data rates, showing higher interference tolerance (lower BER) for lower data rates.

100MHz [12], [10]). Hence, there is no band limitation of the transmitted signals and it is not necessary to have any equalization at the transmitter end.

## 4.4 Measurement Results

The proposed Broadband I-DDR receiver has been fabricated in TSMC 65nm CMOS technology with an active area of 0.122mm2. The die is wire-bonded to a PCB for measurements. The interference robustness of the receiver is determined by measuring the BER under the presence of interference of different types (CW, AM, FM, multi-tone) and different amplitude (varying Signal to Interference Ratio).

### 4.4.1 BER Performance with CW Interference

Fig. 4.8 (a) shows the BER performance bathtub curve of the receiver for different data rate of operation, with varying timing offset between the data and the receiver

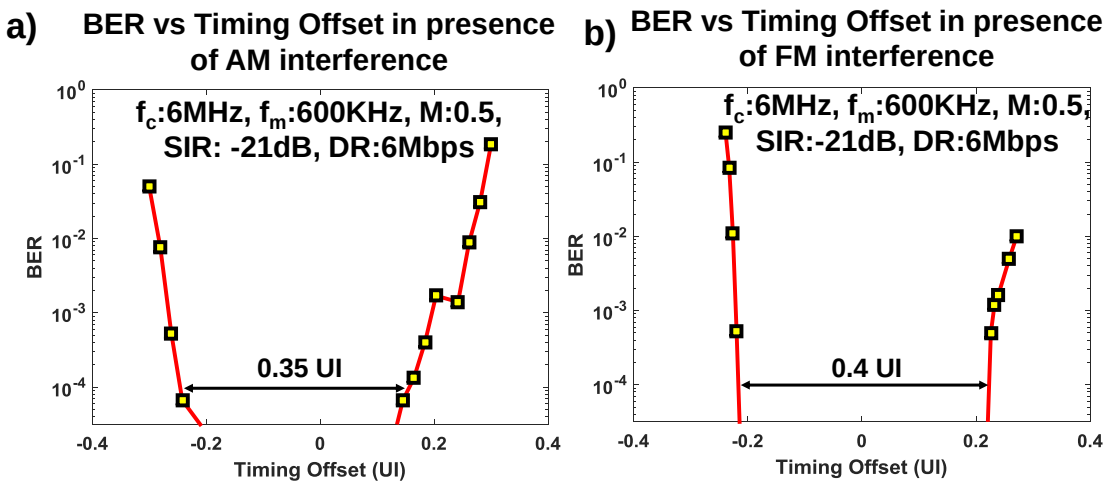


Fig. 4.9. a) Bathtub curve in presence of a) AM interference, b) FM interference.

clock in the absence of any external interference. It can be seen that, for the same timing offset, the BER increases as the data rate increases. The horizontal opening of the bathtub curve also decreases for higher data rates. For the highest data rate of 30Mbps, a 0.2UI eye opening is achievable for a BER limit of $10^{-5}$. To test the interference robustness of the receiver, CW interference of varying amplitude is applied, keeping the data rate fixed at 30Mbps. BER measurements show (fig. 4.8 (b)) a horizontal bathtub curve opening of 0.19UI (BER limit $10^{-3}$) in presence of a CW interference of 60MHz frequency and a SIR of -30dB. Fig. 4.8 (c) shows the BER vs SIR performance of the receiver for different data rates. As the SIR reduces (less signal, more interference), BER increases for all data rates. Consistent with the earlier experiments, the BER for higher data rate operation is more under the same interference condition. It can also be seen that until 30Mbps data rate the BER is $< 10^{-3}$ even in the presence of interference with a SIR of -30dB. Extrapolating the measurement results linearly shows interference tolerance of -32dB for a BER of $10^{-3}$ even at the highest data rate of 30Mbps.

### 4.4.2 BER Performance with AM, FM Interference

Fig. 4.9 (a) shows the bathtub curve of the I-DDR receiver in the presence of AM interference of modulation frequency = 600 KHz, carrier frequency = 6 MHz and modulation index = 0.5. The receiver performance under FM interference of 6MHz carrier frequency, 600 KHz modulation frequency and 0.5 modulation index is shown in fig. 4.9 (b). The bathtub curve shows a 0.4 UI horizontal opening for FM interference and 0.35UI opening ($< 10^{-4}$ BER) for AM interference rejection. This shows the interference tolerance of the receiver to AM, FM interferences.

### 4.4.3 BER performance in presence of DCC

In presence of interferences which are not an integral multiple of the data rate, the sampled integrated interference is not zero at the end of the integration period. As a result, the BER performance of the receiver degrades in presence of interferences of such frequencies. Fig. 4.10 shows the BER at the receiver end, as the ratio between the interference frequency and the data rate is varied from 1-3, keeping the data rate fixed at 15Mbps. As can be seen, for non-integral ratios such as 1.5 or 2.5, the BER is almost two orders of magnitude more than the case for integral ratios of interference to data frequency. However, by adjusting the duty cycle of the integrating clock to an appropriate value through DCA, the BER can be significantly improved even for non-integral relation between interference and data rate. This validates the theory of variable frequency rejection through duty cycle adaptation while keeping the data rate fixed. It is also interesting to note that even without duty cycle adaptation, the BER of the receiver in presence of -25dB SIR interference is $< 10^{-3}$ for all different non-integral ratios of interference frequency and data rate. This shows the efficacy of integration followed by periodic sampling to achieve interference robust operation.

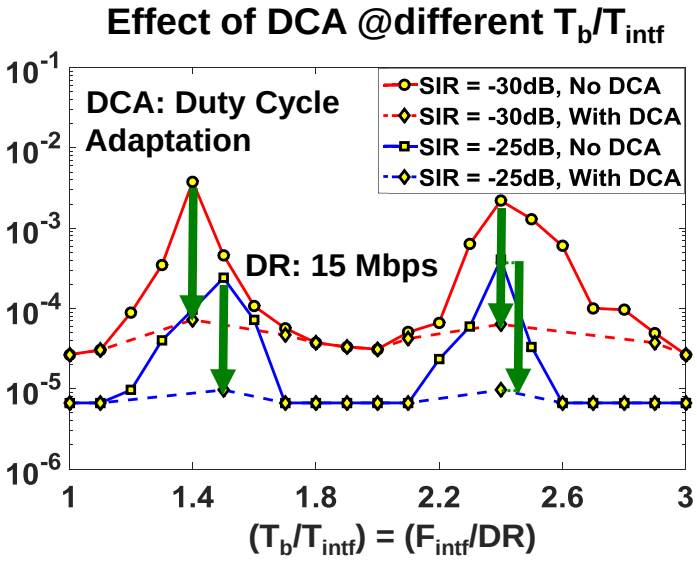


Fig. 4.10. Interference rejection property of the receiver under varying interference frequency (frequency response), showing lower interference tolerance (higher BER) for interference frequencies which are a non-integral multiple of the data rate. Duty Cycle Adaptation reduces the BER for these scenarios by adjusting the duration of integration.

### 4.4.4 BER performance for Multitone Interference

In the previous experiments we have looked into the performance of the I-DDR receiver in presence of a single frequency. Here we look into the efficacy of the proposed I-DDR receiver in the presence of multiple interferences of different frequencies. The data rate is fixed at 6Mbps and interference of 5 different frequencies (6MHz, 6.3MHz, 6.6MHz, 6.9MHz, 7.2MHz for Fig. 4.11 (a); 5.4MHz, 5.7MHz, 6MHz, 6.3MHz, 6.6MHz for Fig. 4.11 (b)) are injected into the data transmission. Each interference corresponds to an SIR of -15dB. The BER bathtub curve shows a horizontal opening of 0.09UI in fig. 4.11 (a) and 0.05 UI in fig. 4.11 (b) for a BER limit of $10^{-3}$, showing interference rejection even in the presence of multi-tone interference.

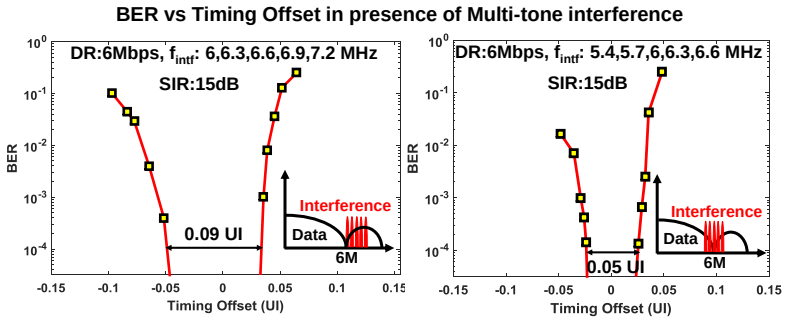


Fig. 4.11. Bathtub curve in presence of Multi-tone (5 tone) Interference : a) Interference frequencies only higher than the data rate, b) Interference frequencies both higher and lower than the data rate.

### 4.4.5 Frequency Response of I-DDR receiver

The BER performance of the receiver provides a measure of its interference rejection property. A lower BER signifying high interference rejection and vice versa. Hence, the frequency response of interference rejection for the I-DDR receiver can be measured by varying the interference frequency and measuring the BER in presence of those different interferences. Fig. 4.10 shows the frequency response of the I-DDR receiver, showing BER $< 10^{-4}$ for interference frequencies which are integral multiple of data rate, showing high interference rejection. The BER increases to $> 10^{-3}$ for interference frequencies, which are non-integral multiple of data rate, showing lower amount of interference rejection as expected.

### 4.4.6 BER Variation with Interference frequency and SIR

Fig. 4.12 shows the BER variation with changing interference frequency and SIR. The data rate is chosen to be 15Mbps and the interference frequency is varied from 15-45 Mbps. For each frequency, the SIR is also varied to change the strength of interference. The measured BER is high for non-integral relation between the interference and data frequencies. Also as SIR reduces (stronger interference), the BER increases, as seen in other measurements also. The two peaks in fig. 4.12 show

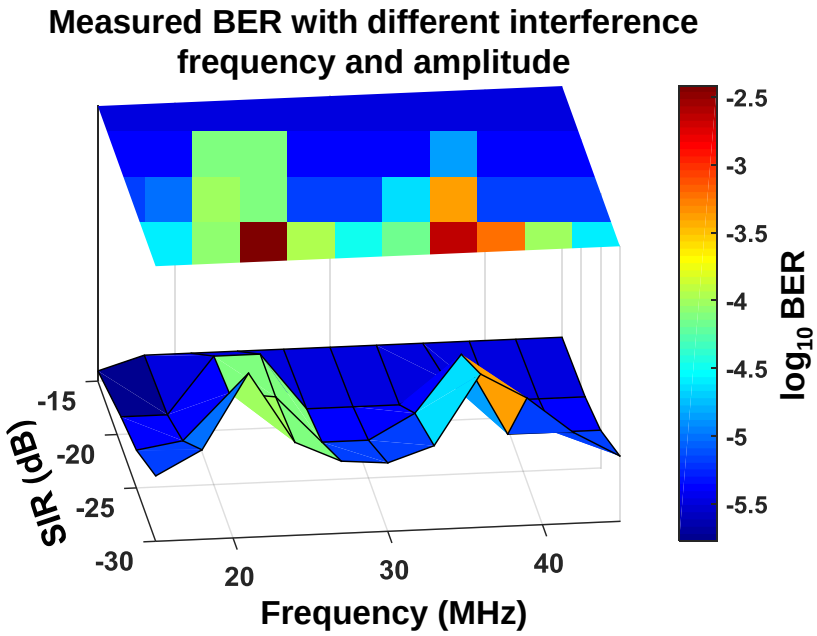


Fig. 4.12. Shmoo plot showing the variation of measured BER in presence of interference of varying frequencies and amplitude (different SIR) for a data rate of 15Mbps.

the range of frequency and SIR for which the BER is high. The BER at the second peak is higher, showing lower interference tolerance for higher frequencies.

### 4.4.7 Image Transmission and Recovery

In this setup (fig. 4.13 (a)), an image is transmitted from an Arbitrary Waveform Generator (AWG) to the receiver, which is then streamed to a PC for reconstruction using MATLAB. The amplitude of the transmitted signal for image transmission is determined through experimental calibration of the HBC channel. For channel measurements, a wearable battery powered device is used for transmission and the received signal is measured in an oscilloscope. However, as reported in previous literature, HBC channel measurements show lower loss when measured with a ground connected instruments. To compensate for this the channel loss is recalibrated for

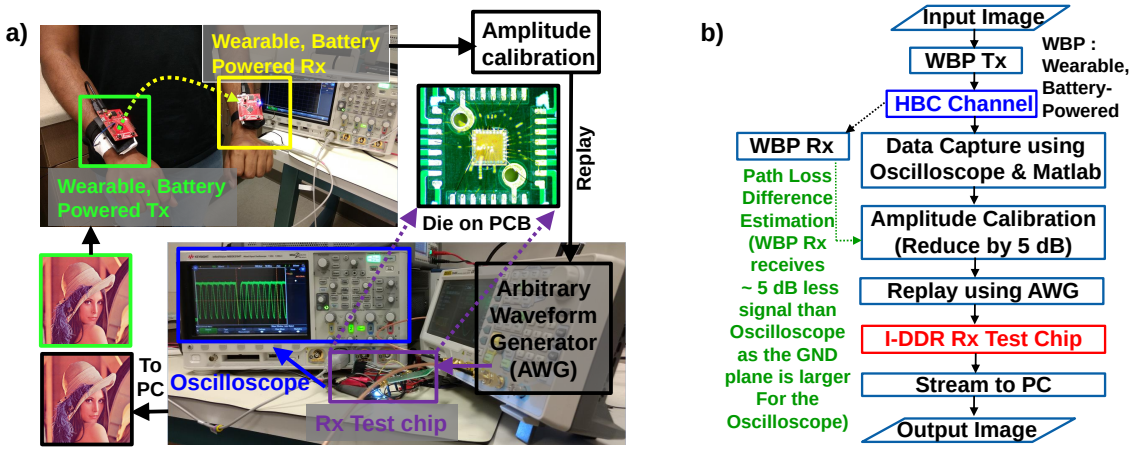


Fig. 4.13. a) Experimental setup of image transfer through HBC. b) Flowchart showing the steps used to convert the image into a stream of bits and re-playing it through an AWG by applying attenuation corresponding to channel loss. The signal amplitude is determined by measuring channel loss and recalibrating it to a wearable transmitter, receiver scenario.

the scenario of a wearable transmitter and wearable receiver as reported in [12], [29]. The signal amplitude of the AWG is determined assuming a transmission voltage of 1V at the transmitter end, going through a channel loss of a wearable-wearable measurement scenario. The image is digitized and the corresponding bit stream is transmitted from the AWG, with proper channel attenuation, to the receiver. The receiver decodes the incoming signal and the received bit-stream is transferred to a computer and the image is reconstructed through MATLAB. The PSNR of the receiver signal is found to be $> 50$dB showing a BER $< 10^{-5}$. The steps followed for amplitude re-calibration and image transmission is shown in the flowchart of fig. 4.13 (b).

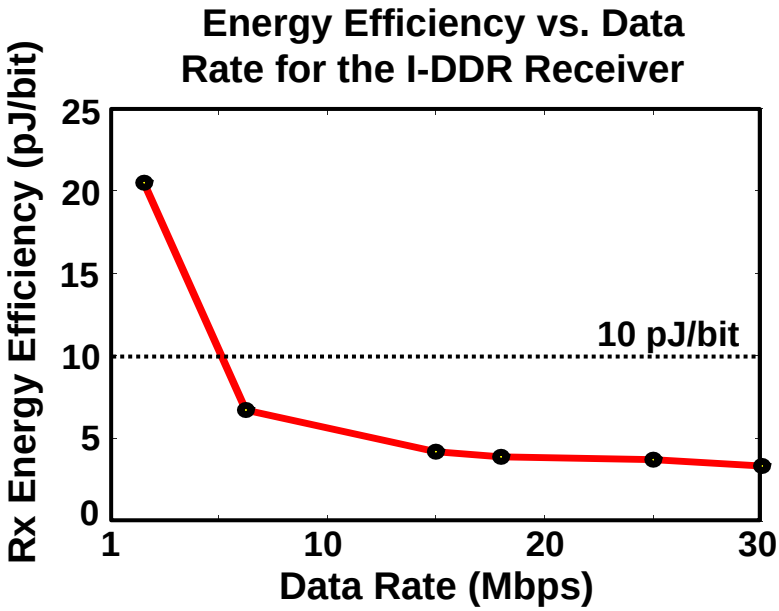


Fig. 4.14. Plot of receiver energy efficiency over different data rates, showing higher energy efficiency with increasing data rate.

### 4.4.8 Energy Efficiency

Fig. 4.14 shows the energy efficiency of the receiver for different data rates. The static DC power consumption of the receiver front end components (integrator bias current, sampler offset generation current etc.) does not scale linearly with the data rate. Also the leakage power is independent of the data rate of operation. As a result, the energy efficiency of the receiver reduces for lower data rates, with maximum energy efficiency of 3.27pJ/bit for the maximum data rate of 30Mbps.

### 4.4.9 Comparison with State of the Art HBC Transcievers

Fig. 4.15 shows the comparison of the proposed HBC transceiver with other state-of-the art HBC transceivers. Other than [35], all the previous designs [33], [34], [36], [37] use narrowband modulation technique for signal transmission. At the peak data rate of 30Mbps the proposed receiver achieves an energy efficiency

| | N.Cho JSCC '09 | J.Bae JSSC '12 | J. Lee ISSCC '14 | H. Cho ISSCC '15 | W. Saadeh JSSC '17 | This Work |
|---|---|---|---|---|---|---|
| **Process** | 180nm CMOS | 180nm CMOS | 65nm CMOS | 65nm CMOS | 65nm CMOS | 65nm CMOS |
| **Supply Voltage** | 1 | 1 | 1.1 | 1.2 | 1.1 | 1 |
| **Modulation** | AFH FSK | Double FSK | 3-Level Walsh Coding | Coherent BPSK | 8 P-OFDM BPSK | NRZ |
| **Maximum Data Rate** | 10Mb/s | 10Mb/s | 60Mb/s | 80Mb/s | 2Mb/s | 30Mb/s |
| **Tx Power** | 2.4mW | 2mW | 1.85mW | 2.6mW | 0.87mW | 93uW |
| **Rx Power** | 3.7mW | 2.4mW | 9.02mW | 6.3mW | 1.1mW | 98uW |
| **Energy/bit (Tx)** | 240pJ/b | 200pJ/b | 31pJ/b | 32.5pJ/b | 435pJ/b | 3.1pJ/b |
| **Energy/bit (Rx)** | 370pJ/b | 240pJ/b | 150pJ/b | 79pJ/b | 550pJ/b | 3.27pJ/b |
| **SIR (@ $10^{-3}$ BER)** | -28dB | -20dB | -20dB | NA | NA | -30dB |
| **Sensitivity** | -65dBm @ $10^{-5}$ BER | -62dBm @ $10^{-5}$ BER | -58dBm @ <$10^{-5}$ BER | -58dBm | -83.1dBm @ $10^{-3}$ BER | -63.3*dBm @ $10^{-3}$ BER |
| **Input Impedance** | <100 Ω | 100-600 Ω | 10KΩ | _ | >> 50Ω | 22* KΩ, (Capacitive) |
| **Area ($mm^2$)** | 2.3 | 12.5 | 1.12 | 5.93 | 0.542 | 0.122 |
| **Interference Robust** | Yes | Yes | Yes# | No | No | Yes |
| **Broadband** | No | No | Yes | No | No | Yes |

# In robust mode using a separate band-stop filter, not at the highest data rate
* Capacitive input termination, input impedance calculated at the Nyquist frequency of 15MHz corresponding to highest data rate of 30Mbps. Sensitivity corresponding to 6mV input swing for this input impedance

Fig. 4.15. Performance Summary and comparison with related literature

of 3.2pJ/bit and the transmitter has an energy efficiency of 3.1pJ/bit, making the overall transceiver energy efficiency 6.3pJ/bit. This is an 18x improvement over the previously reported best HBC transceiver energy efficiency of 111.5pJ/bit [34] and a >100x improvement over state-of-the-art wireless transceivers (fig. 4.16), which achieves an energy efficiency of 1nJ/bit. For a BER of $< 10^{-3}$, the proposed receiver

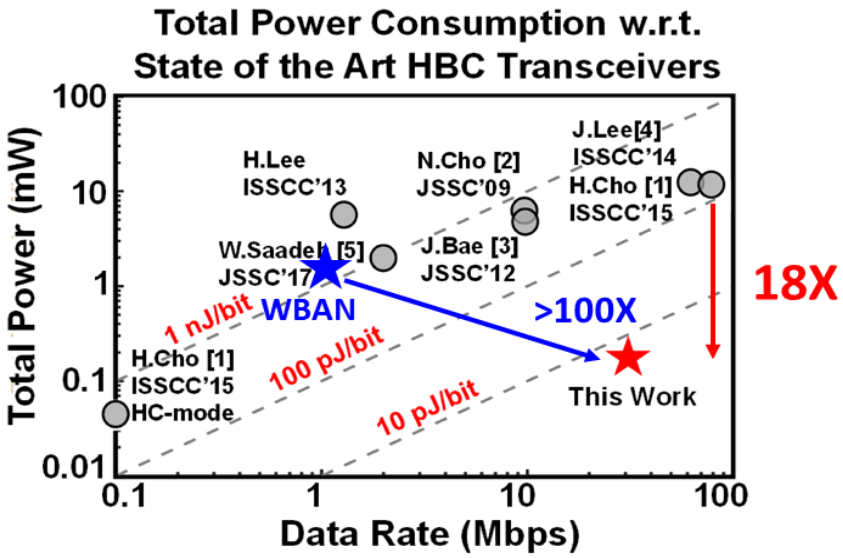


Fig. 4.16. Comparison of the proposed I-DDR transceiver with other state of the art HBC transceivers in terms of total power and data rate. The proposed transceiver is the only transceiver to show <10pJ/bit energy efficiency, making it 18x energy efficient than state of the art HBC transceivers.

also achieves an interference tolerance of -30dB, which is higher than other interference robust HBC transceivers. The input impedance of the receiver is made capacitive to provide wider bandwidth as discussed in Section IV. The input capacitance is primarily determined by the ESD diodes connected to the signal input pin. The input impedance of the receiver is 22K at the Nyquist frequency of 15 MHz, corresponding to the maximum data rate of 30Mbps. The sensitivity of the receiver is calculated using this value as the input impedance of the receiver. The proposed transceiver also has an active area of $0.122mm^2$, which is a 4X improvement compared to state-of-the-art HBC transceivers. The die micrograph and the area breakdown of the individual blocks are shown in fig. 4.17.

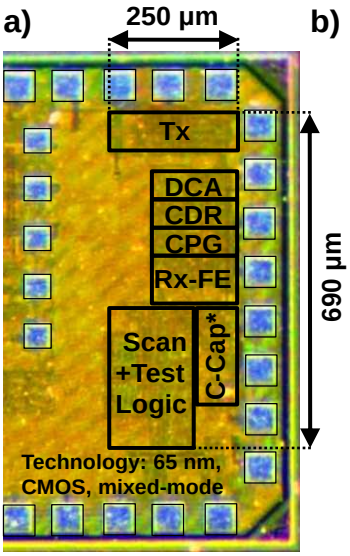


| Block | Sub-block | Power @30Mbps |
|---|---|---|
| Rx | Integrator + Sampler (RX-FE) | 9µW |
| | Clock Data Recovery (CDR) | 20µW |
| | Duty Cycle Adaptation (DCA) | 5µW |
| | Clock Phase Generation (CPG) | 64µW |
| Tx | | 93µW |
| Total | | 191µW |

| Block | Area |
|---|---|
| (Rx-FE)+CDR+DCA+CPG+(C-Cap) | 0.102 $mm^2$ |
| Tx | 0.02 $mm^2$ |

***C-Cap: 250 fF AC coupling cap for RX-FE input**

Fig. 4.17. a) Die Micrograph showing the I-DDR transceiver fabricated in 65nm CMOS technology. b) Power and area breakdown of different blocks.

## 4.5 Conclusion

This chapter presents an interference robust broadband HBC transceiver system achieving 6.3pJ/bit operation, making it 18x more energy efficient than state of the art HBC transceivers. System level techniques such as capacitive termination and voltage mode operation are used to utilize the body as a wire-like broadband channel enabling broadband receiver operation. The interference robustness is achieved through an I-DDR receiver employing TD-SIS technique for interference rejection. Measurement results from a 65nm CMOS implementation of the receiver shows -30dB interference tolerance with maximum achievable data rate of around 30Mbps.

# 5. *BODYWIRE*: ENABLING NEW INTERACTION MODALITIES BY COMMUNICATING STRICTLY DURING TOUCH USING HUMAN BODY COMMUNICATION

Most of the materials in this chapter have been extracted verbatim from the paper: S. Maity et al. "*BodyWire*: Enabling New Interaction Modalities by Communicating Strictly During Touch using Human Body Communication" submitted to ACM Transactions on Computer Human Interaction.

Decades of rapid advancement in semiconductor technology has enabled computing in cheap, small form factor everyday devices. Human users are now submerged in a sea of computers in the environment, with which they are constantly interacting. User interaction with the surrounding environment is one of the key aspects of ubiquitous computing. Communication between devices during a touch based interaction will significantly enhance the effect of a touch event and open up new interaction modalities in Human Computer Interaction. The standard method of achieving this is through coupling touch (fig. 5.2 (a)) and communication (fig. 5.2 (b)) separately. That can be done by utilizing a touch sensor (example: capacitive touch sensor) along with some wireless communication protocol such as Bluetooth, Near Field Communication (NFC) (fig. 5.2 (c)). These protocols use radio waves, utilizing air as the communication medium. Wireless radio wave communication suffers from the problem of security and selectivity, as the signal gets transmitted through air medium and is available to any device within a certain range. As a result information may get communicated even when the devices are in close proximity even before touch. So, communication strictly during a touch event in a secure, selective manner is difficult to achieve with radio communication.

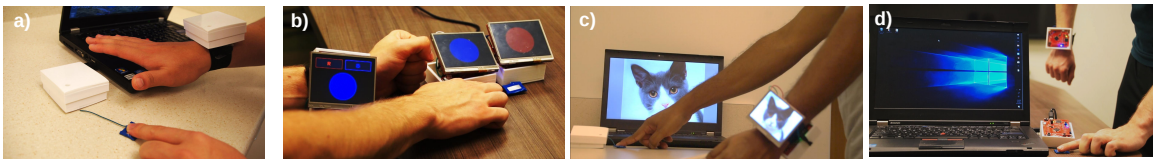


Fig. 5.1. a) *BodyWire* utilizes Electro-Quasistatic HBC technique to communicate through the body without radiating signal out of the body enabling selective and secure communication strictly through touch. a) A wearable transmitter communicating with a receiver connected to a laptop which enables human computer interaction, b) Demonstration showing selectivity of *BodyWire* transmission, c) Information exchange between a wearable and a computer, d) Secure Authentication through *BodyWire*.

Imagine if it is possible to communicate securely and selectively strictly during a touch event (fig. 5.2 (d)). Human Body Communication (HBC) [1], [25], [2] potentially provides such a secure, selective, natural way of touch based interaction between users and the environment, turning everyday objects into an interactive computing platform as well as providing a trusted communication channel. HBC uses the human body as the communication channel for interactions between devices on and around the body. The transmitter couples the signal into the body through a metal electrode. The signal goes through the skin layer and gets transmitted through the conductive tissues and fluids in the body and is picked up at the receiver end when it is in touch with the skin. As a communication method, HBC provides three key advantages over radio wave communication: a) security, b) selectivity, c) enhanced device lifetime.

These potential advantages coupled with the natural and seamless integration of touch in everyday life, make HBC a promising alternative to radio wave communication for acting as the communication medium during interactions between a wearable and any computing device in the surrounding environment. Coupling communication strictly with a touch event can open up new interaction modalities utilizing everyday conductive objects as a potential touch sensor. Human Computer Interaction

through HBC can enable different applications such as authenticating a door with touch through transfer of a key, transferring data between a computer and smart watch, information exchange between smart watches of two people during a meeting or some other social gathering [25] etc. In this chapter we develop a HBC system *BodyWire* (fig. 5.1), which utilizes electro-quasistatic transmission of electrical signals through the human body to achieve enhanced selectivity and security by minimizing signal leakage out of the body into the air medium. The receiver and transmitter communicate with each other only when both devices are in direct contact with the human body and there is no communication even when the devices are in very close proximity to the body. Electro-quasistatic HBC transmission requires operating at a low frequency range to minimize signal leakage out of the human body. Previous studies characterizing the human body channel as a communication medium has shown the body to be a high loss channel at low frequencies, making it undesirable to operate HBC systems at low frequencies. Hence, certain system design techniques have to be followed to enable HBC signal transmission at low loss at these low frequencies to minimize signal leakage. The main contributions of this chapter are the following:

1. **Introduction of Electro-Quasistatic (EQS) HBC-HCI and development of and optimized EQS-HBC system:** We demonstrate that system level techniques such as capacitive termination and voltage mode transmission, reception can be used to utilize the human body as a wire-like broadband communication channel. As a result, low frequency signal transmission can occur through minimal transmission loss within the body. This enables electro-quasistatic transmission, which helps in containing the signal within the human body. We use Commercial Off-the-Shelf (COTS) components to implement these techniques and demonstrate electro-quasistatic HBC with minimal leakage.

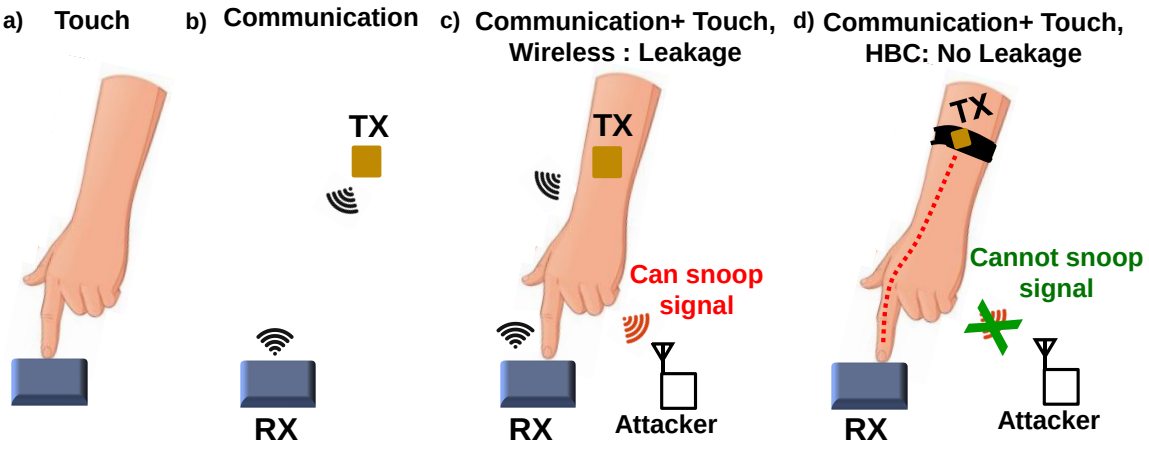


Fig. 5.2. Different possible interaction scenarios between a body worn wearable and off-body computing device. a) Only Touch: where a touch sensitive surface is used to detect a touch event, b) Only communication: a wearable and machine communicating with each other through wireless communication, c) Communication while touch through wireless communication radiates the signal, resulting in communication even without touch and also enabling data snooping from an attacker, d) Communication during touch through Human Body Communication confining the signal within the body enabling communication strictly during touch.

2. **Selective Human-Computer Interaction using HBC-HCI:** In our demonstrations the receiver and the transmitter communicate only through direct touch with the body. This is achieved by electro-quasistatic HBC transmission, which minimizes the signal radiated out of the body. As a result, even if the transmitter or receiver is in close proximity to the body, there is no communication between them. Hence this enables highly selective human computer interaction strictly through touch.

## 5.1 Motivation

### 5.1.1 Touch Based Interaction

Touch has been widely used a medium for humans to communicate with devices around them. Touchscreen displays on mobile devices, computers provide an interactive way to communicate with those devices. Touch has also been used as an interaction technique for 3D interactive environments [39], [40] and haptics. Even touch based interaction has been recommended for older users due to its limited cognitive, spatial and attentional demand [41], [42]. However, adding interaction along with touch, which enhances the effect of touch, is seen as a promising application area [43], [44]. One example of such application is using mobile phones to interact with larger public displays [45]. Paying through mobile applications is also one such example, where the user has to authenticate himself/herself by touching a fingerprint sensor and subsequently use NFC based communication to finish the payment. Enhancing touch based interaction by combining it with communication can increase the convenience of such applications significantly. In this chapter, we utilize HBC to enable communication strictly during touch, enhancing the effect of touch based interactions.

### 5.1.2 Previous HBC Demonstrations

There have been previous studies showing both system level and circuit level implementation of HBC based system for interactions between wearable devices and computers. Microchip Technologys Bodycom system [46] show interaction between a wearable transmitter on a pocket and other everyday objects such as a car / home door, power drill etc. The communication also occurs when the transmitter is kept in the pocket, showing that direct touch is not a strict requirement for communication. [32] shows the demonstration of a ring being used as an intermediate device for exchanging data between two computers. The data is downloaded from a computer

into the ring while touching a pair of electrodes attached to the computer. But in this scenario the communication is done by the touch of two fingers, which forms a closed path between the transmitter and receiver through the electrodes making it unusable for wearable devices, like a smartwatch / smart-band. The demonstrations in [47] show the transfer of an image between a mobile transmitter and a receiver terminal connected to the wall. It also shows that even when the transmitter and the receiver are a few centimeters away from each other, they can communicate with only just the transmitter being held in hand and the receiver not in touch with the body. [48] shows applications where the colour of the clothing of a person or a ball changes depending on the colour displayed at the transmitter end. Various demonstrations of cabinet unlocking, authentication on doors are shown in [49]. However, in this case also the demonstrations work when the person is not in direct contact with both the transmitter and receiver devices. [50] shows multiple applications utilizing HBC for human computer interaction, such as playing interactive games by touching or walking on floor tiles. The authors show that even when the person wearing the transmitter is standing on one floor tile, there is signal leakage into the adjacent floor tiles. Also, there is communication between the wearable and the floor tiles through the shoes of the user, showing touch is not a strict necessity for communication. The demonstrations in [51] show the usage of commodity devices such as smartphone and touchpads to transmit secret keys through the body for user authentication. The achievable data rate in this scenario is a few hundred bits per second, which is sufficient for the authentication demonstrations shown but not sufficient for information transfer. The studies discussed so far focuses on system level demonstration of HBC. There have also been previous studies [33], [34], [36], [27], [37] which focus on specific circuit design techniques for HBC. Most of these designs also operate at high frequencies, making them prone to signal leakage out of the body.

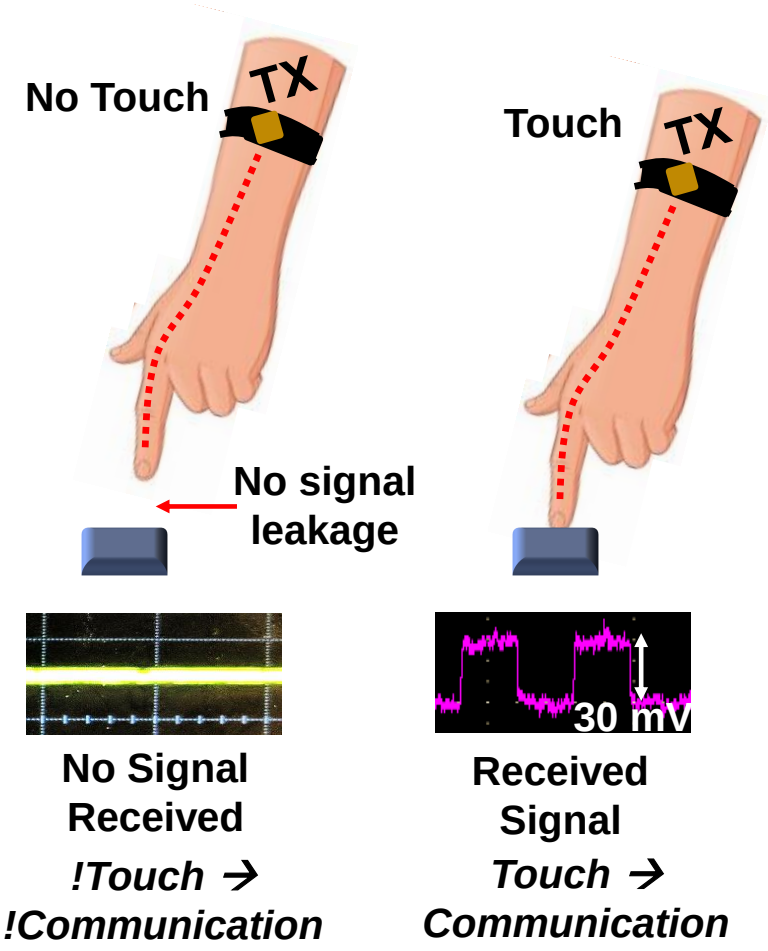


Fig. 5.3. a) EQS-HBC enables signal confinement within body. So, there is no signal leakage out of the body. b) This results in communication strictly during touch.

### 5.1.3 Open Problems (HBC-HCI)

The previous demonstrations of HBC show information exchange when there is a path between the transmitter and the receiver. However most of them suffer from the problem of signal leakage, which results in the receiver getting triggered even when there is no direct physical contact with the receiver. [47] shows information getting transferred even when the transmitter is a few centimeters away from the receiver. The authors in [50] show that signal leaks into the adjacent floor tiles even when the

person with the transmitter is standing on a separate floor tile. Other demonstrations also show communication when the device is not in direct touch with the body. This shows that there is signal leakage out of the body, which results in communication between the devices even without direct physical touch. As a result of which, these demonstrations does not have the property of information exchange strictly during touch. However, the goal of this chapter is to design systems such that a touch event is the necessary and sufficient condition for signal transmission (fig. 5.3). This can be written as

$$Touch \implies Communication \tag{5.1}$$

$$!Touch \implies !Communication \tag{5.2}$$

Each of the individual equations provides a necessary condition for communication, however both of them combined provides the necessary and sufficient condition for strictly touch based communication. We design our systems following system level techniques such that signal leakage out of the body during HBC transmission is minimized and we can demonstrate data transmission strictly during touch.

## 5.2 Fundamental Techniques

In our current demonstration, we have used certain system level design techniques and parameter choices to minimize the signal leakage out of the body and provide us with selectivity and security during Human Computer interactions. The key system level design techniques utilized to achieve this are: a) Electro-quasistatic HBC, b) Capacitive receiver termination, c) Voltage mode transmission and reception. In this section we discuss the effect of each of these techniques in achieving the goal of higher selectivity and security.

- **Electro-quasistatic (EQS) HBC:** In EQS-HBC, the signal transmission between the transmitter and the receiver occurs through electric fields, which are contained within the human body. The signal propagation occurs primarily

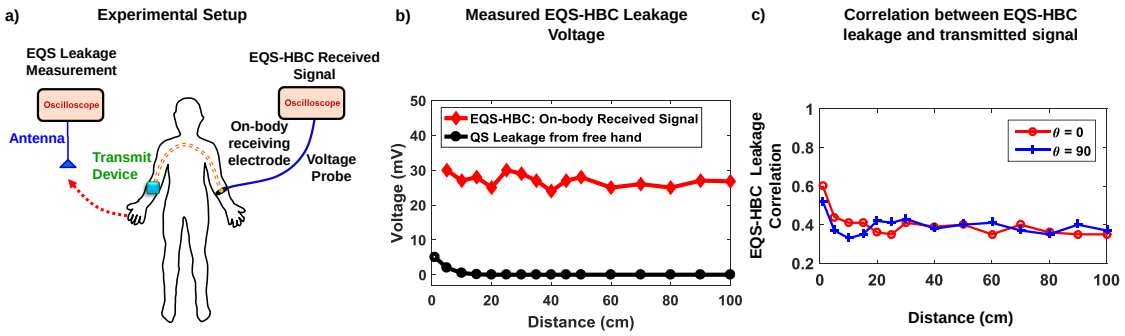


Fig. 5.4. Measurement of signal leakage into the air, as the receiver is moved away from the body. a) Measurement setup showing leakage measurement and on-body signal transmission measurement b) Plot of measured voltage with distance away from body, c) Correlation between the measured and transmitted voltage over distance at different angles. The correlation is <0.5 even for distances a few cm away from the body, highlighting the difficulty for an attacker to snoop an ongoing transmission.

through the low impedance tissue layers underneath the skin. Propagation of electro-magnetic waves is not the primary mode of communication in this scenario. Hence, there is minimal signal leakage out of the body during ongoing signal transmission within the body. The low frequency operation of the HBC system enables electro-quasistatic operation and is the primary reason for the confinement of the transmitted signals within the body. Fig. 5.4 shows the measured voltage at different distances from the body when there is a signal transmission going on within the body at 1 MHz frequency. It can be seen that the amount of signal leakage in the air falls below 10 millivolts even 1 centimeter away from the human body, showing signal confinement primarily within the body. The signal received only a few centimeters away from the body also shows minimal correlation with the transmitted signal. Hence, it will be nearly impossible for an attacker to successfully decipher the data transmission going on even from a distance of a few centimeters away from the body. However, to

achieve electro-quasistatic operation, it is important to operate at low frequencies to minimize signal radiation. Previous studies characterizing the human body [12], [10], [5], [19], [7] had shown high signal attenuation at low frequencies, making it an undesirable frequency band for HBC transmission. However for our current system design, we use capacitive termination and voltage mode operation to reduce the human body channel loss at low frequencies and extend the bandwidth of the human body. This enables using the body as a wire-like communication channel, even utilizing the low frequencies.

- **Capacitive Termination:** The value and type of termination impedance of the human body channel at the receiver end is an important parameter in determining the operable frequency range of the HBC system. Resistive termination is the commonly used termination methodology in most previous studies. However, in our design, the termination at the receiver end is done through a high impedance capacitor. Because of the capacitive return path between the transmitter and the receiver, using a capacitive termination at the receiver end creates a loss response independent of frequency. This reduces low frequency loss and enables HBC at these frequencies. In our current demonstration, the receiver is carefully designed such that its input impedance and hence the termination impedance seen by the channel is primarily capacitive.

- **Voltage mode transmission and reception:** Previous HBC system designs primarily use signal power as the metric for communication between devices. However, power transmission requires low impedance termination at the receiver end, which is not suitable for low frequency signal transmission through HBC. In our demonstrations we use voltage mode operation, where the transmitter sends out voltage through the system and the receiver is designed to pick up voltage. Voltage mode operation requires high impedance termination at the receiver end, which also enhances the amount of signal received for low frequency HBC operation. Hence, design of voltage mode systems also help reduce the low

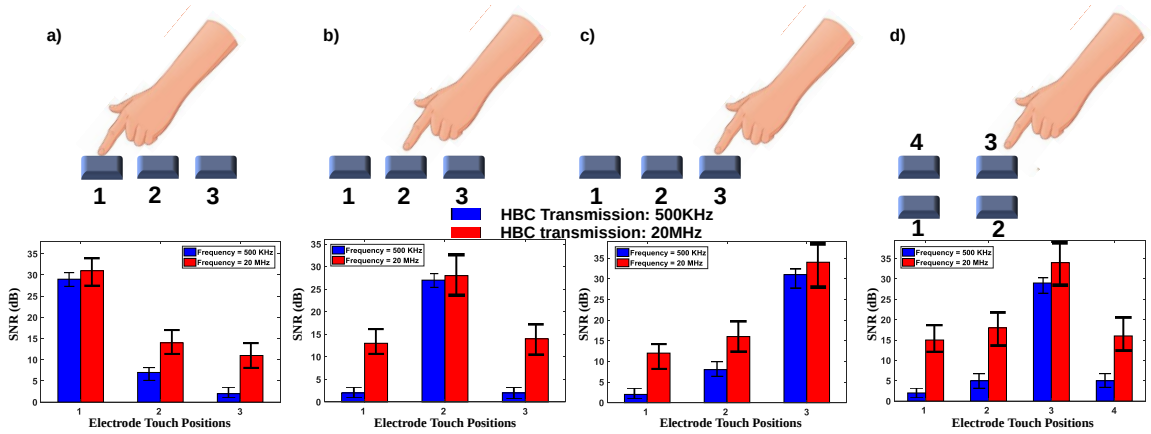


Fig. 5.5. Measurement of received SNR for different electrode configurations: User touching a) electrode 1, b) electrode 2, c) electrode 3 respectively for a three electrode configuration. d) User touching electrode 3 in a four electrode configuration. All measurements show more than 20dB degradation in SNR on adjacent electrodes compared to the electrode being touched when the transmission frequency is 500KHz, showing signal confinement in EQS HBC. Measurements at 20MHz show significantly more signal leakage to adjacent electrodes as well as variation in measurement.

frequency loss. This in turn enables electro-quasistatic HBC, providing signal confinement within the body.

## 5.3 Design Goals

- **Touch Based Communication:** The primary design goal of the demonstrations is to show communication strictly during touch events. The transmitter and the receiver communicate only when there is a direct conductive path through the human body. This can only be achieved if there is no communication through the air medium by signal leakage out of the body. Hence, to ensure communication strictly through touch, the system has to be designed to ensure minimal signal leakage out of the body. For this, we have utilized

signal transmission at frequencies lower than 500 KHz. The low frequency operation enables EQS-HBC and results in minimal signal radiation out of the body. The experiments in fig. 5.5 shows the viability of strictly touch based communication. Three electrodes are kept 1 cm away from each other. The user touches one of the electrodes and the received signal is measured through a spectrum analyzer at all of the electrodes. The peak value of the measured spectrum at each electrode is shown in fig. 5.5 corresponding to each posture for two different frequencies. It can be seen that for low frequencies used in EQS-HBC, the adjacent electrodes receive at least 20dB less signal compared to the electrode that is being touched directly through the fingertip, with SNR of 5 dB or less. On the other hand, for a high frequency transmission at 20MHz, the received SNR at the adjacent electrodes are 15dB, which makes it possible for a receiver connected to the adjacent electrode to get activated. Also the measured spectrum shows higher variation at 20 MHz frequency, making it difficult for a receiver to differentiate between actual data transmission and leakage. This shows that the low frequency operation enables the selectivity of the touch events achievable through EQS-HBC in our current system design.

- **Posture Independence:** For signal transmission between a wrist worn/ handheld device and a computer, the hand posture affects the amount of signal received at the receiver end. Specifically, the distance of the hand from the torso of the user affects the amplitude of the received voltage. Experiments in fig. 5.6 shows four different postures of the hand with the transmitter and the corresponding received signal at the receiving electrode when the other hand is touching it. It can be seen that there is 7 dB difference in the amount of received signal depending on the posture of the hand. Maximum amount of signal is received for the posture with an outstretched hand. As the hand with the transmitter is brought closer to the torso, the received signal amplitude decreases. Touching the torso with the transmitting hand shows minimum received signal at the receiver end. The *BodyWire* system should be designed

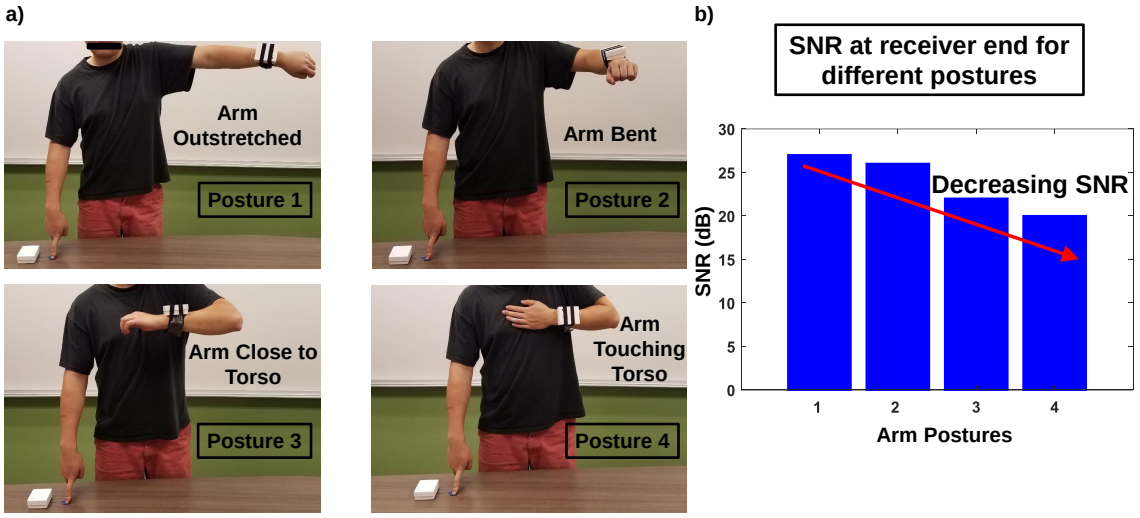


Fig. 5.6. The effect of transmitting hand posture on received signal strength. a) The transmitting hand moves closer to the torso from its outstretched position, b) the received signal strength reduces as the hand moves closer to the torso.

to operate across all these posture variations. The receiver should be sensitive enough to operate during the posture with minimum received voltage but should not get saturated when the amount of received signal increases to maximum for a different posture.

- **Convenience:** One of the primary goals of HBC is to enhance convenience during user interaction by combining communication with touch. The combination of communication and touch results in combining multiple user interaction steps into one single step, which enhances the ease of use. *BodyWire* system is designed to provide secure communication during touch and enhance user convenience during human-computer Interaction.

- **Wide Applicability:** The *BodyWire* system serves as the communication backbone infrastructure for any application requiring transmission of information strictly through touch. The system is designed to take data from a trans-

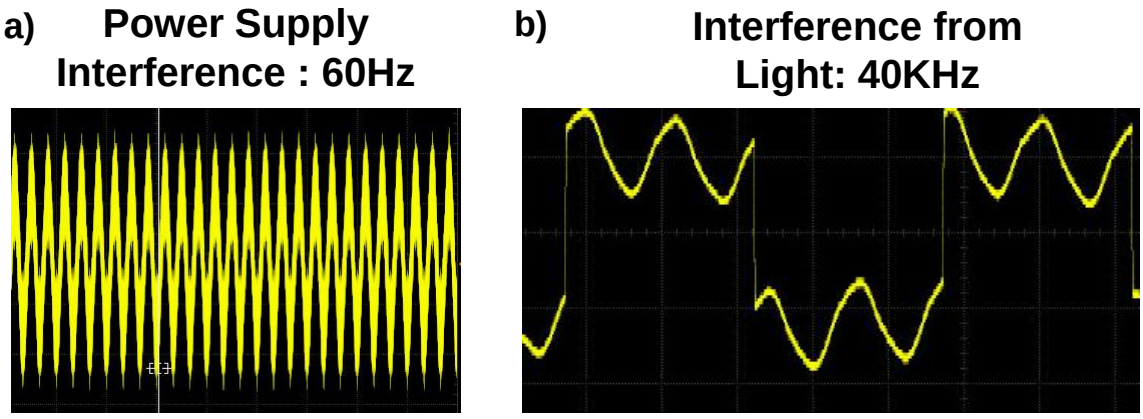


Fig. 5.7. Interferences picked up by the body during transmission in EQS-HBC. a) 60Hz building power supply noise, b) Additional 40 KHz interference present in the laboratory environment.

mitter device, transmit it through EQS-HBC and decode it at the receiver end. The type of transmitter, receiver device does not affect the hardware / software of the *BodyWire* system. This will allow wide applicability of the *BodyWire* system for different application scenarios such as data transfer, secure authentication etc.

- **Interference Tolerance:** The human body picks up any interference present in the environment due to the human body antenna effect [33]. This interference affects any ongoing HBC data transmission, resulting in bit errors. Since the frequency of operation of the *BodyWire* system is in the range of 100s of KHz, any environmental interference in this frequency range has an effect on data transmission. Fig. 5.7 shows two of the prominent source of interference present in the laboratory environment, as measured through an oscilloscope. The 60 Hz noise (fig. 5.7 (a)) originates from the supply mains within the building, which will be present in an actual application scenario within any building. The interference around 40 KHz (fig. 5.7 (b)) is due to the light sources present in the laboratory. The hardware of the *BodyWire* system is designed to filter

a) **ICNIRP safety limits**

| Frequency(f) | RMS Current Density ($mA/m^2$) | Whole Body SAR (W/Kg) |
|---|---|---|
| <1Hz | 8 | - |
| 1-4 Hz | 8/f | - |
| 4Hz – 1KHz | 2 | - |
| 1-100 KHz | f/500 | - |
| 100KHz – 10MHz | f/500 | 0.08 |
| 100MHz – 10 GHz | - | 0.08 |

b) **Simulated EQS-HBC current density compared to safety limits**

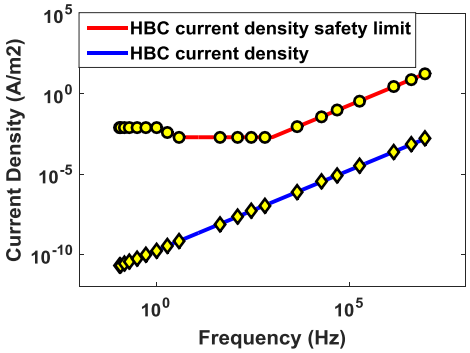


Fig. 5.8. a) Safety limit table of current density and SAR provided by the ICNIRP guidelines b) Current density of EQS-HBC from simulated circuit models , showing >10000x lower current density compared to the safety limits

out the different interferences present within the environment. The software also needs to have error detection/ correction mechanisms to tolerate bit errors happening due to any interference affecting transmission.

- **Form Factor:** The *BodyWire* system is designed for applications involving Human Computer Interaction. Hence, one of the devices involved in the interaction will be a wearable or a hand-held device. So both the transmitter and the receiver should be designed to have a wearable form factor. This puts a limit on the battery life and the processing power of the computing unit (microcontrollers) present on these devices.

## 5.4 Safety

HBC requires transmission of electrical signal through the human body. Hence safety limits of electrical signal transmission are one of the primary concerns of any HBC system. Every HBC based system should be designed to adhere to the safety lim-

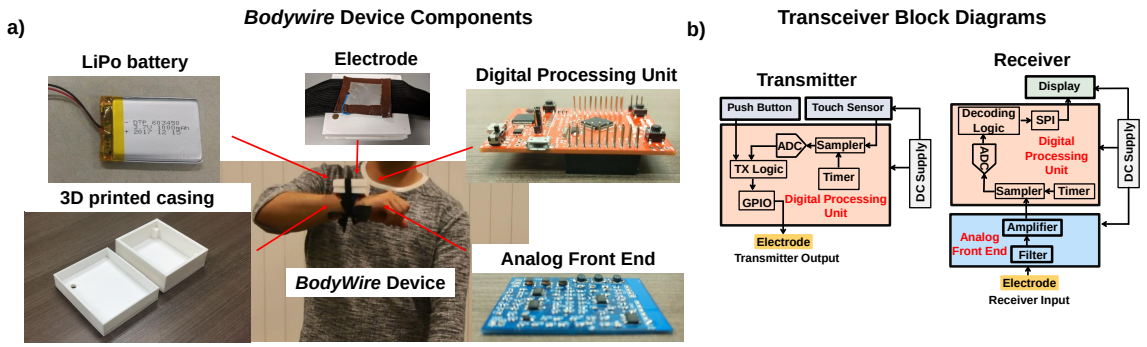


Fig. 5.9. a) *BodyWire* device components: PCB of the analog front-end, TM4C123G microcontroller acting as the Digital Processing Unit, Lithium Poly Battery used as power source, 3D printed casing for packaging the device. b) Block diagram of the transmitter and receiver showing the basic building blocks and how they are interconnected.

its of current and radiation (fig. 5.8). The International Commission on Non-Ionizing Radiation Protection (ICNIRP) provides guidelines for limits of human exposure to time varying electric, magnetic and electro-magnetic fields up to 300 GHz frequency. Since the *BodyWire* system operates in the frequency range of a few 100s of KHz, we are primarily focused on the low frequency range. The rms current density through the body is the primary bottleneck at this frequency range. The 4Hz-1KHz frequency range has the most stringent current density requirement as the current at these frequencies has effect on nerve stimulation. Fig. 5.8 shows the safety requirement of current density for different frequencies. Simulating an EQS-HBC circuit model [28] shows that the current density in EQS-HBC is ¿10000x lower than the safety limits imposed by the guidelines. This is primarily due to the high resistance provided by the return path capacitance at the low frequency of operation, limiting the overall current through the system.

## 5.5 System Level Implementation

The complete *BodyWire* transceiver is implemented using Commercial Off-The-Shelf components, as shown in fig. 5.9. The receiver consists of an Analog Front End (AFE) designed on a custom PCB for signal processing and a Digital Processing Unit (DPU) to run the software and interface with the external world. The AFE primarily consists of filters and amplifiers to process the received signal. The transmitted signal gets attenuated and is affected by environmental interference when it is received at the receiver end. Hence appropriate analog signal processing needs to be performed to recover the received bits from the noisy, attenuated signal, before it can be utilized by the DPU. The DPU is implemented on a Texas Instruments TM4C123G microcontroller, which has a 32bit 80 MHz, ARM Cortex M4 processor. The board consists of 32KB SRAM and 56KB flash memory. Two 12 bit, 2MSPS ADCs are used to sample the signal coming out of the AFE and these act as an interface between the AFE and the DPU. 32 bit Timers internal to the microcontroller is used to provide precise timing necessary for ADC sampling operation. The DPU performs basic error correction on the received bits and decodes the data from its packetized form. The DPU also acts an interface to the touchscreen display unit through the Serial Peripheral Interface (SPI). A BOOSTXL-K350QVG-S1 QVGA touchscreen display is used for taking external touch input and display images or text. The transmitter also has a TM4C123G microcontroller unit as its DPU. The transmitter packetizes the data payload and transmits it through one of the General Purpose Input Output (GPIO) pin present in the microcontroller. The transmitter can also receive external input through touch screen display (BOOSTXL-K350QVG-S1) or push buttons present on the microcontroller board. Both the transmitter and receiver is provided power supply through rechargeable Li ion batteries to reduce noise and comply with the wearable form factor. The data rate of transmission achievable in the prototype *BodyWire* system is 8 Kbps.

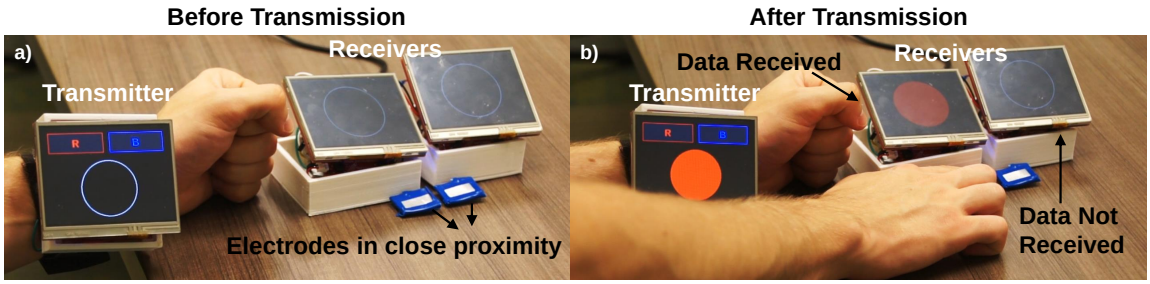


Fig. 5.10. Selective information transmission from a transmitter to a receiver: a) Two receivers kept in close proximity to each other, b) Data transmitted to the receiver, whose electrode is touched by the user. The adjacent receiver does not receive the signal.

## 5.6 Applications

We show three example demonstrations of the *BodyWire* system and illustrate how it can be used for strictly touch based communication. The first application demonstrates the selectivity and the strict touch requirement of communication through HBC, where the data intended for a particular receiver is not picked up by an adjacent receiver in close proximity. The second application shows transfer of information from a wrist watch to a computer through the touch of an electrode, highlighting the convenience aspect. Demonstration 3 shows secure authentication through touch by unlocking a computer when a person wearing the appropriate key touches an electrode connected to the computer. This illustrates the security aspect of HBC.

### 5.6.1 Selectivity: Data Transmission with multiple receivers

Selectivity is one of the key advantages of signal confinement within the body, achieved by *BodyWire*. The selectivity aspect of *BodyWire* is the focus of this current demonstration. In this scenario there are two receivers, which are kept in close proximity to each other. The transmitter transmits a code corresponding to the color chosen by the user on the touchscreen display. The data only gets transmitted to the

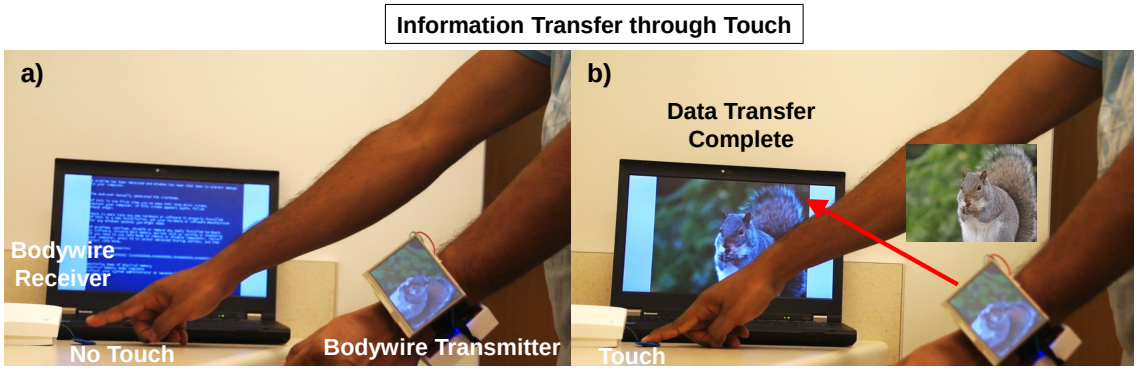


Fig. 5.11. Information transmission from a wearable device to a computer through touch. a) user about to touch the electrode , b) information transfer during touch of electrode resulting in image displayed in the computer.

receiver whose electrode is touched by the user (fig. 5.10). Although the electrode of the other receiver is in close proximity, it does not receive the signal (fig. 5.10 (b)), showing selectivity provided by the *BodyWire* prototype. The signal confinement property of EQS-HBC makes selective information transmission possible, as shown through this demonstration. This selectivity property can be utilized for applications requiring precise location tracking and localization.

### 5.6.2 Data Transfer: Wearable to Computer Data Transfer

In this demonstration we utilize the *BodyWire* framework to transfer information from a wearable device such as a smart watch to a computer (fig. 5.11). A *BodyWire* receiver is connected to the computer, which uses serial USB to communicate with the receiving computer. When the user touches the electrode connected with the receiver, it forms a communication channel between the devices. The code corresponding to the image being displayed in the wearable gets transferred to the *BodyWire* receiver through EQS-HBC, which is subsequently transferred to the receiving computer through USB serial communication. The receiving computer displays the

image corresponding to the code it receives on its display. This demonstration shows information exchange between a wearable transmitter and a computer. This can be extended to image transmission also but that requires higher data rates than 8kbps supported through the *BodyWire* prototype. The receiver device in this demonstration is implemented as a separate device connected to the computer through USB for the ease of implementation. However, it can always be integrated within the computer as a separate module with only the electrode acting as the external interface. This example illustrates the possible usage of *BodyWire* framework for entertainment purposes. Transferring data from one device to another just through touch provides a very natural and intuitive way of information exchange and enhances user convenience significantly. This demonstration can also be utilized for other usage scenarios such as downloading map information from computer to a smart-watch or using a body worn wearable as an intermediate device for data transfer between two computers.

### 5.6.3 Secure Authentication: Unlocking Computers

This demonstration of the *BodyWire* system shows the unlocking of a computer screen with the touch of an electrode connected to a HBC receiver, as seen in fig. 5.12 (a)-(d). The computer unlocks only when the user with the correct key touches the electrode connected to the computer, through the HBC receiver. It can also be seen from our experiments that the computer does not unlock when the fingertip of the user is very close ($<$ 1cm) to the receiver electrode but not touching it. This shows that there is very little signal leakage out of the body, demonstrating the additional physical layer security provided by EQS-HBC compared to radio communication. Hence, utilizing EQS-HBC is advantageous for applications like secure authentication as shown here. This demonstration can also be seen as part of a two factor authentication system, where the unique key of the transmitter acts as a substitute to password. For two factor authentication systems the user has to use both his/her biometric identification (like fingerprint) and a passcode for authentication.

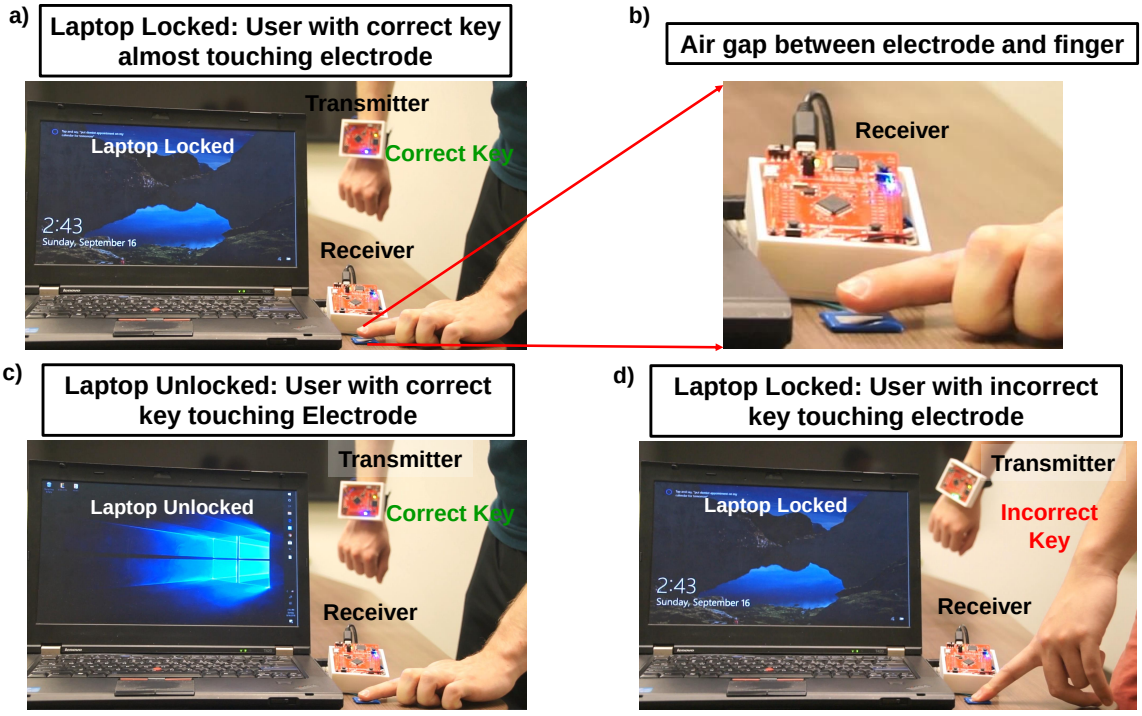


Fig. 5.12. Demonstration showing secure authentication of a computer through the key transmitted by a body worn device. a) The computer is locked and does not get unlocked even when the user with correct key is in close proximity to the electrode, b) Zoomed in diagram showing air gap between the finger and electrode, c) Computer gets unlocked when the user with the correct key is touching the electrode, d) Computer does not unlock when the user with the incorrect key touches the electrode.

This requires two separate steps of scanning fingerprint and entering the passcode. However, by doing communication through touch it is possible to perform two factor authentication through fingerprint matching and also authenticating through the key sent by the transmitter. This enhances the convenience of such applications by reducing the number of steps performed by the user. Through EQS-HBC, it is possible to utilize the human body as a physical communication channel, where the signal is primarily confined within the channel itself and there is minimal radiation out of the body. This enables additional physical layer security which can be utilized to create

secure channels during pairing of devices, such as a streaming device and a TV. Traditionally, in wireless protocols such as Bluetooth, such pairing process begins by key exchange over non-secure air medium, making them vulnerable to malicious attacks. This demonstration shows the possibility of key exchange through EQS-HBC, which can be utilized for establishing secure channels for wireless communication.

## 5.7 Conclusion

Touch acts a natural way of interaction between a human and computing resources present in the environment. Coupling communication with touch will enhance its effect significantly opening up new interaction modalities in human computer interaction. In this chapter we demonstrate *BodyWire*, which uses EQS-HBC to minimize signal leakage out of the body and hence enable communication strictly during touch previously not achievable through wireless radio wave communication or other HBC based systems. The low frequency operation of EQS-HBC helps it reduce signal leakage out of the body significantly, enabling communication strictly through touch. Design techniques, such as capacitive termination and voltage mode transmission / reception has been used to minimize loss through the human body at low frequencies to enable EQS-HBC. The system has been designed to tolerate variation of signal strength due to posture variation of the user and interferences present at low frequencies. The *BodyWire* system has been used to show data (payment, image, medical data) transmission selectively and strictly during touch events and demonstrate applications such as transfer of an image from a wearable to computer, secure authentication (doors, pairing a smart device) of a computer through a body worn key. As computers increasingly become part of our environment, systems coupling communication and touch will provide new modalities to interact with them. *BodyWire* provides such a platform for communication strictly during touch. We hope this will stimulate future research on new human computer interaction modalities which benefits from the coupling of communication and touch.

# 6. PHYSICALLY SECURE WEARABLE-WEARABLE INTER-BODY HUMAN BODY COMMUNICATION

Most of the materials in this chapter have been extracted verbatim from the paper: S. Maity et al. "Physically Secure Wearable-Wearable Inter-Body Human Body Communication" submitted to UbiComp 2019.

## 6.1 Introduction

Improvements in solid-state circuit design over the last several decades have enabled the widespread proliferation of wearable devices and personal computing resources to a diverse number of users. Many daily functions such as financial transactions, SMS, health monitoring, telecommunication have either been off-loaded to these devices or assessed as necessary features to carry everywhere. Because of this phenomenon, technology and interfaces that supports the usability and interactions between these wearable devices continue to become more important from both a security as well as a usability perspective. Electronic communication between these devices is an essential feature for the functionality of these phones, smartwatches etc., whether that comes in the form of secure key exchange between two devices or SMS data/notification from a mobile phone to a smartwatch. Traditionally, these devices utilize Bluetooth to form this communication channel. In this paper, we present an alternative communication using BodyWire, a single-wire communication technique that enables secure covert communication between wearable devices surrounding the body. BodyWire uses Electro-Quasistatic Human Body Communication (EQS-HBC) accompanied with several critical design techniques that enable biological and environmental independent operation for mobile wearables. EQS-HBC enables communication through the conductive properties of the human body and uses the

body as a wire while limiting the physical signal leakage out of the body by operating at the Electro-Quasistatic (lower frequency) regime. Firstly, this enhances the security of ubiquitous wearables by eliminating the access of the physical signal from a nearby malicious attacker. This may seem like small concern with software encryption; but, researchers have demonstrated the hacking of critical life-saving medical devices through these encrypted radio networks. Secondly, it enables communication initiated through touch alone, eliminating the complicated setup process completely. Considering the growing number of ubiquitous devices surrounding the human body, this is an important aspect of keeping high accessibility and usability for a diverse group of users. BodyWire creates an intuitive interface of touch that every human is familiar with and can use. Simple touch is now augmented with the ability of electronic data transfer through a small form factor device that can be adorned on the human body to another worn device or any number of machines/terminals that we interact with today.

In this paper we explore the different environmental and human factors that affect the communication between two wearable devices during communication through HBC. The transmitter and the receiver device has been designed following techniques such as capacitive excitation into the body, high impedance capacitive termination at the receiver and voltage mode operation to enable its operation through EQS-HBC. Experiments are carried out on multiple subjects over two months to assess the effect of different factors on the overall channel loss and ensure repeatable measurement results. We identify the key factors such as the surrounding environment and human body postures that affect the channel loss and determine it under varying conditions to quantify the effect of those individual factors. We also identify the amount of signal leakage out of the body at different distances and identify the range of distances over which channel loss measurements can potentially be affected by the signal leakage.

The rest of the paper is organized as follows: Section 2 provides a background of the HBC technology and compare the EQS-HBC implementation of this paper with previous implementations. Section 3 discusses the key design techniques that en-

**Comparison of BodyWire with State-of-the-art HBC Implementations**

| | Communication between a wearable and earth ground connected device | Communication between two wearable devices | | **Small device:** (4.5cm x 5cm) | **Physically Secure:** Signal contained <1cm from body surface and <25cm from device |
|---|---|---|---|---|---|
| | | Intra-body | **Inter-body** | | |
| Challenge | | Variation in received signal due to environment, posture variation | **Higher Loss** | Small Ground → Low Return Path Capacitance → Higher Loss → Lower SNR | Signals radiated out of Body in previous implementation; e.g. in [53] carrier frequency is 8 MHz which shows higher leakage |
| Comparison with Previous Literature | [46],[48],[57],[51],[47],[56],[54],[55],[52] | [53] | **This work*** | **This work*** | **This work* (EQS-HBC) 415 KHz lower leakage** |

*This work shows the first Inter-body capable, Physically Secure wearable-wearable HBC, with a small form-factor device that is easier to wear

Fig. 6.1. Comparison of Bodywire Implementation with state-of-the-art HBC demonstrations. The key challenges associated with small factor inter-body HBC demonstration is also highlighted.

ables EQS-HBC. Section 4 discusses the key experimental constraints that need to be maintained to ensure repeatability and correctness of the experiments. Section 5 talks about the different experiments that are carried out to characterize the channel loss and quantify the effects of different factors on the overall channel loss. Section 6 provides a demonstration of information exchange between devices worn by two persons and we conclude in Section 7.

## 6.2 Human Body Communication: Background

BodyWire uses Human Body Communication (HBC), also commonly known as Body Channel Communication (BCC) as the underlying communication method between the devices. HBC has been a field of active research over the last two decades since it was proposed by Zimmerman [1] in 1994 for Personal Area Networks (PAN). It was proposed to capacitively couple pico-amps current into the body to communicate between devices around it. Since then, there has been multiple aspects of HBC that has been explored, namely the channel characteristics of the human body, integrated circuit design specific for HBC, complete system design demonstrating information

exchange between devices. In this section we provide a brief overview of HBC on these different aspects and identify the key limitations present in modern day HBC, highlight the possible solutions to alleviate those and enable the demonstration of information exchange between appropriately ground isolated wearable devices.

One of the critical element in any HBC system is the channel characteristics provided by the human body. However, measuring the body channel characteristics without affecting it requires careful experiment design with sufficient isolation between the ground of the measurement instruments and the measured devices. As a result, there is a wide variation in the measured channel response available in literature [4, 5, 7–10, 12]. Some of the measurements show low channel loss ( 20dB) due to improper ground isolation [9, 13], as a result of which the wearable device gets a larger ground than a practical wearable device. HBC systems, which are designed based on these measurements, will not have the sufficient sensitivity to function in an actual scenario where the channel loss is significantly higher. A separate group of measurements [4, 5, 7] show the channel loss to be significantly high (>90 dB) at low frequencies (<10MHz), showing that frequencies ¿10MHz is the optimum frequency for designing HBC systems. However, this limits these systems in terms of security and selectivity, as there is significant signal leakage out of the body. We will discuss in detail about the signal leakage aspects in detail in the later sections. However, this shows the importance of proper channel characterization for the design of an HBC system. We have characterized the human body channel with proper ground isolation and termination at the receiver end to establish it as a broadband channel and utilize the measurements to design the BodyWire prototype. We discuss about the measurement setup and the corresponding results in detail in the following sections.

There has also been multiple studies for designing integrated circuits specific for HBC applications [33], [34], [36], [27], [37]. The relatively lower loss of the broadband human body channel makes it possible to design energy efficient circuits compared to traditional wireless circuits such as Bluetooth. However, the focus of this paper is on Commercial off-the-shelf (COTS) component based system design for demonstration

of HBC. There has been multiple studies for the system level demonstration of HBC. The demonstrations primarily show communication between a wearable and an earth ground connected device. Moreover, these demonstrations suffer from the problem of signal leakage out of the devices even when the person is not in direct physical contact with it. This makes the interactions not selective and the data transmission prone to attacks from an unintended recipient. One of the earliest commercial implementation of HBC is through Microchip Technology's BodyCom system [46]. They show the unlocking of car or home door using a wearable transmitter device. The devices communicate even with the transmitter in the user's pocket showing no strict requirement of direct contact with the body for communication. [32] shows the use of a ring as an intermediate data transfer device for information exchange between two computers. There are demonstrations shown in [47] where an image gets transferred from a mobile transmitter to a wall connected device. However, from the demonstrations we can clearly see information getting transferred between the devices even when the user is far away from the receiver and only holding the transmitter device. [48] shows transfer of colour information from a wrist watch to the clothing of another person when the persons come in contact with each other. The authors of [52] show the example of a game where the users communicate with floor tiles with a wearable watch like device. The devices can communicate even when the user is wearing a footwear showing communication without direct physical contact with the devices and the potential for signal leakage. As a follow-up work [53], the authors provide SNR measurements for different intra-body and inter-body scenarios for communication between wearable devices and provide guidelines for design of groundless BCC systems. As a demonstration, the authors show an application of music streaming through BCC headphones, operating at a carrier frequency of 8MHz, which can again potentially suffer from signal leakage out of the body. The authors in [51] re-purpose the finger print sensors of commodity devices such as smartphones for sending signals through the body for authentication purposes at a data rate of 100s of bits per second.There are other implementations, such as TAP [54], Earthlings

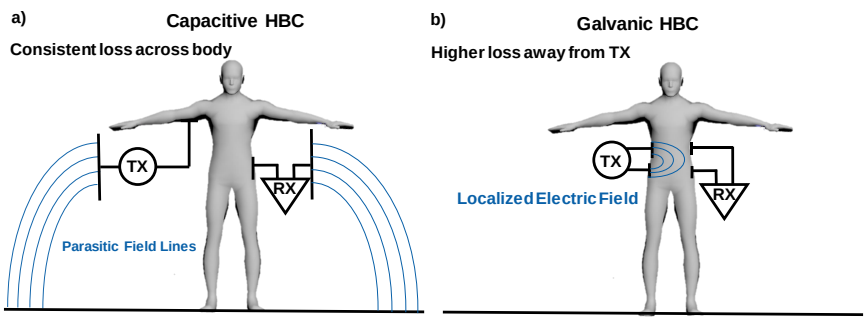


Fig. 6.2. Human body communication using a) capacitive coupling mode versus b) galvanic coupling mode. Capacitive coupling HBC is advantageous for wearable devices as the loss is consistent across the entire body.

Attack! [55], Wearable Key [56], CarpetLAN [57], which uses human as the communication medium for interaction between devices. Through BodyWire, we show the first implementation of physically secure inter-human information transfer, utilizing channel loss results obtained from thorough characterization of the effect of different factors. The associated challenges and comparison with state-of-the-art is shown in figure 6.1.

On a broader sense HBC can be classified as one of those human computer interaction techniques which enables interaction between devices through touch using electrical signal transmission through the body. There are multiple studies which identifies either single/ multiple touches on a screen such as Field mice [58], Smartskin [59], Diamond Touch [60], Swiss-cheese extended [61], Opencapsense [62], DGTS [63], Tile Track [64]. BodyWire enables communication between devices only when they are in direct touch contact with the body but does not provide the capability to find the location of the touch. Skintrack [65] , Aurasense [66], High5 [67], Living Wall [68], iSphere [69] enables gesture recognition using interaction between electric field and the human body.

## 6.3 Electro-Quasistatic Human Body Communication (EQS-HBC)

The fundamental idea behind EQS-HBC is to work a frequency low enough to be in the electro-quasistatic region. In case of a electromagnetic transmission the electric and magnetic fields are related to each other through the Maxwell's equations 6.1, 6.2 6.3 6.4).

$$\nabla \cdot \mathbf{E} = \frac{\rho}{\varepsilon_0} \tag{6.1}$$

$$\nabla \cdot \mathbf{B} = 0 \tag{6.2}$$

$$\nabla \times \mathbf{E} = -\frac{\partial \mathbf{B}}{\partial t} \tag{6.3}$$

$$\nabla \times \mathbf{B} = \mu_0 \mathbf{J} + \mu_0 \varepsilon_0 \frac{\partial \mathbf{E}}{\partial t} \tag{6.4}$$

In case of electro-quasistatic or magneto-static scenario one of the time deravite becomes negligible. Hence in a electro-quasistatic scenario equation 6.3 gets modified to

$$\nabla \times \mathbf{E} = 0 \tag{6.5}$$

Similarly for magneto-quasistatic scenario equation 6.4 is updated to

$$\nabla \times \mathbf{B} = \mu_0 \mathbf{J} \tag{6.6}$$

Operating in the electro-quasistatic regime in HBC enables the signal to be primarily confined within a short distance from the body and have minimal leakage out of the body. Traditional wireless communication like Bluetooth results in the signal being radiated isotropically in all directions and hence lack the security aspect (figure 6.3). However, EQS-HBC enables the secure transmission of information between devices by minimizing the signal leakage out of the body .

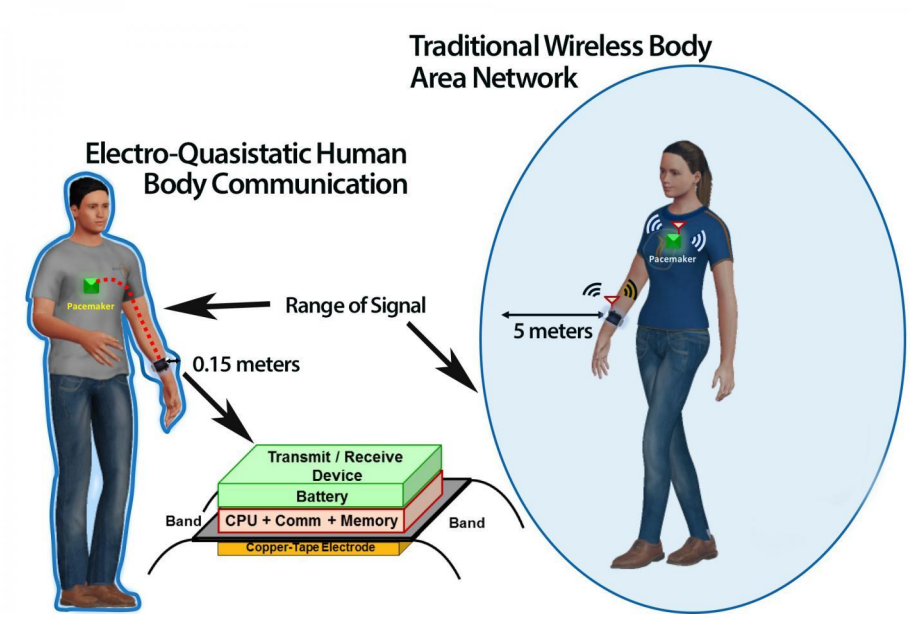


Fig. 6.3. EQS-HBC vs. WBAN: An Overview of the Data Privacy Space. In case of EQS-HBC the signal is primarily confined within a small distance of the body. Whereas in WBAN the signal can be snooped at distances up to 5 meters, providing significantly lower security and privacy.

## 6.4 Key Design Techniques

### 6.4.1 Capacitive vs Galvanic Coupling

The theory of operation behind capacitive coupling [1] (figure 6.2a) HBC can be understood by the use of traditionally parasitic capacitances as the return path for what would otherwise be a traditional wireline channel. On the other hand, galvanic coupling [2] (figure 6.2b) of signal to the body involves applying a differential excitation where the signal path is localized in the human.

There are two key reasons for choosing capacitive coupling for a fully wearable application over galvanic coupling. Firstly, capacitive coupling introduces much less current in the body, and hence makes it more attractive from a safety perspective, as the current is heavily limited by the return path capacitances. The more important

reason, is that since the communication utilizes capacitance between the the devices to ground and this capacitance (few pF) has significantly higher impedance than the rest of the closed loop path, most of the signal loss occurs across this parasitic capacitance. Hence, the received signal strength across different parts of the body is almost equal. In later sections we carry out experiments to highlight this particular benefit of capacitive coupling.

### 6.4.2 High Impedance Termination

Proper termination at the receiver end is another key factor in determining the overall channel loss between the transmitter and receiver devices. A simple circuit theoretic analysis of the HBC channel model shows that the overall channel loss will reduce if a high impedance termination is used at the receiver end. Similarly, a capacitive termination at the receiver end will reduce the low frequency channel loss and make the channel loss almost independent of frequency. A detailed theoretical analysis and experimental results of the channel loss based on a bio-physical model can be found in [70]. The HBC receiver circuit needs to be designed taking the constraint of high impedance capacitive termination into account to enable low loss low frequency operation.

### 6.4.3 Electro-Quasistatic Human Body Communication

The high impedance capacitive termination at the receiver end reduces the human body channel loss at low frequencies and extends the frequency range of its operation. This opens up a new frequency band of operation in the sub-MHz range, which was previously deemed unusable due to the high channel loss reported in previous literature. We utilize this low frequency band to enable Electro-Quasistatic Human Body Communication (EQS-HBC) and use it for our demonstrations. In EQS-HBC, the wavelength of the transmitted signals are significantly larger than the size of the human body, as a result of which the signal is constant across the body. This also helps

reduce the leakage out of the body significantly as the signal leakage is proportional to the frequency of the transmitted signal [71]. The low leakage helps in characterizing the human body channel with minimal effect from inter-device coupling, which can provide optimistic channel loss measurements. It also enhances the security of the HBC devices as the signal is confined within a small distance around the body and reduces the probability of an unintended attacker snooping the signal.

### 6.4.4 Voltage Mode Operation

In the design of the BodyWire system we send the signals between the transmitter and the receiver as voltage instead of power which is traditionally used in other systems [53]. Using voltage for information transfer benefits from the high impedance capacitive termination at the receiver as it maximizes the amount of voltage at the receiver end. Maximizing the power at the receiver requires different design constraints for optimization compared to voltage mode operation, which makes the design of the current receiver different compared to earlier HBC implementations. From a circuit design perspective maximization of power transfer requires the impedance at the receiver end to be low. However, since the body channel itself has a high impedance,a low impedance at the receiver end results in a lower received power. Hence, voltage mode circuit design is beneficial for the operation of wearable-wearable HBC systems, where the received signal is low due to ground isolation.

## 6.5 Experimental Measurement Control Variables

As described previously, wearable to wearable Human Body Communication is challenging to design due to the variations in channel loss due to the nature of capacitive mode HBC systems. However, if the capacitive termination voltage mode technique is utilized properly, these variations can be measured and quantified into manageable design constraints for any wearable Human Body Communication system. This section will explain the custom experimental setups (figure 6.4) and control

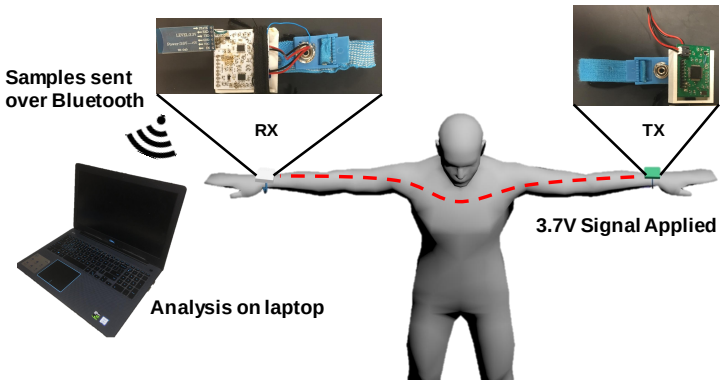


Fig. 6.4. Experimental setup for wearable to wearable channel loss measurements. The transmitted signal is received and sampled using an ADC, which is sent over Bluetooth to a laptop for analysis and channel loss calculations. This ensures that the measurements are not perturbed by a strongly ground connected device, which results in optimistic channel loss results.

variables required to carry out these measurements. We consider five main design factors when attempting to design repeatable and controlled wearable to wearable HBC experiments. These include 1) Proper earth ground isolation 2) Device size 3) Signal leakage 4) Device-to-Body Ground Isolation 5) Environment induced variations.

### 6.5.1 Earth Ground Isolation

The most important control factor for wearable-wearable HBC is proper ground isolation on both the transmitter and receiver devices. As actual wearable systems will have ground isolation from earth ground, the measurement equipment must also have complete ground isolation. Therefore, the use of any measurement device requiring a building power supply would result in inaccurate measurements as one would be boosting the signal strength by introducing a much more convenient return path between the devices through the measurement equipment. To achieve proper ground isolation, a custom printed circuit board in wearable form factor including a microcontroller with 12-bit ADC, embedded Bluetooth module, and signal conditioning analog

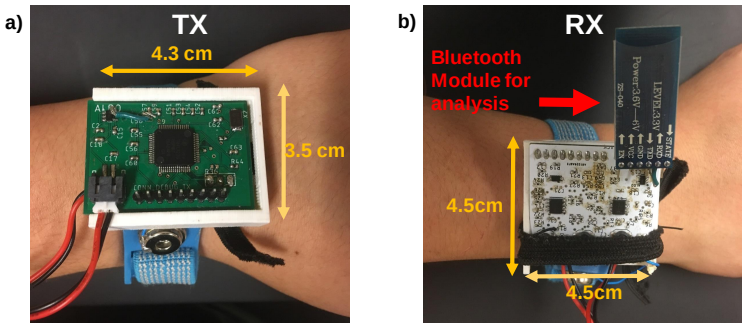


Fig. 6.5. Image of the measurement setup boards with dimensions a) The TX board features a form factor of 43 by 35 cm, the RX board features a form factor of 45 by 45 cm with a Bluetooth module that transmits the sampled ADC values for analysis.

front end was fabricated. This enables the experimental data to be accumulated in a wearable form factor, and transmitted wirelessly to a laptop for post-processing. The Bluetooth module transmits the sampled received Human Body Communication signal to a computer serially and the channel loss is calculated taking the account of the gains and losses introduced by the measurement setup,as shown in figure 6.4. This process eliminates any earth ground from affecting the channel loss numbers. A 3.7V transmit signal is coupled onto the body through a printed circuit board at 415 KHz and measured at a high impedance termination receiver that has the same analog signal front-end as the final demonstration shown through the handshake example.

### 6.5.2 Device Size and Packaging

The size of the transceiver and receiver printed circuit boards with their wearable packaging is 4x4 cm and is coupled to the body through a 2x3 cm electrode which is secured by a wearable band as shown in figure 6.5. The device size must be strictly controlled in order for the experiments to be repeatable. This phenomenon can be explained using the theory of operation for capacitive voltage mode HBC. Increasing the size of the device gives the return path capacitance a larger value and hence reduces the loss in the channel. A dangling component or a longer connecting wire

can result in a change in the return path capacitance and hence change the measurement result. So it is important to ensure that the device is packaged identically (no loose components, minimal size wire for connection) between different measurement sessions across multiple days. Similarly the environment around the device is also an important factor in determining the return path capacitance in a capacitive HBC scenario. Hence, it is necessary to keep the environment around the person identical for measurements corresponding to the same experiment across multiple days and subjects. This not only ensures repeatability of results but also enables us to quantify the effect of each factor on the overall channel loss.

### 6.5.3 Signal Leakage

Leakage from circuit components can affect HBC channel measurement results through two primary methods. The first is improper shielding of the signal being applied to the body. Electrical wires between the body and the device that are not properly shielded will act as a source of leakage for the HBC signal and hence would result in inaccurate loss measurements that are optimistic for packaged wearables. It is obvious that this effect is not an important factor for some applications, but in order to achieve the security and low leakage of EQS-HBC, this is an important consideration. The second method is improper packaging of the battery. Allowing the battery to be exposed, enables ground coupling between the TX and RX which gives lower channel loss. Hence, proper wire shielding and battery packaging are required to set up fundamental HBC measurements, so that the measured channel loss is not affected too much by the signal leakage. Moreover, this also reduces the security aspect of HBC systems as the signal can be snooped by an attacker at distances far away from the body.

### 6.5.4 Device Ground To Body Isolation

It is necessary to ensure appropriate isolation between device ground and human body to ensure capacitive excitation of signals into the body. If there is direct connection between the device ground plane and the skin or close proximity of the ground plane to the body (<2-3mm), it will effectively result in galvanic operation as the excitation/termination will be differential. There will be a local loop formed through the body between the signal and ground terminal of the device, where most of the signal will be localized. This effect is observed to be much larger with the battery specifically, since it forms part the ground plane. Improper device-to-body ground isolation would shunt signal away from the intended receiver either on a different user or the other side of the body. Effectively, the wearable devices' signal and ground planes are being electrically shorted through a small coupling formed between the TX device ground and the body. This isolation must be present in order for fully wearable HBC to be functional. Hence, it is important to package the device ensuring that no part of the ground plane is directly touching the body. This is a key constraint in the design of any wearable capacitive HBC device.

### 6.5.5 Environmental Control

The environment around the body also has an important role in determining the overall channel loss, since the return path capacitance between the transmitter and the receiver is dependent on the coupling of the devices with the environment. As already mentioned, the return path capacitance plays an important role in determining the overall loss between the transmitter and receiver. As part of the characterization process we carry out measurements in different environments such as in an office, lab, outdoors. It is essential to ensure that the environment remain the same among different set of measurements carried out across multiple days and on multiple subjects. This requires careful design of the experiments to ensure repeatability of the setup.

## 6.6 Intra-body Channel Characterizations

This section will explore the various experiments performed in order to identify the different factors that affect channel loss in a wearable-wearable HBC scenario and help us realize the fully wearable HBC communication device. Following are the different sets of experiments that are carried out for wearable-wearable HBC characterization: 1) Channel Loss on Multiple Users 2) Inter-device coupling 3) Intra-body Posture and Environmental Dependency 4) Channel Loss across Various Body Locations 5) Electro-Quasistatic Leakage Measurements. To ensure proper ground isolation and true wearable to wearable measurements the signal received at the receiver end is sampled through an ADC and transmitted over Bluetooth to a computer for further analysis and loss characterization as shown in figure 6.4.

### 6.6.1 Channel Loss on Multiple Users

The channel loss study for multiple users is necessary to ensure a design that is robust to biological variations between users. The theory of operation for wearable-wearable HBC device is inspired from the biophysical circuit model presented from [70]. The parameters of the body is characterized in order to ensure that wearable-wearable HBC is possible to realize. The variation in channel loss across users are important to ascertain the range of signals (dynamic range) that is expected at the input of the receiver device. The dynamic range plays an important role in determining the design complexity of the receiver front-end circuit. Subjects are measured for channel loss at different times of day over a period of two months. This experiment covers subjects that have different physical parameters (age, height, weight, sex, etc.) and provides a sample of channel loss that designers of fully wearable HBC systems must anticipate. These measurements can be used to develop a signal conditioning front end that enables reliable communication through this technology. Channel loss for multiple users is measured in a laboratory environment. Other known factors that affect the return path such as posture, environmental coupling, and device package

positions are kept strictly controlled and in order to provide an accurate understanding of the isolated effect of different user parameters on this devices' channel loss. The results of the channel loss across multiple subjects is plotted in figure 6.6a. Channel loss for the fully wearable HBC system falls within a range of 69dB to 75 dB. These numbers present a worst case number for most applications given the minimal ground size of the devices used to carry out the experiments in this paper.

### 6.6.2 Inter-device coupling

Inter-device coupling describes the interaction in which the ground planes of the transmitter and receiver devices are coupled. This enables the return path of communication to be between the coupling of the device rather than the ambient parasitic environment. This coupling dominates the return path and thus the channel loss at close distances.

The inter-device coupling is measured by bringing the transmitter device very close to the receiver without any direct contact and measuring the received signal. This is repeated over multiple distances up to 25 cm, beyond which the received signal falls below the receivers' sensitivity. The measurement results shown in figure 6.6b show that the inter-device coupling loss can be lower than the channel loss through the body for distances up to 10cm. This shows that intra-body channel loss measurements for channel lengths less than 10cm can be heavily affected by the inter-device coupling rather than the actual body channel loss. Hence, any measurements characterizing body channel loss should be carried out for channel lengths $> 10$ cm.

### 6.6.3 Intra-body Posture and Environmental Dependency

Practical implementations of wearable HBC devices require the communication through the body to be functional irrespective of environment and posture variations. So the devices need to be designed to be able to tolerate the variation introduced by user posture and surrounding environmental effects. Posture varies channel loss pri-

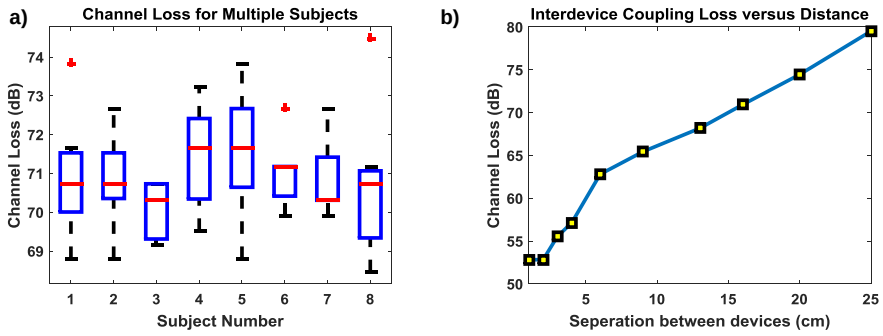


Fig. 6.6. a) Box and whisker plots of channel loss for eight users over two months. The range of loss falls between 68 to 75 dB b) inter-device coupling measurements without the body shows that under 10cm the communication happens mostly between the two devices.

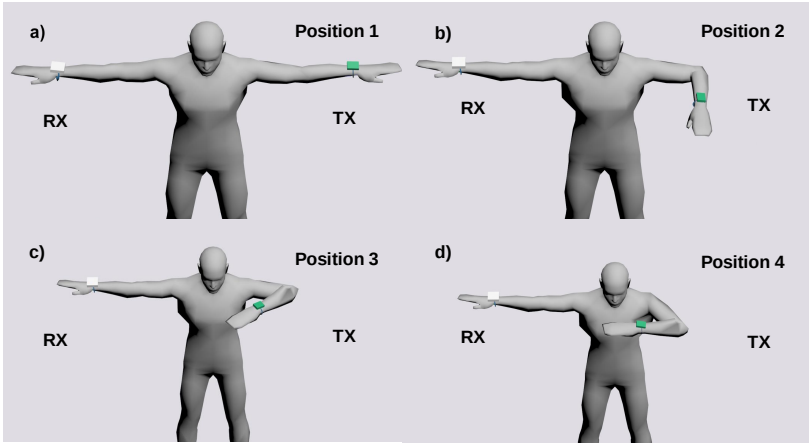


Fig. 6.7. Sample human model illustrating human arm postures: a) RX position 1 and TX position 1, b) RX position 1 and TX position 2, c) RX position 1 and TX position 3, d) RX position 1 and TX position 4.

marily from the geometric positioning of the device ground plane with respect to earth ground, which varies the capacitance in the return path similar to size of the device and battery positioning. Similarly, having many physical objects in the environment can introduce additional signal or ground planes depending on user contact or proximity. These objects can potentially affect the path of transmission which in turn changes the loss introduced by the capacitive voltage division between the

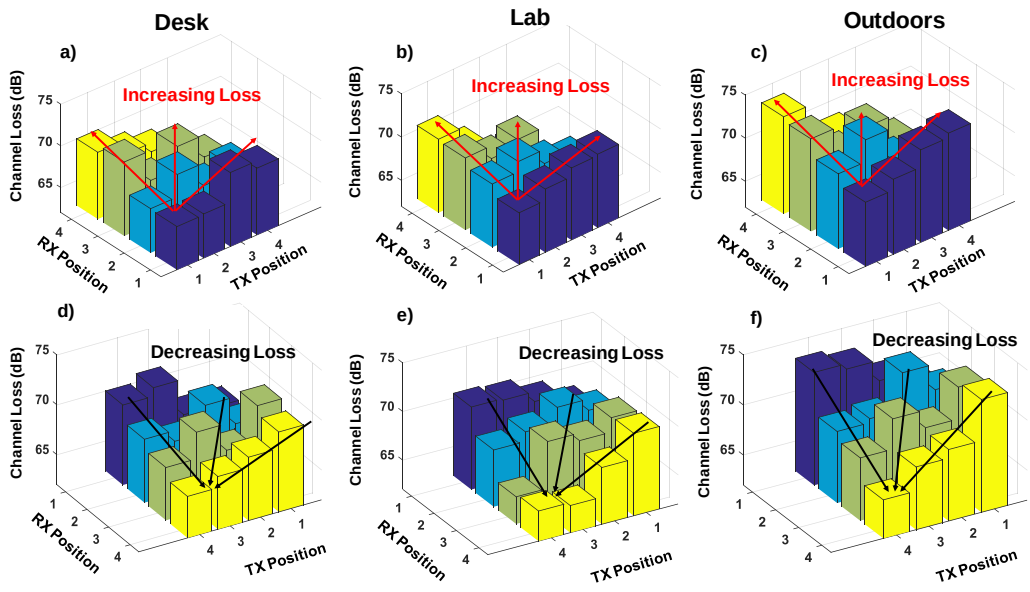


Fig. 6.8. Channel loss vs TX and RX posture: a) in desk environment front view, b) in lab environment front view, c) in outdoors environment front view, d) in lab environment back view, e) in lab environment back view, f) in outdoors environment back view. The plotted data is an average of collected measurements on two subjects over ten measurements sessions across two months.

capacitance of the body and that of the environmental surroundings. For example, if the experiments for channel loss were performed with both the receiver and transmitter over a large table, the capacitance formed between the devices' return path is varied as the return path is now both through the table, when otherwise the field lines would have terminated to the floor. However, the behavior of this coupling is very difficult to predict in theory due to the slight changes in conductivity and positioning between every environment and posture. Like the multi-user channel loss setup, the goal for these series of measurements is to determine if a dynamic range problem exists for the signal conditioning front-end. The reason the design of the experiments for environmental and posture studies were coupled is due to the close nature of their respective effects on the channel loss as a phenomenon of physical device placement and geometry. Also, the experimental setup was designed to ensure that they stay

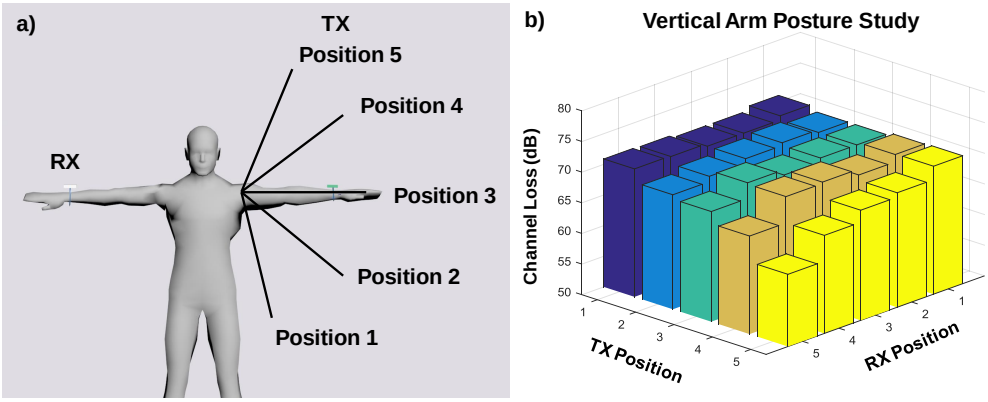


Fig. 6.9. a) Human figure demonstrating vertical arm positions 1-5 b) Channel loss versus position of TX and RX arm. Channel loss is agnostic to vertical position of arms with the exception of the lower loss due to inter-device coupling in: 5-5, 4-5, 5-4.

consistent across multiple days and users for repeatable measurements and proper attribution of the effect of different factors on the channel loss.

### Posture Results

The user posture experiments are carried out with the transmitter and receiver devices fixed onto the subject's wrists. From this point, two separate characterizations are performed, one where the users arm moves horizontally, the other where the user arms move vertically with respect to the body. Figure 6.7 and figure 6.9 gives an overview of the positions of the users arm during the horizontal and the vertical experiments respectively. These measurements provide interesting insight as to the postures and fundamental effects that varies channel loss. For control, all posture and environmental studies are completed on the same subjects over similar times of day. There are two main driving forces that affect channel loss for the horizontal posture: 1) Shunt capacitance as a result of body coupling 2) Inter-device coupling. As observed in any of the posture plots in figure 6.8a,b,c , the loss is driven up as the devices move inwards closer to the core of the body (position moves from 1 to

3). This is due to the effect of coupling between the central/lower parts of the body surfacing. This capacitance shunts signal away from the receiver to the ground plane. Since the subject is standing on the floor, the body capacitance inevitably shunts some signal away from the receiver thus increasing loss. As the arm moves closer to the center/core of the body, the channel loss increases. The trend described above is dominant over the trend of channel loss until the devices are close together (approx. $<$ 10cm). At which point, the ground plane coupling of the transmitter and receiver device forms the dominant physical phenomenon in determining loss. The inter-device coupling, can be observed in the figure 6.8d,e,f where as we move to the 4-4 position the loss is less. In the 4-4 position, the device is touching the main part of the body, effectively short circuiting the shunt capacitance of the body, enabling the body to become the signal plane. It can be observed that 3-3 position, which maintains both devices close to the center body but not touching, shows high loss as signal is being shunted to the body and cannot be measured by the receiver. Furthermore, in figure 6.8d,e,f, it can be seen that as the device moves closer (4-4 to 4-1 or 1-4 to 4-4) the channel loss decreases - illustrating the effect of inter-device coupling. Despite all the variations due to the two phenomenon, the channel loss introduced by the posture is still tolerable for a system, showing a maximum variation of 6 to 7dB, suggesting that no significant dynamic range problem arises from variation in posture. The vertical posture study result shown in figure 6.9b shows the inter-device coupling effect in the 5-5,5-4, and 4-5 positions. Outside of the inter-device coupling all other postures show consistent average measurement result, giving the insight that vertical posture is not a factor that affects channel loss.

**Environmental Dependency Results**

The posture experiments are carried out in three different settings - a controlled lab environment, a desk setup, and an open outdoor area. The desk represents the best case scenario for channel loss measurements as the return path has the assistance

of nearby chair and table. The user is sitting in a chair and the devices are over a table. The outdoor measurements represent a worst case scenario, where there are no objects for the devices to couple within tens of meters. Hence, the return path capacitance will be minimum increasing the channel loss. The motivation is to investigate the signal coupling differences between the devices in a sample of different environments and understand channel loss within these different environments. As can be seen in figure 6.8, as the environment changes from a desk to a laboratory, the channel loss goes up across the board. This result is in line with theoretical expectations, since as the number of objects increase around the user, the distance to a terminating common ground is reduced. Once again, these ambient objects increase the return path capacitance and thus reduce the loss in the channel. Finally, the outdoor measurements give a worst-case scenario sample. Despite the variations observed in figure 6.8 the average channel loss between the best and worst case samples only vary by 1.8dB, from 67.8dB to 69.6dB channel loss. This result confirms that environmental coupling has minimal effect on channel loss measurements and hence does not cause a significant dynamic range issue for the device designer. In order to characterize the distance up to which objects will be effectively coupling and affecting the channel loss, an experiment targeted at measuring channel loss from a single isolated source of coupling is executed as shown in figure 6.10a. The channel loss for a user is measured in a nominal posture at predefined distances away from a large coupling object. The averaged channel loss results are presented in figure 6.10b. It can be seen that coupling effect has approximately a 4dB effect on the channel loss up to around 50cm. Beyond 50cm, the large coupling object pose little to no effect to the wearable to wearable communication. This shows that for enclosed indoor environments, the objects around the users can have a reducing effect on the channel loss. Outdoor environments provides a worst case scenario in terms of channel loss. However, this experiment again shows that the dynamic range is 4dB for the indoor channel loss, not posing too strict a constraint on the receiver design.

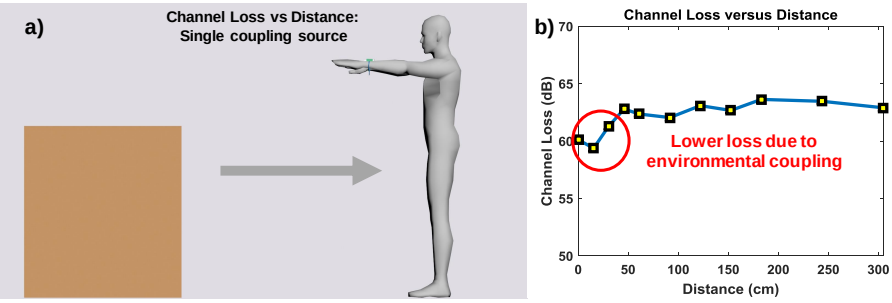


Fig. 6.10. a) Experiment setup for experiment illustrating the effect of environment on channel loss b) After a distance of 50cm, the effect of the environment is not observable on the subject.

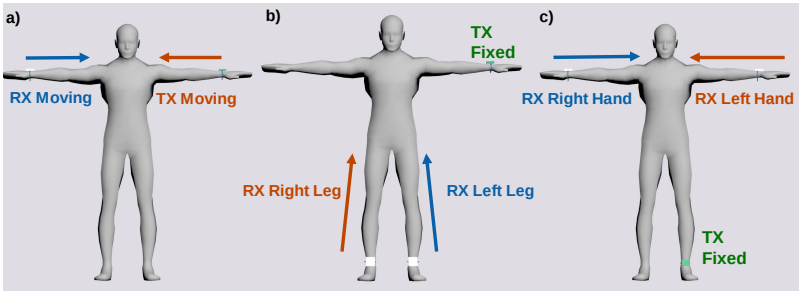


Fig. 6.11. Illustration of experiments performed to verify equal signal strength on the entire body: a) TX and RX devices affixed to the arm and measured along arm b)TX fixed to the left arm and measured along the legs c) TX fixed the the left leg and characterized along the arms.

### 6.6.4 Channel Loss across various body locations

As described in the overview of HBC, capacitive voltage HBC systems give uniform channel loss across all parts of the body. This effect is contrary to the results galvanic approach, in which the signal is localized between the transmitter and receiver. Galvanic coupling suffer for transmission across long lengths within the body, which degrades the usability of this technology significantly as you would only be able to transmit very short distances on the body. BodyWire implements capacitive mode HBC which opens up this technology to many more applications.

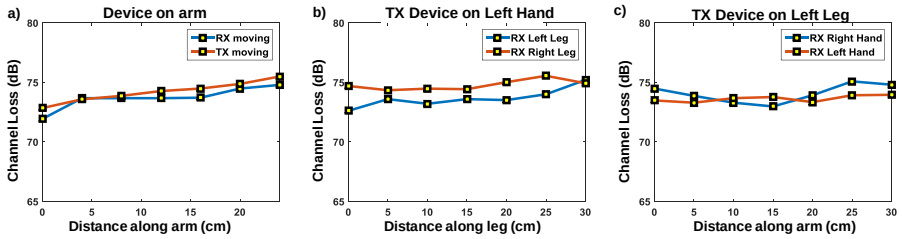


Fig. 6.12. Results of experiments performed to verify equal signal strength on the entire body: a) A small 3dB variation can be observed due to the devices moving towards the torso b) loss is higher in general for the opposite leg but only around 3dB c) loss is similar for both arms showing no difference in channel loss.

This set of measurements is carried out to provide a characterization of the performance of capacitive voltage mode HBC along different paths across the body. In one set of experiments the transmitter device is moved across the arm keeping the receiver fixed on the other arm and vice versa (figure 6.11a). For the second experiment the transmitter is kept fixed on the left arm while the receiver is moved across both legs as shown in figure 6.11b. The final experiment keeps the transmitter fixed on the left leg, and characterizes the loss along both arms 6.11c. Channel loss is characterized in each of these six scenarios and the variation between transmissions across different parts of the body is characterized as shown in figure 6.12. The results from the experiments show that the channel loss remains within a range of 3 dB across various channel lengths. This illustrates the advantage of constant loss across the body provided by capacitive HBC.

### 6.6.5 Electro-Quasistatic Leakage Measurements

Currently, wireless technologies like Bluetooth uses radio waves, which results in electromagnetic radiation up to several meters in every direction and result in the signal getting intercepted. BodyWire implements the technique of Electro-Quasistatic Human Body Communication, which aims to confine the communication signal near

and within the body [71]. This technique prevents a potential malicious attacker from intercepting sensitive communications from far away and gives body area networks an additional layer of physical security.

Hence, an important characterization of any on-body communication between two wearable devices lie in determining the extent to which the signal is available away from the body.These experiment setups are depicted in figure 6.13. For both set of experiments, a human with a transmitter transmits a test signal through their body. This signal represents the sensitive information that the user could potentially be protecting. The signal is received either using a dipole antenna or using the human body as an antenna. Furthermore, for both experiments, the leakage is measured for both a "line-of-sight" leakage as well as a "body obstructed" leakage. Line-of-sight leakage describes a transmitter device with a direct coupling path to the measurement setup. Body obstructed constitutes the other scenario, where the device is on the opposite side of the body. In other words, the body obstructed measurements represents a device facing away from the attacker. In the first experiment depicted by figure 6.13a, a second subject is connected to the measurement setup, utilizing the person as the antenna, and the leakage is measured as a function of distance. This result is plotted in figure 6.14a, which shows the SNR vs distance of the leakage signal that is available to the second subject. The second experiment is illustrated in figure 6.13b has the same setup as the first, with the exception of the removal of the second subject and only having the antenna sense the received signal and the measured SNR at different distances are shown in figure 6.14b. The SNR for both experiments is measured relative to the noise floor of the receiver device, which is the spectrum analyzer in this case.

From the results in figure 6.13 it can be seen that the leakage between the devices without the presence of a human is significantly lower compared to the case when the second person is used as the antenna to receive the signal. This shows that the signal leakage is more as the coupling between the two person is more than the coupling between a person and the standalone antenna at the receiver end. Another

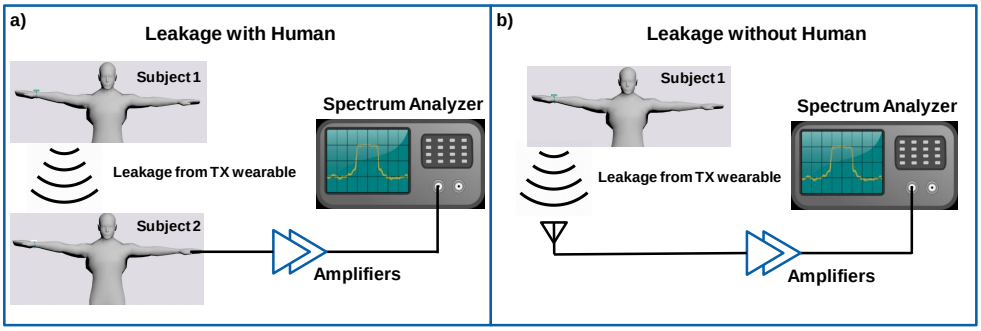


Fig. 6.13. Measurement setup for leakage experiments a) with human b) without human. The extra human introduces an increased coupling between the devices which increases the leakage as compared to the non-human measurement setup. The device leakage is characterized from a minimum distance of 30cm.

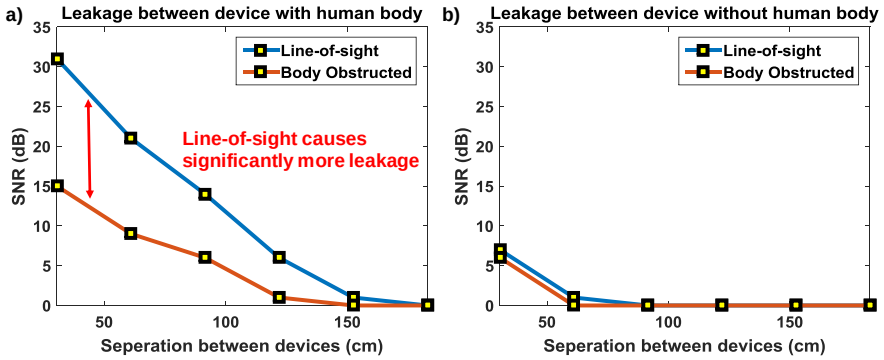


Fig. 6.14. Leakage measurements between two HBC devices a) with the presence of the human bodies and b) without the presence of human bodies. SNR is measured between the leakage signal and that of the spectrum analyzer noise floor. Line-of-sight leakage results in higher leakage compared to an obstructed device.

important takeaway is that body-obstructed leakage has even lower SNR giving some directional protection from malicious attackers. Moreover, it's important to note that these measurements were performed with a spectrum analyzer using a 1kHz resolution bandwidth - which should be a good approximation for the fundamental limitation of what an attacker can detect. The noise floor of the spectrum analyzer is about -140dBm, which acts as the sensitivity limit at the receiver end.

## 6.7 Wearable Wearable HBC Demonstration

Human body communication can enable many convenient new interactions between devices and humans. For example, secure authentication benefits greatly by being able to covertly transmit information through the body to a lock or secured device. Touch activated communication systems would no longer require separate hardware or software overhead to incorporate a touch sensor, as the touch and communication are both integrated into the interaction. Information exchange between two wearable devices (smartwatches, smartbands) or a wearable device and a computer are examples of possible use cases of HBC. To show this technology in practice, we implemented a simple demonstration to illustrate the elegance and potential of BodyWire to benefit current human computer interaction applications. To the best of the authors knowledge, this demonstration shows the smallest form factor and lowest frequency groundless state-of-the-art HBC system.

One of the interesting use case of HBC is inter-body information exchange between two users during a touch event, such as a handshake. BodyWire shows a demo of two users using a groundless HBC system. The channel loss in a inter-body scenario is slightly higher than the intra-body case. The user with the transmitter device is able to toggle the color they want to send through the touch screen. The transmitter packetizes the sixteen bit code corresponding to the color displayed on the screen and sends it through the human body using HBC. The receiver's signal conditioning front-end processes the noise and interferences for the digital processing unit. Next, the receiver decodes the compressed data in software to display the corresponding color on the display. The details of the demonstration is shown in figure 6.15. Figure 6.15a) shows information is not transmitted between the devices when the persons are not in direct contact, showing signal confinement very close to the body. When the two persons handshake the green color information gets transmitted to the receiver as shown in figure 6.15b). The transmitted color is changed (figure 6.15c) and the subsequent color is received at the receiver end (figure 6.15d).

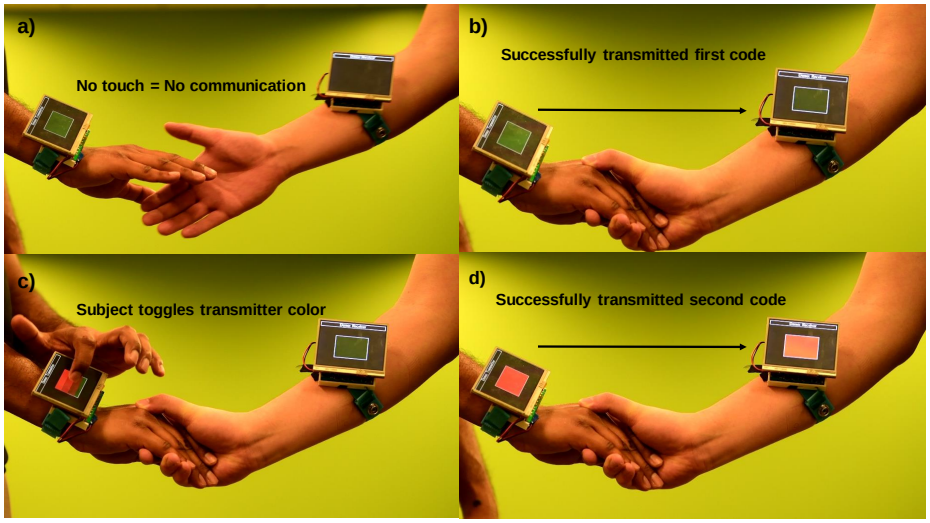


Fig. 6.15. Demonstration of inter-human information exchange through BodyWire prototype. a)No communication without physical touch illustrating signal confinement very close to the body b) Successfully transmitted initial color information from one to the other c) Subject toggles to different color information to transmit d) Second successful transmission of color information.

### 6.7.1 Hardware Implementation Details

The HBC transceiver is fabricated on a custom two-layer printed circuit board with a size of 4.5 x 5 cm. The transceiver includes an analog front end, which preconditions the signal by filtering and amplifying the signal for detection by a digital processing unit. The design techniques such as capacitive excitation, high impedance capacitive termination at the receiver end described in previous sections are used in the design of the receiver. The digital processing of the signal from the analog front-end is done using a TI TM4C123GH6PM microcontroller; BodyWire utilizes analog comparators in the microcontroller for interfacing with the analog hardware and detecting the bits. At the transmitter end, we use the same microcontroller to digitally synthesize the transmitted signal and couple it to the body directly.

## 6.8 Conclusion

In this chapter we introduce BodyWire, which demonstrates communication between two wearable devices through Electro-Quasistatic Human Body Communication. We carry out experiments to characterize the channel loss across different human subjects,environments, postures and locations on the body. We discuss about the different factors such as ground isolation, device size, packaging etc. that can potentially affect the experimental results and provide suggestions about taking these factors into account while designing experiments to ensure repeatable measurements. The measurement results show that the channel loss variation across subjects, different postures and environment is about 15dB, providing a design constraint for receiver design. The results also show that the channel loss reduces by 3-4 dB in presence of a big object around the body, such as an office desk. This shows that the loss in a office/lab environment will be slightly better than an outdoor environment, which can be explained from the higher return path capacitance due to the parasitic coupling of the device ground with the environment. The almost constant channel loss for measurements across different locations of the body also shows the advantage of capacitive coupling over galvanic coupling. These characterizations were taken into account to design a prototype device demonstrating information exchange between two person during handshake, showing the smallest form factor wearable-wearable HBC information exchange according to the authors' best knowledge.

# 7. ON THE SAFETY OF HUMAN BODY COMMUNICATION

Most of the materials in this chapter have been extracted verbatim from the paper: S. Maity et al. "On the Safety of Human Body Communication" to be submitted to IEEE Transactions on BioMedical Engineering

## 7.1 Safety Limits of Human Body Communication

There are multiple standards specifying the safety limits on the exposure of human body to electric/magnetic fields. We look into the safety limits provided by three primary safety standards in this section.

### 7.1.1 International Commission on Non-Ionizing Radiation Protection (ICNIRP) Standard

In HBC systems, the impact of signal transmission through human body and its safety limits must be carefully addressed. The International Commission on Non-Ionizing Radiation Protection (ICNIRP) [72] provides the exposure limit of Non Ionizing Radiation for humans. Depending on the frequency of the field, different physical quantities are used to set the restriction of exposure. For frequencies in 1Hz-10MHz range, *current density* provides the restriction to prevent effects on central nervous system. In the 100MHz-10GHz range restrictions are provided on *Specific energy Absorption Rate (SAR)* to prevent heat stress on the body. Between the 10GHz-300GHz frequency range, power density is restricted to prevent heating in body tissue or near the skin surface. The limits on these restrictions are shown in graphical form in Fig. 7.2. As can be seen from the plots, the most stringent requirement on *current den-*

*sity* is in the 4Hz-1KHz frequency range due to the low threshold current required for nerve stimulation at this frequency range. In addition to the whole body SAR requirement of 0.08W/Kg , the restriction of localized SAR in head and trunk is 2W/Kg and limbs are 4W/Kg. Apart from these, reference level for time varying contact current, when the human body comes in contact with an object of different electrical potential, are provided in order to avoid shock and burn hazards. For frequency of <2.5 KHz the maximum contact current is 0.5mA, whereas for 2.5-100KHz the limit is 0.2f (f= frequency in KHz) and for >100KHz the limit is 20mA. In later sections we carry out circuit simulations and FEM based simulations to investigate the compliance of different type of HBC to the safe exposure limits specified in this standard.

### 7.1.2 Institute of Electrical and Electronics Engineers (IEEE) Standard

The IEEE standard also provides guidelines for Basic Restrictions (BR) and Maximum Possible Exposure (MPE) limits of the human body to time varying electric, magnetic fields and contact currents in the 3kHz to 300 GHz frequency range. Separate restriction limits are provided for sinusoidal and pulsed electric fields and contact currents, as well as for fields and signals with multiple frequency components. Most of this limits show close correspondence to the ICNIRP guidelines discussed in the previous subsection. The standard also looks into multiple previous studies which has explored different cancer and non-cancer related effects of these radiations. It looks into studies which takes care of the established thermal effects of RF frequencies above 100 kHz and electrostimulation effect below 100 kHz. A review of non-cancer studies about the effect of these fields on thermoregulation, neurochemistry, neuropathology teratogenicity, reproduction, development, auditory pathology, membrane biochemistry is provided with most of them showing minimal or no effects. Cancer related studies on DNA damage, cell cycle elongation, cell toxicity, gene and protein expression and activity also does not show any clear or consistent role of RF radiation on

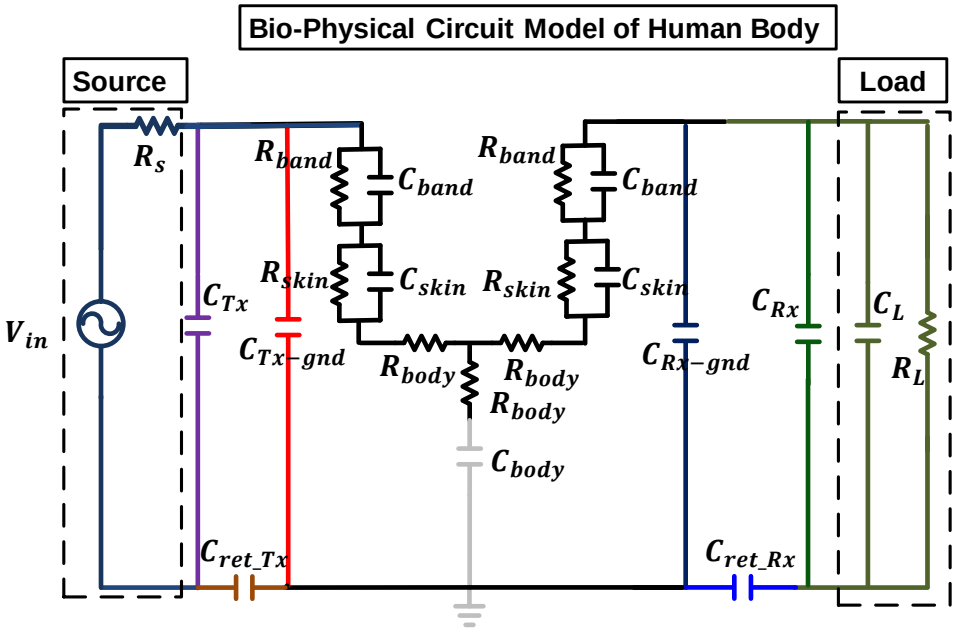


Fig. 7.1. Detailed Bio-physical model of HBC [29] showing the different biological parameters and load conditions. The different parameters are as follows: $R_s$: Source Resistance, $C_{Tx}$: Transmitter ground to body capacitance, $C_{Tx-gnd}$: Capacitance between body and ground at the transmitter end, $C_{ret\_Tx}$: Return path capacitance of the transmitter, $R_{band}$: Resistance of the coupling electrode, $C_{band}$: Capacitance of the coupling electrode, $R_{skin}$: Skin resistance, $C_{skin}$: Skin capacitance, $R_{body}$: Tissue resistance, $C_{body}$: Capacitance between feet and ground, $C_{Rx-gnd}$: Capacitance between body and ground at the receiver end, $C_{ret\_Rx}$: Return path capacitance of the receiver, $C_{Rx}$: Receiver ground to body capacitance, $C_L$: Load capacitance, $R_L$: Load resistance.

human cancer. It also provides recommendations such as usage of bi-phasic signal to avoid harmful electro-chemical action on the electrode, skin interface.

### 7.1.3 The National Institute for Occupational Safety and Health (NIOSH) Standard

While the previous two standards primarily looks into the effect of current density and field intensities of lower values on the human body, the NIOSH standards looks into the effect of high voltage and current on the human body. Electric current chooses the path of least resistance within the body, and dissipates heat during the passage, which can cause thermal damage to tissue along the path of current. The skin provides the highest resistance to flow of current. Skin resistance, when dry, is about 300 times greater than the resistance of internal organs. This high resistance of skin is lowered in several ways: by cuts and abrasions, by immersion in water, by breakdown of outer layer of skin by high voltages $> 600$ Volts, thereby allowing large amount of current to pass and cause greater damage. The tissues that sustain highest damage from electrical injury are nerve, muscle, bone and skin. Nerves sustain direct damage from the passage of electricity, with proprioceptive nerves being the most susceptible. The passage of current can also overstimulate the nervous system, and cause varying degrees of damage to internal organs.

The physiological effect of electric injury is determined by the magnitude of the current passing through the human body. The estimated effects that 60 Hz AC currents passing through the chest can cause are tabulated below:

Higher voltage generally causes greater acute injury to the human body, however, the reverse can be true as well. High-voltage ($\sim$103 Volts) arcing can often throw the victim off by blast effect, thereby limiting contact and hence extent of injury; whereas a much lower voltage 60-Hz AC current can cause an involuntary muscle contraction with protracted gripping, prolonging contact and leading to far more severe injury.The outcome of electrical injuries, whatever the mode of causation, is heavily dependent

| Current (60 Hz) | Physical Effect |
|---|---|
| 1mA | Barely Perceptible |
| 16 mA | Maximum current an average man can grasp and let go |
| 20 mA | Paralysis of respiratory muscles |
| 100 mA | Ventricular fibrillation threshold |
| 2 A | Cardiac standstill and internal organ damage |

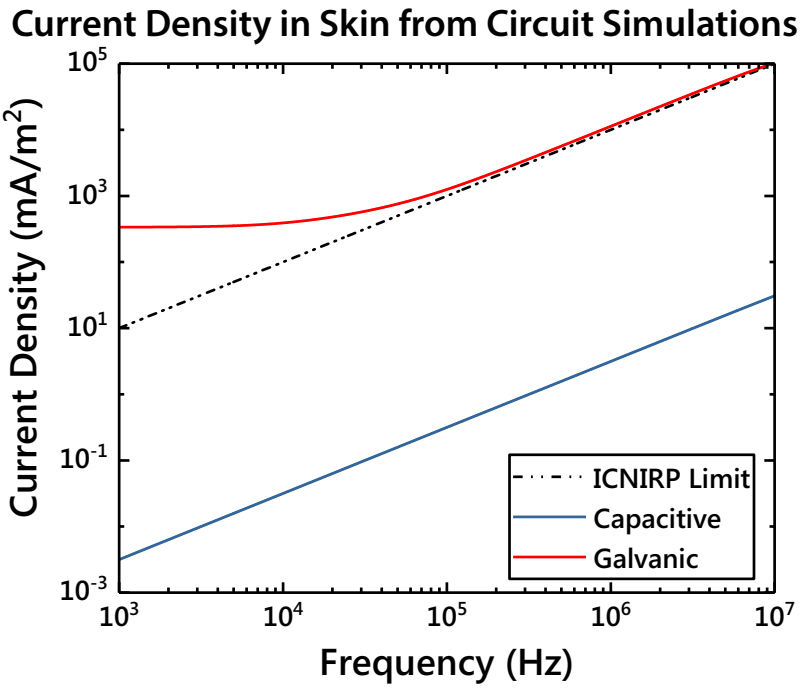


Fig. 7.2. Current density in the skin adjacent to the device, calculated from circuit model.

on the speed of initiation of initial resuscitative measures.

In the subsequent sections we will carry out circuit and FEM based simulations to compare the induced current and field densities with the safety limit established by the standards discussed in this section.

## 7.2 Theoretical Safety Analysis

We carry out theoretical studies through circuit and FEM modeling and simulations to analyze the safety compliance of HBC in terms of current and field constraints respectively. This section looks into the setup for both these analysis and provide a quantitative measure of safety.

### 7.2.1 Bio-Physical Model of HBC

We use an experimentally validated Bio-Physical model [29] of the human body to find a reasonable estimate of the current and field densities within the body and analyze the safety aspect. The model consists of different human body biological parameters along with the different parasitic capacitance for Capacitive HBC. The load conditions are also included in the circuit models, although they do not play a critical role in determining the current density or field intensity within the body, The details of the Bio-Physical model along with the component values in a tabular form can be found in [29] and is provided in Fig. 7.1. In this paper we use a relatively simplified version of the complete Bio-Physical model, consisting of the components required to explain the field distribution and current density within the body.

### 7.2.2 Current Density Limits: Circuit Simulation

Theoretical simulations are carried out for both Capacitive and Galvanic HBC to find the current density within the body resulting from voltage excitation provided to the skin. A Bio-Physical model [29] of the human body is used for simulation purposes. An AC analysis of the circuit provides us with the current being injected into the body across different frequencies. This is then compared with the safety limit provided by the guidelines.

As seen from the detailed Bio-Physical model in Fig. 7.1 and the simplified versions in Fig. 7.3c,f, the return path in capacitive HBC is closed by the parasitic

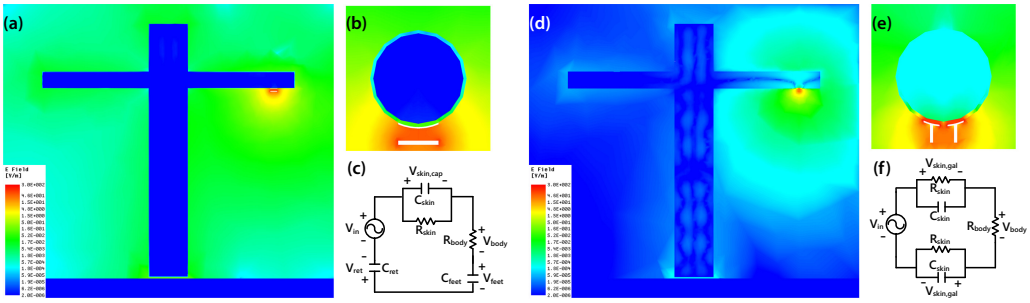


Fig. 7.3. **Capacitive HBC:** Electric field distribution along (a) a cross-section plane of the dummy model of Fig. 7.4 and (b) a cross-section of the arm and the device as shown in Fig. 7.4b, (c) simplified channel model. **Galvanic HBC:** Electric field distributions (d) across the body and (e) near the device, (f) simplified channel model. All simulations for these field distributions were carried out at 400 kHz, for a 1 V p-p sinusoidal excitation voltage.

capacitances between the ground plane of the transmitter, receiver devices and the surrounding environment. The impedance of this parasitic capacitance is the primary limitation in the amount of current flowing through the body for capacitive HBC. The value of this capacitance is in the order of a few picofarads, Hence, the impedance provided by the return path is few MΩ for frequencies less than the MHz range. This limits the current to a few $\mu$amps for capacitive HBC, The maximum current density will be close to the electrodes used for excitation. Taking a cross sectional area equal to the size of the electrode (4 $cm^2$) close to it, the current density is plotted across different frequency, as shown in Fig. 7.2, for an excitation voltage of 1V. It can be seen that the current density is orders of magnitude smaller than the safety limits suggested by the ICNIRP guidelines for the general public. This shows that capacitive HBC complies with the safety limit.

In case of Galvanic HBC, the signal is applied differentially between two electrodes, both connected to the body. Hence there is a closed loop formed between the signal and ground terminal ( Fig. 7.3f) , through the body. The skin provides the impedance between the signal and the ground electrode and is in the order of few tens of KΩ. Hence, the amount of current injected into the body is significantly

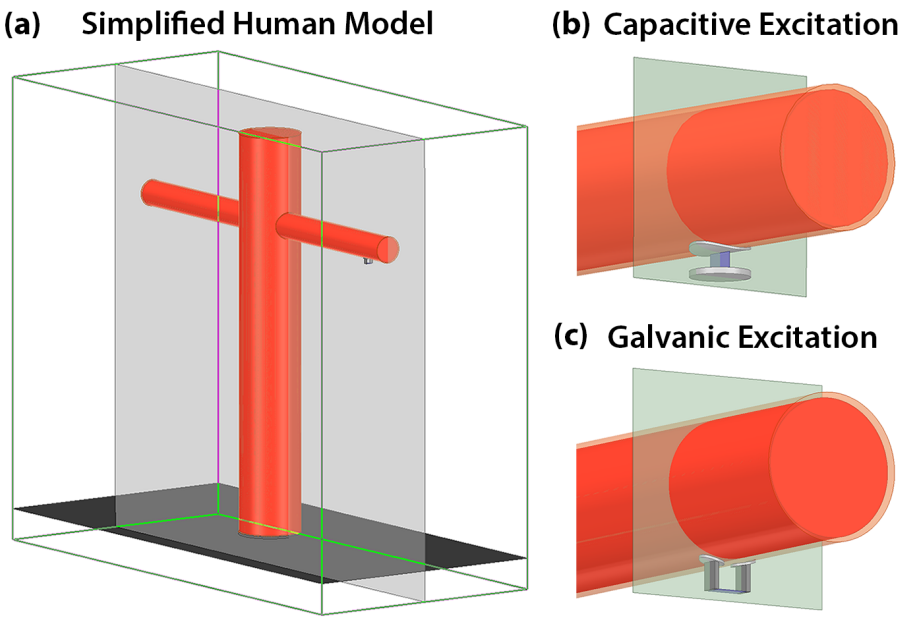


Fig. 7.4. (a) Dummy human model consisting of two crossed cylinders with muscle interior and 4mm thick skin shell. The cross-section plane shown is used for E field plots in Fig. 7.3a and Fig. 7.3d. (b) Excitation structure for capacitive HBC. A potential difference is maintained between a copper disc of 2 cm radius attached to skin and a floating copper ground plate. The cross-section plane is for E field plot in Fig. 7.3b. (c) Excitation structure for galvanic HBC. A potential difference is maintained between two copper discs of 1 cm radius, placed 2 cm apart on the skin. The cross-section plane is for E field plot in Fig. 7.3e.

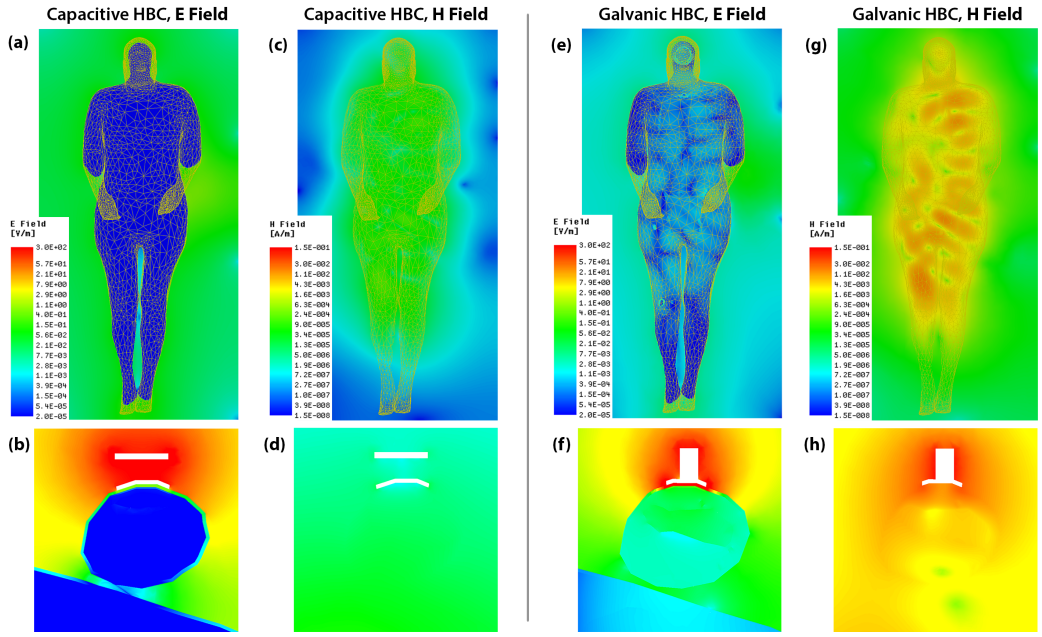


Fig. 7.5. Field plots along different cross section planes of the detailed human model shown in Fig. 7.6 at 400 kHz, 1 V p-p sinusoidal excitation voltage. **Capacitive HBC:** (a) E field across the body, (b) E field near the device, (c) H field across the body, and (d) H field near the device. **Galvanic HBC:** (e) E field across the body, (f) E field near the device, (g) H field across the body, and (h) H field near the device.

higher compared to capacitive HBC. As shown in Fig. 7.3e, most of the current is primarily contained within the surface of the skin. Hence, the cross sectional area of the current transmission is taken considering the thickness of the skin (4mm maximum). The plot of current density is shown in Fig.7.2, for an excitation voltage of 1V applied through excitation at the wrist with a distance of 2cm between the electrodes. This shows that applying signals to the wrist, as done in several previous studies, can result in localized current densities, which is significantly higher than the recommended general public safety limit, at the skin close to the signal electrode. To ensure safety compliance in case of galvanic HBC, a *current limiting circuit* can be used at the output of HBC devices to ensure that the current injected into the body is within the recommended safety limits for general public exposure.

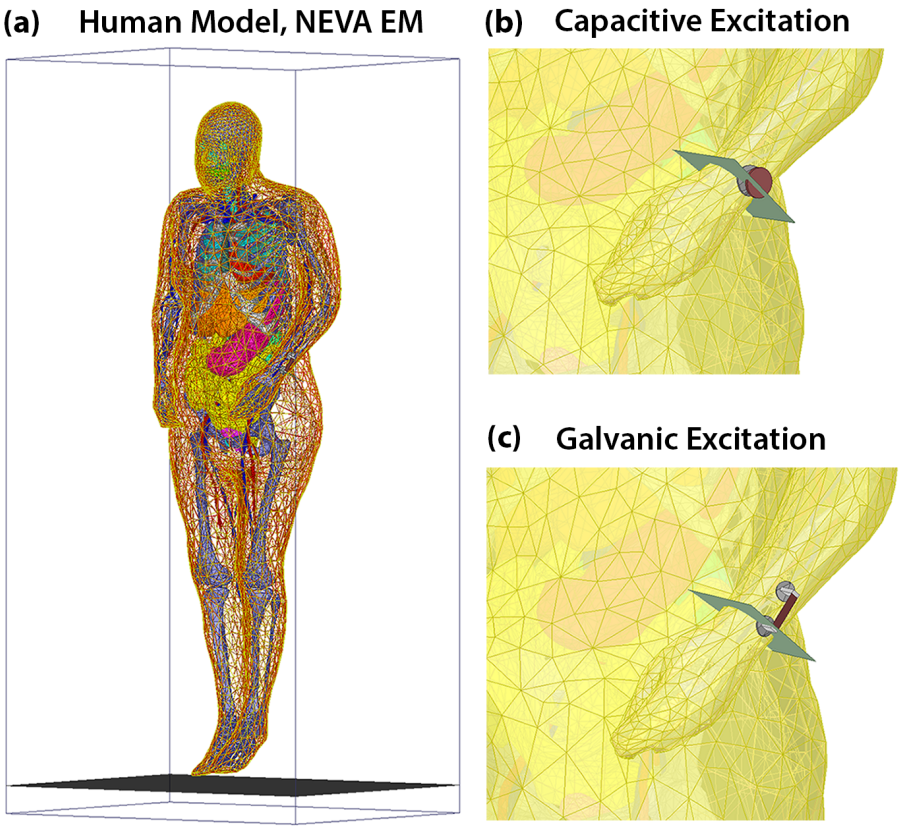


Fig. 7.6. (a) Detailed human model for FEM simulations: VHP-Female v2.2 from NEVA Electromagnetics LLC, with cross-section plane for E and H field plots of Fig. 7.5a, 7.5c, 7.5e and 7.5g. (b) excitation method for capacitive HBC and cross section plane for obtaining field plots of Fig. 7.5b and 7.5d, and (c) excitation method for galvanic HBC and cross section plane for obtaining field plots of Fig. 7.5f and 7.5h.

### 7.2.3 Field Limits: FEM Simulations

To understand the E and H field distributions in and around the human body for both capacitive and galvanic HBC, simulations were performed in Ansys HFSS, which is an FEM based EM solver. First, simulations are carried out using a simplified model consisting of two crossed cylinders as shown in Fig. 7.4 to develop an idea of the expected field distributions for both Capacitive and Galvanic HBC. The dielectric properties of this model is assigned as that of an average human muscle, and it is given a 4mm thick skin shell. Dielectric and conductive properties of human body tissues found by Gabriel et. al. [73] is used for all EM simulations in this section. The simplified model enables us to explain the field distribution intuitively from the voltage drop obtained through circuit models and provide a connection between the field and circuit simulations; this will later be backed by detailed full-body simulations derived from the model shown in Fig. 7.6. For capacitive HBC, the excitation is provided by a single disc shaped conductor attached to the skin, and an alternating potential difference is maintained between this and another disc shaped plate hanging in the air that is supposed to serve as the ground plate of the device (Fig. 7.4b). As shown in the simplified circuit representation of this modality in Fig. 7.3c, derived from Fig. 7.1, the signal return path from the subjects body to the device ground plate is formed via parasitic capacitance to earths ground. The impedance of this capacitance is high compared to the resistance provided by human muscle, and the potential drop inside the subjects body should be negligible. This in turn implies that the electric field inside the body should be low, which is confirmed from the E Field plots from the simulation (Fig. 7.3a and Fig.7.3b). For Galvanic HBC, the excitation is provided by two disc shaped conductors placed 2 cm apart on the skin (Fig. 7.4c), and an alternating potential difference is maintained between the two. This results into a high potential difference at the skin over a short distance, resulting into a high local electric field inside the subjects body, especially at the skin (Fig. 7.3e). For both capacitive and galvanic styles of excitation, a voltage source is used

in HFSS. A voltage source is preferred over a lumped port style excitation, because the results from a lumped port has possibilities of getting affected by port impedance and reflections at the excitation point depending on the model design, whereas a voltage source in HFSS basically represents an ideal voltage source, maintaining an alternating potential difference of 1V between the points of excitation, no mater what the design is. This provides us with a more fundamental platform to study field and current patterns in HBC.

This basic simulation setup is now carried over to a detailed model of human body, to find out values of E and H fields that different body parts would experience for a certain HBC operating voltage. The human body model used for all the simulations was obtained from NEVA Electromagnetics LLC. The specific model used is the VHP-Female v2.2, which was generated from a 162 cm tall, 60 year old female subject [**?**]. The HFSS simulation setup used is shown in Fig. 7.6. Similar to the simulations of the cylindrical dummy, the excitations were provided by a single disc and a floating ground plate in Capacitive HBC (Fig. 7.6b), and two spaced disc in case of galvanic HBC (Fig. 7.6c). As mentioned before, the dielectric properties of the body tissues were adapted from the works of Gabriel et al. [73]; we did not use the material properties that came packaged with the HFSS version of the NEVA EM model, as the HFSS model did not incorporate tissue properties for frequencies less than 10 MHz. The field plots resulting from simulations of the detailed model are shown in Fig. 7.5 suggest the same key points noted in the simulations of the dummy, i.e. lower fields inside the body for capacitive HBC compared to galvanic, and high local fields near the device, notably in the skin, for galvanic HBC. Simulations were performed for multiple frequencies in the 100 kHz$-$1 GHz range, and maximum RMS E and H field values were recorded at the skin patch below the device, as well as a few vital organs such as brain, heart and the spinal cord. The comparison of these values with the ICNIRP limit for general public exposure is shown in Fig. 7.7 and Fig. 7.8. It is evident that for 1V excitation, the fields at brain, heart or spinal cord remain well below the ICNIRP threshold for both capacitive and galvanic HBC. Additionally

for capacitive HBC, the fields at the skin adjacent to the HBC device are below the safety limit as well, whereas these local fields ride above the threshold for galvanic HBC with fixed potential and without any current limiting circuit at the output of the transmitter. This indicates the need for current limiting circuits at the output of HBC transmitters to ensure compliance of current density and field limits under all usage scenarios.

### 7.2.4 Field Estimation from Circuit Model

The Bio-Physical circuit models of Capacitive (Fig. 7.3c) and Galvanic HBC (Fig. 7.3f) provides an intuitive explanation to the expected electric field and explains which mode of operation creates higher fields. As seen from the EM simulations the field density is highest near the skin where the signal is injected. The voltage drop across the skin determines the electric field density ($E = \frac{V}{d}$). From the Bio-Physical model of capacitive HBC (Fig. 7.3 ) the voltage drop across skin and the field density can be obtained as in equation (7.1) and (7.3) respectively.

$$V_{skin,cap} = \frac{V_{in} * \frac{1}{sC_{skin}}}{Z_{skin} + \frac{1}{sC_{ret}} + \frac{1}{sC_{feet}} + R_{body}} \tag{7.1}$$

$$Z_{skin} = R_{skin} \parallel \frac{1}{sC_{skin}} \tag{7.2}$$

$$E_{skin,cap} = \frac{V_{skin,cap}}{t_{skin}} \tag{7.3}$$

The impedance of the skin is in the range of 10s of KΩ, varying with body conditions. The return path capacitance is dominated by the self-capacitance of the device and is around a few pFs [29]. Only when the transmitter comes in very close proximity of the ground plane (few cms) the distance between the device and the external ground has an effect on the return path capacitance . Hence, for all practical purposes, the return path capacitance is almost independent of the distance of the transmitter from the ground. Since the return path impedance is significantly larger

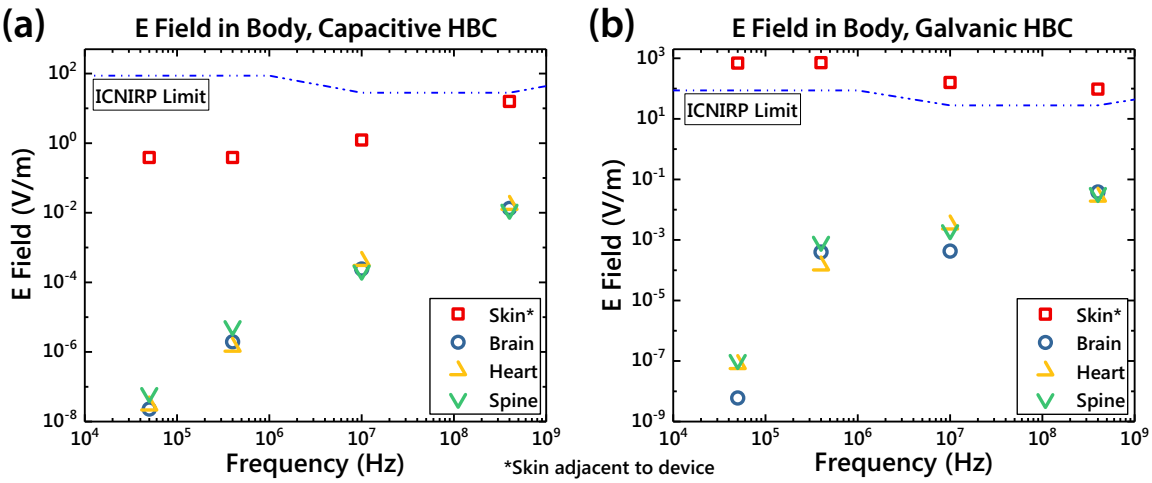


Fig. 7.7. Maximum RMS E fields at different parts of the body from simulations of the detailed human model of Fig. 7.6 with 1 V p-p sinusoidal excitation for (a) capacitive HBC, and (b) galvanic HBC. For galvanic HBC, the fields at the skin adjacent to the device is above the ICNIRP limit.

than the skin impedance for frequencies up to 10s of MHz range, the voltage drop across the skin is significantly small. As a result, the generated field is also small across the skin, whose thickness is presented as 4 mm.

The Bio-Physical model for galvanic HBC (Fig. 7.3f) shows that the impedance across the transmitter is primarily dependent on the skin impedance. The impedance provided by the internal tissue layers are in the order of few 100s of Ωs and smaller than the skin impedance (10s of KΩ). Hence, for galvanic HBC, the voltage drop across the skin (eq. (7.4)) is a significant portion of the applied voltage. So, the electric field density across the skin (eq. (7.5)) for galvanic HBC is significantly higher compared to capacitive HBC. This can be validated from the field plots obtained through HFSS simulations in Fig. 7.3a and Fig. 7.3b.

$$V_{skin,gal} = \frac{V_{in} * Z_{skin}}{2Z_{skin} + R_{body}} \tag{7.4}$$

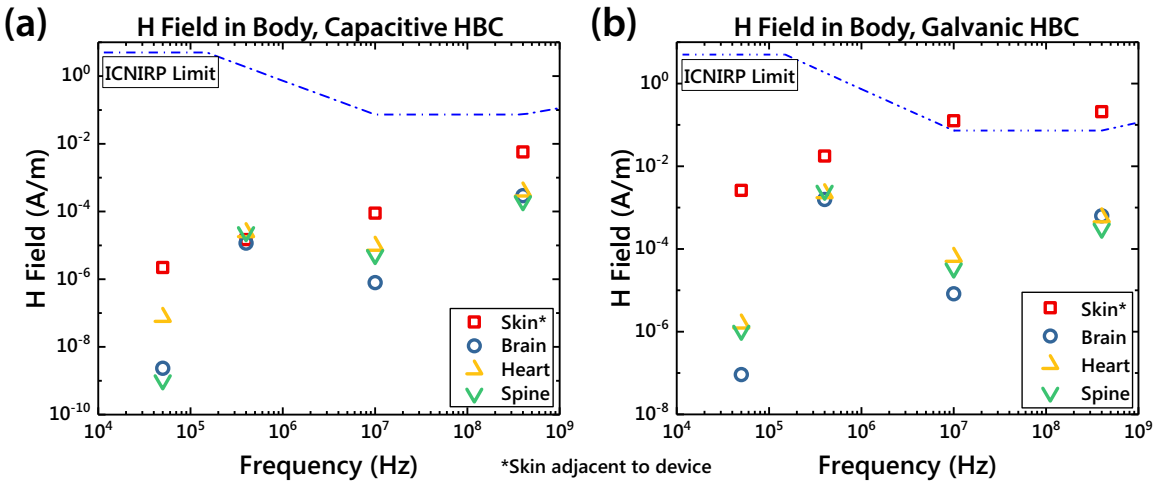


Fig. 7.8. Maximum RMS H fields at different parts of the body from simulations of the detailed human model of Fig. 7.6 with 1 V p-p sinusoidal excitation for (a) capacitive HBC, and (b) galvanic HBC. For galvanic HBC, the fields at the skin adjacent to the device is above the ICNIRP limit at frequencies over 10 MHz

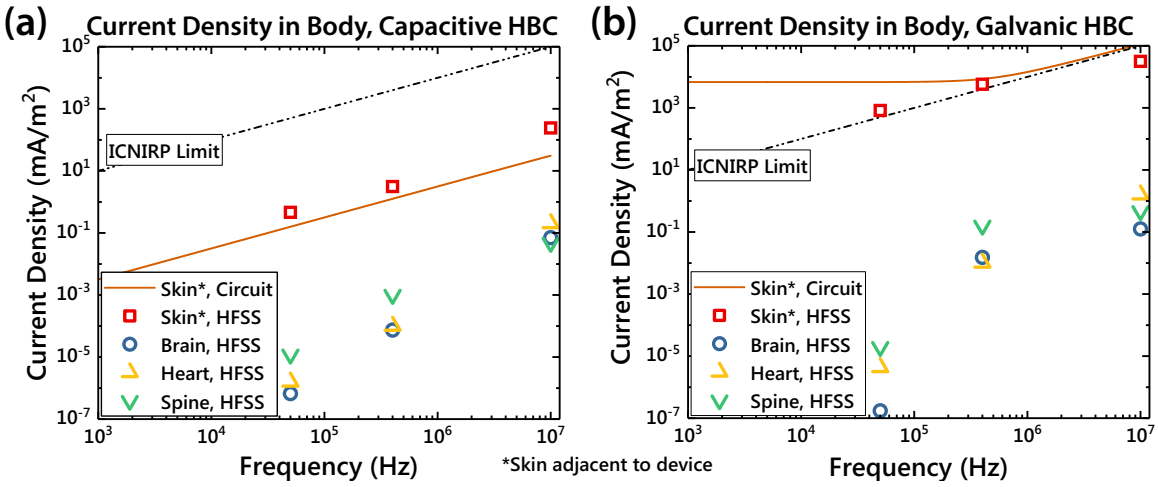


Fig. 7.9. RMS current densities at different parts of the body from simulations of the detailed human model of Fig. 7.6 with 1 V p-p sinusoidal excitation for (a) capacitive HBC, and (b) galvanic HBC. The current density at the skin adjacent to the device is also computed using a circuit theoretic model, and all values are compared with the ICNIRP limit for general public exposure.

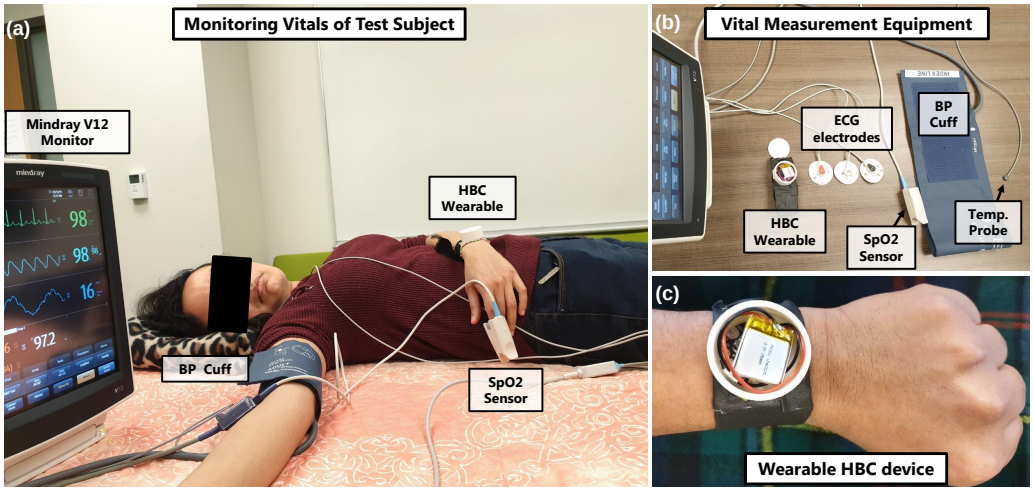


Fig. 7.10. Diagram showing the experimental setup for measuring the vital parameters of human subjects. a) Vital recordings carried out on a test subject, wearing a HBC transmitter device, using the Mindray V12 patient monitor, b) Details showing the equipment used for different measurements with the patient monitor, c) The HBC wearable device showing on the wrist of a test subject.

$$E_{skin,gal} = \frac{V_{skin,gal}}{t_{skin}} \tag{7.5}$$

### 7.2.5 Current Density Limits: FEM Simulations

Similar to the electric and magnetic field limits, the current density within the body can also be estimated from the HFSS simulations. Fig. 7.9 shows the current density on different parts of the body for a 1 V p-p sinusoidal excitation for capacitive (Fig. 7.9a) and galvanic HBC (Fig. 7.9b). The current density limits for capacitive HBC is significantly smaller than the safety limits imposed by the guidelines. In case of galvanic HBC though, the current density on the skin near the excitation point is close to the safety limits. The current density results on the skin obtained from circuit simulations of the bio-physical model is also shown in Fig. 7.9 and corroborates the safety of capacitive HBC in terms of current density.

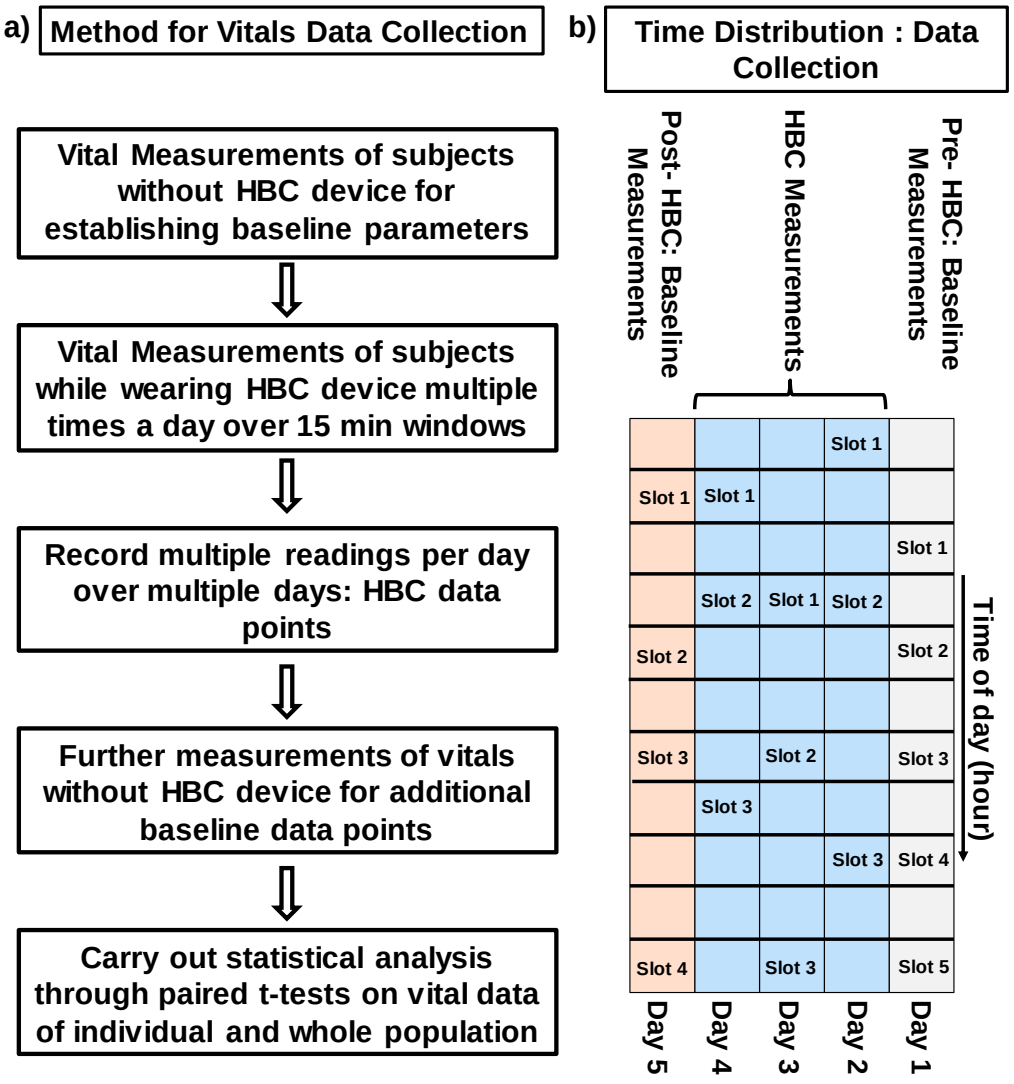


Fig. 7.11. a) Flow graph showing the method of vital data collection on test subjects. Measurements are first carried out to establish the baseline for each subject. Multiple following measurements were carried out with the HBC device worn by the test subjects on multiple days. Further baseline measurements are done following the completion of the tests with the HBC wearable device. b) Time slot distribution showing the type of data collected (baseline vs HBC data) over the different days of experiment.

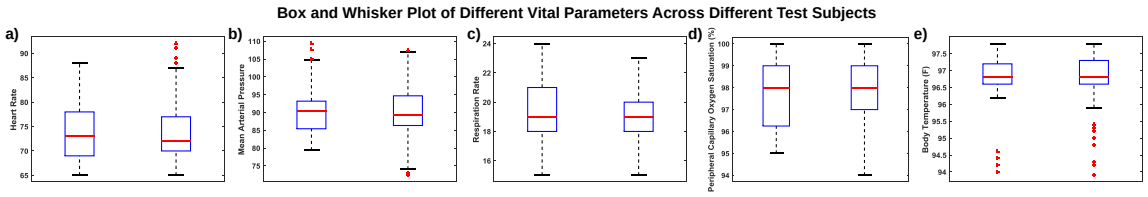


Fig. 7.12. Box and Whisker plot for the different vital parameters of the human subjects with and without wearing the HBC enabled device: a) Heart Rate (HR), b) Mean Arterial Pressure (MAP), c) Respiration Rate (RR), d) Peripheral Capillary Oxygen Saturation ($SpO_2$), e) Body Temperature. There is minimal change in the mean value and ranges of the vital parameters across the entire population in presence of signal transmission through HBC, compared to a normal scenario, showing HBC does not affect the vitals of the body.

## 7.3 Safety Analysis: Experiments

The previous sections theoretically establishes the safety of Capacitive HBC, both in terms of current density and electric/magnetic field intensity, through circuit and FEM simulations. The results show order of magnitude difference between the safety limits and the simulated current density, fields compared to the safety limits. To further corroborate and support the safety of HBC, we collect the vital parameters of human subjects and carry out a bio-statistical analysis and provide experimental evidence that HBC does not show any early signs of affecting the vital parameters of subjects.

### 7.3.1 Experimental Design and Methods

#### Study Design

To ascertain the existence of any short-term effect of HBC on the human body, a study was designed to non-invasively measure a set of commonly used five vital

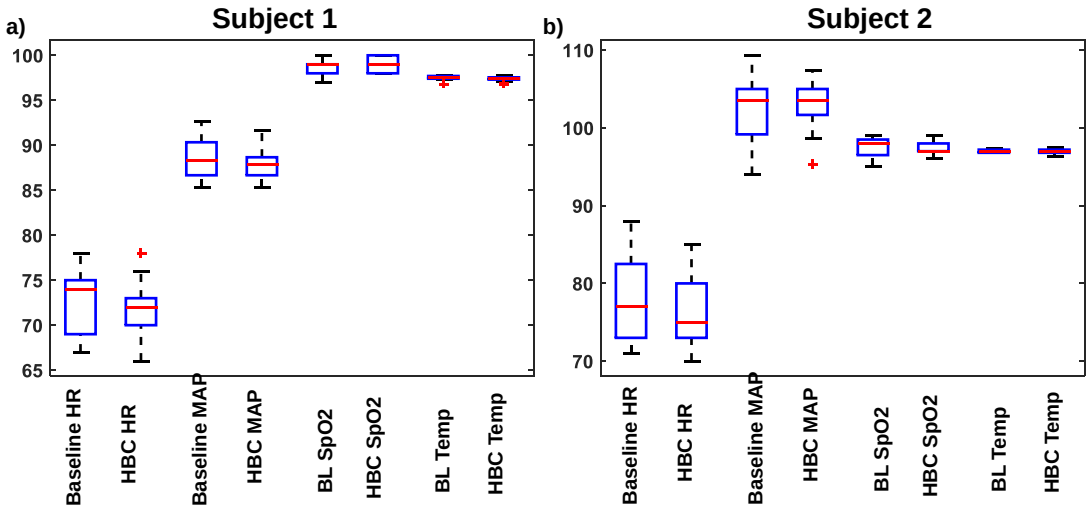


Fig. 7.13. Box and Whisker plot of HR, MAP, $SpO_2$, Body Temperature of two test subjects. Similar to the population ranges, the individual plots also do not show any significant change in the mean value and ranges of the vitals.

parameters from human subjects both in and without the presence of HBC devices. The study was approved by the Institute Review Board (IRB). Seven subjects took part in the experiments through voluntary consent. The vital parameters observed are the Heart Rate (HR), Blood Pressure (BP), Respiratory Rate (RR), oxygen saturation of hemoglobin ($SpO_2$) and body temperature (Temp) of the test subject.

**Experimental Procedure**

The volunteers were first monitored for their baseline vital parameters for a day. On the following three days the volunteers wore the HBC enabled watch-like wearable (Fig. 7.10c), during which their vital parameters were recorded for three time slots on each day. Following the set of measurements with the HBC device on, more baseline measurements are carried out for the vital parameters. The time slot distribution for these experiments are shown in Fig. 7.11b. These set of measurements were carried out multiple times almost over a month.

**Equipment and Facilities**

A medical grade patient monitor (MindRay V12), was used for measuring the vitals. The sensors used are ECG probes and gel electrodes, $SpO_2$ sensor, BP cuff and Temperature probe sourced from Mindray. The study design, preparation of subjects, experimental data collection and results of data analysis were supervised by a medical doctor.

**HBC Device Design**

The wearable 'watch-like' HBC device (Fig. 7.10c) consists of a microcontoller, a LiPo battery, a custom-made stretchable band with a copper electrode on the underside of the band touching the human skin, all housed in a small 3D printed round housing for easy all-day wearability for the volunteers. The device consists

of a 32-bit Cortex M0+ ATSAMD21E18 microcontroller is programmed to digitally synthesize the electrical excitation at 400 KHz with 3.3V peak to peak amplitude. This signal is then coupled into the body through a 2cmx2cm copper electrode. For all our experiments we carry out measurements for capacitive HBC, as this is our preferred mode of HBC, based on the theoretical analysis presented above. A single electrode is used to excite the signal into the body and the ground electrode remains floating. The HBC device is worn on the wrist of the volunteer.

**Data Collection and Statistical Analysis**

To ascertain the effects of HBC compared to a normal scenario, baseline data of the vital parameters of these subjects were also recorded on separate days, before and after they had put on the HBC enabled wearable. The goal of the experiments is to observe whether wearing the HBC enabled device has an effect on the vital parameters of the person through statistical analysis. Fig. 7.10 shows the details of the experimental setup. Fig. 7.10a shows the vital monitoring being carried out on one of the volunteers with a Mindray V12 patient monitor. The details of the different sensors used for the vital measurements are shown in Fig. 7.10b.

Each recording was made as a set of 5 data points. At the start of each recording, the monitor is connected to the human subject to record the vital information. Three gel electrode leads were placed, one each at the two arms and one at the left leg, and the tracing was chosen similar to that of a standard ECG Lead II. Blood Pressure (BP) was measured by means of an adult-sized BP cuff on the right arm that was set to inflate at intervals of 5 mins. The temperature probe was placed in contact with skin in the left axillary region. $SpO_2$ was measured by the pulse oximeter placed to clasp the tip of the left index finger. After the connection were made and the volunteers vitals attained steady-state, four consecutive readings were taken off the monitor display, concurrent with the 5-minute inflation interval of the BP cuff. Each data collection session lasted about 15 mins. Multiple such sessions of recordings were

made throughout the day on each volunteer over five days. The data recordings were done on 7 human subjects (4 male, 3 female) aged in the twenties and early thirties. a flow graph showing the complete data collection procedure is shown in Fig. 7.11a.

For each vital parameter, baseline readings were pooled together, and readings with HBC device on were pooled together. The range and 95% confidence interval of each subject was constructed from the data, both in the baseline state and Intra-HBC state, for each vital parameter. This allowed us to look for any significant change due to HBC in each individual subject. The Two-Sample t-test was used for this purpose. The p-values are also calculated to understand the statistical significance of the change in parameters, if any, as a result of wearing an HBC enabled device.

### 7.3.2 Results

The statistical analysis is done through Paired t-test of baseline data and the data with HBC wearable on, for each vital parameter. We carry out the t-test on both the individual and population vitals data. Individual t-tests are run to gather more statistical information, which can be limited from the population tests due to the relatively small population size. Hence, baseline and HBC measurements are carried out on individual test subjects multiple number of times to have sufficient statistical significance. The p values obtained from individual t-test results are shown in Table 7.1. It can be seen that the p values for all vital parameters for each individual is $>0.05$, indicating that HBC does not introduce any significant statistical change in the vital parameters of the subjects. The mean values of the vital parameters also show minimal change between the baseline scenario and with the HBC device on the test subject as shown in Table 7.2. Fig. 7.13 shows the box and whisker plot for the HR, MAP, $SpO_2$ and temperature measurements of two individual test subjects, showing small difference in the mean values and the ranges. Similarly the population box and whisker plots (Fig. 7.12) for all the different vital parameters show that there

is little change in the mean and range of the parameters between the states when the subject is wearing the HBC enabled device and when he/ she is not wearing it.

For looking at the changes in parameter in the entire population, the Paired t-test was used with the two variables being the Baseline mean and the Intra-HBC mean for each of the 7 subjects. Five such paired t-tests were done for the five vital parameters under consideration. The p values and the mean differences obtained from these tests also does not show any statistically significant change.

Table 7.1.
p values for t tests of individual subjects

| | HR | MAP | RR | $SpO_2$ | Temp |
|---|---|---|---|---|---|
| S1 | 0.16 | 0.26 | 0.55 | 0.18 | 0.31 |
| S2 | 0.28 | 0.56 | 0.41 | 0.19 | 0.09 |
| S3 | 0.11 | 0.98 | 0.21 | 0.50 | 0.57 |
| S4 | 0.34 | 0.40 | 0.49 | 0.29 | 0.39 |
| S5 | 0.79 | 0.06 | 0.52 | 0.28 | 0.58 |
| S6 | 0.27 | 0.45 | 0.60 | 0.48 | 0.40 |
| S7 | 0.39 | 0.06 | 0.68 | 0.59 | 0.70 |

## 7.4 Discussions

The different safety standards reviewed in this paper shows that the restriction limitations come from the limit on current density, Specific Absorption Rate and maximum field exposure. Certain design practices can be adopted to ensure safety compliance of the HBC devices even under varying conditions of the human body when nominal conditions are not satisfied. For example, the impedance provided by the human body can vary significantly (by orders of magnitude) in presence of sweat or a wound in the skin. This can lead to varying amount of current flowing through

Table 7.2.
Mean Difference for t tests of individual subjects

| | HR | MAP | RR | $SpO_2$ | Temp |
|---|---|---|---|---|---|
| S1 | 1.98 | 0.91 | 0.31 | 0.57 | 0.12 |
| S2 | 2.00 | 0.71 | 0.77 | 0.59 | 0.22 |
| S3 | 1.01 | 0.03 | 0.74 | 0.28 | 0.06 |
| S4 | 1.24 | 0.65 | 0.48 | 0.36 | 0.09 |
| S5 | 0.56 | 2.02 | 0.47 | 0.47 | 0.22 |
| S6 | 2.02 | 1.12 | 0.42 | 0.29 | 0.06 |
| S7 | 0.76 | 1.46 | 0.18 | 0.11 | 0.03 |

the body depending on the condition which can lead to currents exceeding the safety limit being injected into the body. From circuit design point of view any HBC device can be designed with a current limiter circuit at the output to ensure the injected current into the body is within the safety limits even under varying physiological condition. Such design practices need to be followed while designing HBC circuits and systems to ensure compliance with the safety limits at all frequencies and different mode of operation of the device.

## 7.5 Conclusion

HBC is a promising alternative to wireless radio wave based communication of devices around the body, due to its enhanced security and energy efficiency. However, the safety aspect of HBC needs to be carefully evaluated as it involves injecting electrical current into the body, This paper, for the first time, provides a thorough analysis of the safety compliance of different types of HBC by FEM, circuit simulations and carries out a small experimental study to observe any effect of HBC on the vital parameters of the human body. The simulations show that the current density and

field intensities in Capacitive HBC are significantly smaller compared to the safety standards. Bio statistical analysis of the vital parameters of human subjects involved in the experimental study show statistically insignificant change due to wearing a HBC device, supporting the simulation results. On the other hand, Galvanic HBC with differential excitation at the wrist can result in localized current densities and field intensities (around the electrode), which are significantly higher than the safety limits and should be avoided. Given that this small non-clinical study didn't show any early sign of the effect of HBC on the vitals of the subjects and the simulations showed large margin of safety, in future longer clinical studies can be done before HBC is adopted as a widely used product. Future studies about the safety aspect of HBC can employ invasive procedures on a wider population to see the effect of electrical signals on extracellular fluids, nerves, muscles and neuromuscular junctions.

## Acknowledgment

This work was supported in part by Eli Lilly through the Connected Health care initiative, Air Force Office of Scientific Research YIP Award under Grant FA9550-17-1-0450 and the National Science Foundation CRII Award under Grant CNS 1657455. The authors would like to thank Mr. Shitij Avlani for his help in designing the HBC wearable device.

# 8. CONCLUSION

Last few decades has seen a tremendous growth in the number of wearable and implantable devices due to scaling of semiconductor technology. A lot of research effort has focused on making these devices energy efficient to potentially enhance their lifetime. Since communication power consists of a significant portion of the overall system power, any communication method reducing energy is of significant interest. Human Body Communication (HBC) provides an alternative communication medium to radio wave communication for Wireless Body Area Network (WBAN) applications. In this thesis, we explore three key aspects of HBC : a) channel characterization b) energy efficient circuit design, c) secure system design. Through high impedance capacitive termination, the human body is shown to exhibit broadband characteristics. A bio-physical model is developed to explain the measured experimental results as well as the discrepancies found in previous literature. The wire-like characteristics of the human body is utilized to develop broadband circuits, which exhibits an energy efficiency of 6.3pJ/bit, achieving the lowest energy BAN IC. Finally it is shown that, through Electro Quasi-Static HBC, by operating at the frequency range of below a few MHz, the signals can be confined within a few cms from the body. This signal confinement enables secure communication through HBC, not possible with previous state-of-the art HBC implementations. COTS based demonstrations are developed to show strictly touch based communication between a wearable and ground connected device for Human-Computer Interaction scenarios such as information transfer and secure authentication. A prototype showing the first secure inter-body communication is also developed using EQS-HBC technique. These shows the possibility of using the human body as a secure energy efficient communication medium potentially making it the physical layer of choice for future Body Area Networks.

# REFERENCES

# REFERENCES


[1] T. G. Zimmerman, "Personal Area Networks: Near-field intrabody communication," *IBM Systems Journal*, vol. 35, no. 3.4, pp. 609–617, 1996.

[2] M. S. Wegmueller, M. Oberle, N. Felber, N. Kuster, and W. Fichtner, "Signal Transmission by Galvanic Coupling Through the Human Body," *IEEE Transactions on Instrumentation and Measurement*, vol. 59, no. 4, pp. 963–969, Apr. 2010.

[3] J. Park and P. P. Mercier, "Magnetic human body communication," in *2015 37th Annual International Conference of the IEEE Engineering in Medicine and Biology Society (EMBC)*, Aug. 2015, pp. 1841–1844.

[4] N. Cho, J. Yoo, S. Song, J. Lee, S. Jeon, and H. Yoo, "The Human Body Characteristics as a Signal Transmission Medium for Intrabody Communication," *IEEE Transactions on Microwave Theory and Techniques*, vol. 55, no. 5, pp. 1080–1086, May 2007.

[5] . Luev, I. Krois, and M. Cifrek, "A capacitive intrabody communication channel from 100 kHz to 100 MHz," in *2011 IEEE International Instrumentation and Measurement Technology Conference*, May 2011, pp. 1–4.

[6] . Lucev, I. Krois, and M. Cifrek, "A capacitive intrabody communication channel from 100 khz to 100 mhz," *IEEE Transactions on Instrumentation and Measurement*, vol. 61, no. 12, pp. 3280–3289, Dec 2012.

[7] J. Bae, H. Cho, K. Song, H. Lee, and H. Yoo, "The Signal Transmission Mechanism on the Surface of Human Body for Body Channel Communication," *IEEE Transactions on Microwave Theory and Techniques*, vol. 60, no. 3, pp. 582–593, Mar. 2012.

[8] J. Hwang, T. Kang, Y. Kim, and S. Park, "Measurement of Transmission Properties of HBC Channel and Its Impulse Response Model," *IEEE Transactions on Instrumentation and Measurement*, vol. 65, no. 1, pp. 177–188, Jan. 2016.

[9] J. A. Ruiz and S. Shimamoto, "A study on the transmission characteristics of the human body towards broadband intra-body communications," in *Proceedings of the Ninth International Symposium on Consumer Electronics, 2005. (ISCE 2005).*, Jun. 2005, pp. 99–104.

[10] M. A. Callejn, D. Naranjo-Hernndez, J. Reina-Tosina, and L. M. Roa, "A Comprehensive Study Into Intrabody Communication Measurements," *IEEE Transactions on Instrumentation and Measurement*, vol. 62, no. 9, pp. 2446–2455, Sep. 2013.

[11] M. A. Callejn, J. Reina-Tosina, D. Naranjo-Hernndez, and L. M. Roa, "Measurement issues in galvanic intrabody communication: Influence of experimental setup," *IEEE Transactions on Biomedical Engineering*, vol. 62, no. 11, pp. 2724–2732, Nov 2015.

[12] J. Park, H. Garudadri, and P. P. Mercier, "Channel Modeling of Miniaturized Battery-Powered Capacitive Human Body Communication Systems," *IEEE Transactions on Biomedical Engineering*, vol. 64, no. 2, pp. 452–462, Feb. 2017.

[13] Y. Song, Q. Hao, and K. Zhang, "Review of the Modeling, Simulation and Implement of Intra-body Communication," *Defence Technology*, vol. 9, no. 1, pp. 10–17, Mar. 2013. [Online]. Available: http://www.sciencedirect.com/science/article/pii/S2214914713000238

[14] R. Xu, H. Zhu, and J. Yuan, "Characterization and analysis of intra-body communication channel," in *2009 IEEE Antennas and Propagation Society International Symposium*, Jun. 2009, pp. 1–4.

[15] ——, "Electric-Field Intrabody Communication Channel Modeling With Finite-Element Method," *IEEE Transactions on Biomedical Engineering*, vol. 58, no. 3, pp. 705–712, Mar. 2011.

[16] W. Wang, Z. Nie, F. Guan, T. Leng, and L. Wang, "Experimental Studies on Human Body Communication Characteristics Based Upon Capacitive Coupling," in *2011 International Conference on Body Sensor Networks*, May 2011, pp. 180–185.

[17] N. Zedong, L. Tengfei, W. Wenchen, G. Feng, and W. Lei, "Experimental Characterization of human body communication in shield chamber," in *Proceedings of 2012 IEEE-EMBS International Conference on Biomedical and Health Informatics*, Jan. 2012, pp. 759–762.

[18] Y. Song, Q. Hao, K. Zhang, M. Wang, Y. Chu, and B. Kang, "The Simulation Method of the Galvanic Coupling Intrabody Communication With Different Signal Transmission Paths," *IEEE Transactions on Instrumentation and Measurement*, vol. 60, no. 4, pp. 1257–1266, Apr. 2011.

[19] B. Kibret, M. Seyedi, D. T. H. Lai, and M. Faulkner, "Investigation of Galvanic-Coupled Intrabody Communication Using the Human Body Circuit Model," *IEEE Journal of Biomedical and Health Informatics*, vol. 18, no. 4, pp. 1196–1206, Jul. 2014.

[20] P. J. H. Christina Skourou and K. D. Paulsen, "Tissue permittivity," *Cancer Biol Ther. 2009 Dec 1; 8(23): 22212227.*, May 2009, arXiv: 1805.02492. [Online]. Available: https://www.ncbi.nlm.nih.gov/pmc/articles/PMC3819449/

[21] R. M. Fish and L. A. Geddes, "Conduction of electrical current to and through the human body: a review," *Eplasty*, vol. 9, p. e44, Oct. 2009.

[22] Y. A. Chizmadzhev, A. V. Indenbom, P. I. Kuzmin, S. V. Galichenko, J. C. Weaver, and R. O. Potts, "Electrical properties of skin at moderate voltages: contribution of appendageal macropores," *Biophysical Journal*, vol. 74, no. 2 Pt 1, pp. 843–856, Feb. 1998.

[23] J. Rosell, J. Colominas, P. Riu, R. Pallas-Areny, and J. G. Webster, "Skin impedance from 1 hz to 1 mhz," *IEEE Transactions on Biomedical Engineering*, vol. 35, no. 8, pp. 649–651, Aug 1988.

[24] S. Maity, D. Das, and S. Sen, "Wearable health monitoring using capacitive voltage-mode Human Body Communication," in *2017 39th Annual International Conference of the IEEE Engineering in Medicine and Biology Society (EMBC)*, Jul. 2017, pp. 1–4.

[25] S. Sen, "SocialHBC: Social Networking and Secure Authentication Using Interference-Robust Human Body Communication," in *Proceedings of the 2016 International Symposium on Low Power Electronics and Design*, ser. ISLPED '16. New York, NY, USA: ACM, 2016, pp. 34–39. [Online]. Available: http://doi.acm.org/10.1145/2934583.2934609

[26] S. Maity, D. Das, X. Jiang, and S. Sen, "Secure Human-Internet using dynamic Human Body Communication," in *2017 IEEE/ACM International Symposium on Low Power Electronics and Design (ISLPED)*, Jul. 2017, pp. 1–6.

[27] S. Maity, B. Chatterjee, G. Chang, and S. Sen, "A 6.3pj/b 30mbps #x2212;30db SIR-tolerant broadband interference-robust human body communication transceiver using time domain signal-interference separation," in *2018 IEEE Custom Integrated Circuits Conference (CICC)*, Apr. 2018, pp. 1–4.

[28] S. Maity, K. Mojabe, and S. Sen, "Characterization of Human Body Forward Path Loss and Variability Effects in Voltage-Mode HBC," *IEEE Microwave and Wireless Components Letters*, vol. 28, no. 3, pp. 266–268, Mar. 2018.

[29] S. Maity, M. He, M. Nath, D. Das, B. Chatterjee, and S. Sen, "BioPhysical Modeling, Characterization and Optimization of Electro-Quasistatic Human Body Communication," *arXiv:1805.05200 [cs]*, May 2018, arXiv: 1805.05200. [Online]. Available: http://arxiv.org/abs/1805.05200

[30] W. R. Smythe, "Charged right circular cylinder," *Journal of Applied Physics*, vol. 33, no. 10, pp. 2966–2967, 1962. [Online]. Available: https://doi.org/10.1063/1.1728544

[31] ——, "Charged right circular cylinder," *Journal of Applied Physics*, vol. 27, no. 8, pp. 917–920, 1956. [Online]. Available: https://doi.org/10.1063/1.1722514

[32] "Investigating Human Body Communications | Intel Newsroom." [Online]. Available: https://newsroom.intel.com/editorials/investigating-human-body-communications-wearables/

[33] N. Cho, L. Yan, J. Bae, and H. J. Yoo, "A 60 kb/s #x2013;10 Mb/s Adaptive Frequency Hopping Transceiver for Interference-Resilient Body Channel Communication," *IEEE Journal of Solid-State Circuits*, vol. 44, no. 3, pp. 708–717, Mar. 2009.

[34] H. Cho, H. Kim, M. Kim, J. Jang, J. Bae, and H. Yoo, "21.1 A 79pj/b 80mb/s full-duplex transceiver and a 42.5W 100kb/s super-regenerative transceiver for body channel communication," in *2015 IEEE International Solid-State Circuits Conference - (ISSCC) Digest of Technical Papers*, Feb. 2015, pp. 1–3.

[35] J. Lee, V. V. Kulkarni, C. K. Ho, J. H. Cheong, P. Li, J. Zhou, W. D. Toh, X. Zhang, Y. Gao, K. W. Cheng, X. Liu, and M. Je, "30.7 A 60mb/s wideband BCC transceiver with 150pj/b RX and 31pj/b TX for emerging wearable applications," in *2014 IEEE International Solid-State Circuits Conference Digest of Technical Papers (ISSCC)*, Feb. 2014, pp. 498–499.

[36] J. Bae, K. Song, H. Lee, H. Cho, and H. Yoo, "A 0.24-nJ/b Wireless Body-Area-Network Transceiver With Scalable Double-FSK Modulation," *IEEE Journal of Solid-State Circuits*, vol. 47, no. 1, pp. 310–322, Jan. 2012.

[37] W. Saadeh, M. A. B. Altaf, H. Alsuradi, and J. Yoo, "A 1.1-mW Ground Effect-Resilient Body-Coupled Communication Transceiver With Pseudo OFDM for Head and Body Area Network," *IEEE Journal of Solid-State Circuits*, vol. 52, no. 10, pp. 2690–2702, Oct. 2017.

[38] K. Mueller and M. Muller, "Timing Recovery in Digital Synchronous Data Receivers," *IEEE Transactions on Communications*, vol. 24, no. 5, pp. 516–531, May 1976.

[39] C. Hand, "A Survey of 3d Interaction Techniques," *Computer Graphics Forum*, vol. 16, no. 5, pp. 269–281, Dec. 1997. [Online]. Available: https://onlinelibrary.wiley.com/doi/abs/10.1111/1467-8659.00194

[40] D. A. Bowman, E. Kruijff, J. J. LaViola, and I. Poupyrev, "An Introduction to 3-D User Interface Design," *Presence: Teleoper. Virtual Environ.*, vol. 10, no. 1, pp. 96–108, Feb. 2001. [Online]. Available: http://dx.doi.org/10.1162/105474601750182342

[41] E. Wood, T. Willoughby, A. Rushing, L. Bechtel, and J. Gilbert, "Use of Computer Input Devices by Older Adults," *Journal of Applied Gerontology*, vol. 24, no. 5, pp. 419–438, Nov. 2005. [Online]. Available: https://doi.org/10.1177/0733464805278378

[42] N. Caprani and N. E. O. a. C. Gurrin, "Touch Screens for the Older User," *Assistive Technologies*, 2012. [Online]. Available: https://www.intechopen.com/books/assistive-technologies/touch-screens-for-the-older-user

[43] K. Cheverst, A. Dix, D. Fitton, C. Kray, M. Rouncefield, C. Sas, G. Saslis-Lagoudakis, and J. G. Sheridan, "Exploring Bluetooth Based Mobile Phone Interaction with the Hermes Photo Display," in *Proceedings of the 7th International Conference on Human Computer Interaction with Mobile Devices & Services*, ser. MobileHCI '05. New York, NY, USA: ACM, 2005, pp. 47–54. [Online]. Available: http://doi.acm.org/10.1145/1085777.1085786

[44] R. Ballagas, M. Rohs, and J. G. Sheridan, "Sweep and Point and Shoot: Phonecam-based Interactions for Large Public Displays," in *CHI '05 Extended Abstracts on Human Factors in Computing Systems*, ser. CHI EA '05. New York, NY, USA: ACM, 2005, pp. 1200–1203. [Online]. Available: http://doi.acm.org/10.1145/1056808.1056876

[45] R. Hardy and E. Rukzio, "Touch & Interact: Touch-based Interaction of Mobile Phones with Displays," in *Proceedings of the 10th International Conference on Human Computer Interaction with Mobile Devices and Services*, ser. MobileHCI

'08. New York, NY, USA: ACM, 2008, pp. 245–254. [Online]. Available: http://doi.acm.org/10.1145/1409240.1409267

[46] "BodyCom Technology | Microchip Technology." [Online]. Available: http://www.microchip.com/design-centers/embedded-security/technology/bodycom-trade-technology

[47] ikinamo, "Human body as a communication medium : DigInfo." [Online]. Available: https://www.youtube.com/watch?v=bgl88nrd7do

[48] "Panasonic's wild new technology transmits data by human touch," Oct. 2016. [Online]. Available: https://www.pcworld.com/article/3128025/wearables/panasonic-has-a-technology-for-transmitting-data-by-human-touch.html

[49] Nextel Italia S.r.l., "Tecnologia NFC RedTacton (En)." [Online]. Available: https://www.youtube.com/watch?v=uAzphwZ8VLY

[50] V. Varga, G. Vakulya, A. Sample, and T. R. Gross, "Enabling Interactive Infrastructure with Body Channel Communication," *Proc. ACM Interact. Mob. Wearable Ubiquitous Technol.*, vol. 1, no. 4, pp. 169:1–169:29, Jan. 2018. [Online]. Available: http://doi.acm.org/10.1145/3161180

[51] M. Hessar, V. Iyer, and S. Gollakota, "Enabling On-body Transmissions with Commodity Devices," in *Proceedings of the 2016 ACM International Joint Conference on Pervasive and Ubiquitous Computing*, ser. UbiComp '16. New York, NY, USA: ACM, 2016, pp. 1100–1111. [Online]. Available: http://doi.acm.org/10.1145/2971648.2971682

[52] V. Varga, G. Vakulya, A. Sample, and T. R. Gross, "Enabling interactive infrastructure with body channel communication," *Proc. ACM Interact. Mob. Wearable Ubiquitous Technol.*, vol. 1, no. 4, pp. 169:1–169:29, Jan. 2018. [Online]. Available: http://doi.acm.org/10.1145/3161180

[53] V. Varga, M. Wyss, G. Vakulya, A. Sample, and T. R. Gross, "Designing groundless body channel communication systems: Performance and implications," in *Proceedings of the 31st Annual ACM Symposium on User Interface Software and Technology*, ser. UIST '18. New York, NY, USA: ACM, 2018, pp. 683–695. [Online]. Available: http://doi.acm.org/10.1145/3242587.3242622

[54] D. G. Park, J. K. Kim, J. B. Sung, J. H. Hwang, C. H. Hyung, and S. W. Kang, "Tap: Touch-and-play," in *Proceedings of the SIGCHI Conference on Human Factors in Computing Systems*, ser. CHI '06. New York, NY, USA: ACM, 2006, pp. 677–680. [Online]. Available: http://doi.acm.org/10.1145/1124772.1124873

[55] M. Takahashi, C. L. Fernando, Y. Kumon, S. Takeda, H. Nii, T. Tokiwa, M. Sugimoto, and M. Inami, "Earthlings attack!: A ball game using human body communication," in *Proceedings of the 2Nd Augmented Human International Conference*, ser. AH '11. New York, NY, USA: ACM, 2011, pp. 17:1–17:4. [Online]. Available: http://doi.acm.org/10.1145/1959826.1959843

[56] N. Matsushita, S. Tajima, Y. Ayatsuka, and J. Rekimoto, "Wearable key: device for personalizing nearby environment," in *Digest of Papers. Fourth International Symposium on Wearable Computers*, Oct 2000, pp. 119–126.

[57] M. Fukumoto and M. Shinagawa, "Carpetlan: A novel indoor wireless(-like) networking and positioning system," in *UbiComp 2005: Ubiquitous Computing*, M. Beigl, S. Intille, J. Rekimoto, and H. Tokuda, Eds. Berlin, Heidelberg: Springer Berlin Heidelberg, 2005, pp. 1–18.

[58] J. R. Smith, "Field mice: Extracting hand geometry from electric field measurements," *IBM Systems Journal*, vol. 35, no. 3.4, pp. 587–608, 1996.

[59] J. Rekimoto, "Smartskin: An infrastructure for freehand manipulation on interactive surfaces," in *Proceedings of the SIGCHI Conference on Human Factors in Computing Systems*, ser. CHI '02. New York, NY, USA: ACM, 2002, pp. 113–120. [Online]. Available: http://doi.acm.org/10.1145/503376.503397

[60] P. Dietz and D. Leigh, "Diamondtouch: A multi-user touch technology," in *Proceedings of the 14th Annual ACM Symposium on User Interface Software and Technology*, ser. UIST '01. New York, NY, USA: ACM, 2001, pp. 219–226. [Online]. Available: http://doi.acm.org/10.1145/502348.502389

[61] T. Grosse-Puppendahl, A. Braun, F. Kamieth, and A. Kuijper, "Swiss-cheese extended: An object recognition method for ubiquitous interfaces based on capacitive proximity sensing," in *Proceedings of the SIGCHI Conference on Human Factors in Computing Systems*, ser. CHI '13. New York, NY, USA: ACM, 2013, pp. 1401–1410. [Online]. Available: http://doi.acm.org/10.1145/2470654.2466186

[62] G. Lan, D. Ma, W. Xu, M. Hassan, and W. Hu, "Capsense: Capacitor-based activity sensing for kinetic energy harvesting powered wearable devices," in *Proceedings of the 14th EAI International Conference on Mobile and Ubiquitous Systems: Computing, Networking and Services*, ser. MobiQuitous 2017. New York, NY, USA: ACM, 2017, pp. 106–115. [Online]. Available: http://doi.acm.org/10.1145/3144457.3144459

[63] I. Habib, N. Berggren, E. Rehn, G. Josefsson, A. Kunz, and M. Fjeld, "Dgts: Integrated typing and pointing," in *Human-Computer Interaction – INTERACT 2009*, T. Gross, J. Gulliksen, P. Kotzé, L. Oestreicher, P. Palanque, R. O. Prates, and M. Winckler, Eds. Berlin, Heidelberg: Springer Berlin Heidelberg, 2009, pp. 232–235.

[64] M. Valtonen, J. Maentausta, and J. Vanhala, "Tiletrack: Capacitive human tracking using floor tiles," in *2009 IEEE International Conference on Pervasive Computing and Communications*, March 2009, pp. 1–10.

[65] Y. Zhang, J. Zhou, G. Laput, and C. Harrison, "Skintrack: Using the body as an electrical waveguide for continuous finger tracking on the skin," in *Proceedings of the 2016 CHI Conference on Human Factors in Computing Systems*, ser. CHI '16. New York, NY, USA: ACM, 2016, pp. 1491–1503. [Online]. Available: http://doi.acm.org/10.1145/2858036.2858082

[66] J. Zhou, Y. Zhang, G. Laput, and C. Harrison, "Aurasense: Enabling expressive around-smartwatch interactions with electric field sensing," in *Proceedings of the 29th Annual Symposium on User Interface Software and Technology*, ser. UIST '16. New York, NY, USA: ACM, 2016, pp. 81–86. [Online]. Available: http://doi.acm.org/10.1145/2984511.2984568

[67] Y. Kim, S. Lee, I. Hwang, H. Ro, Y. Lee, M. Moon, and J. Song, "High5: Promoting interpersonal hand-to-hand touch for vibrant workplace with electrodermal sensor watches," in *Proceedings of the 2014 ACM International Joint Conference on Pervasive and Ubiquitous Computing*, ser. UbiComp '14. New York, NY, USA: ACM, 2014, pp. 15–19. [Online]. Available: http://doi.acm.org/10.1145/2632048.2632072

[68] L. Buechley, D. Mellis, H. Perner-Wilson, E. Lovell, and B. Kaufmann, "Living wall: Programmable wallpaper for interactive spaces," in *Proceedings of the 18th ACM International Conference on Multimedia*, ser. MM '10. New York, NY, USA: ACM, 2010, pp. 1401–1402. [Online]. Available: http://doi.acm.org/10.1145/1873951.1874226

[69] C.-H. Lee and T. Selker, "isphere: A proximity-based 3d input device," in *ACM SIGGRAPH 2004 Posters*, ser. SIGGRAPH '04. New York, NY, USA: ACM, 2004, pp. 72–. [Online]. Available: http://doi.acm.org/10.1145/1186415.1186499

[70] S. Maity, M. He, M. Nath, D. Das, B. Chatterjee, and S. Sen, "Biophysical modeling, characterization and optimization of electro-quasistatic human body communication," *IEEE Transactions on Biomedical Engineering*, pp. 1–1, 2018.

[71] D. Das, S. Maity, B. Chatterjee, and S. Sen, "Enabling covert body area network using electro-quasistatic human body communication," *Scientific Reports*, vol. 9, no. 1, pp. 169:1–169:29, Mar. 2019. [Online]. Available: https://doi.org/10.1038/s41598-018-38303-x

[72] ICNIRP, "Icnirp guidelines for limiting exposure to timevarying electric and magnetic fields (1hz  100 khz)."

[73] S. Gabriel, R. W. Lau, and C. Gabriel, "The dielectric properties of biological tissues: II. measurements in the frequency range 10 hz to 20 GHz," *Physics in Medicine and Biology*, vol. 41, no. 11, pp. 2251–2269, nov 1996.

VITA

# VITA

Shovan Maity received the B.E. degree in electronics and telecommunication engineering from Jadavpur University, India, in 2012, and the M.Tech. degree in electrical engineering from IIT Bombay, in 2014. He was an Analog Design Engineer at Intel, Bangalore, India, from 2014 to 2016. He is currently pursuing the Ph.D. degree in electrical engineering with Purdue University, West Lafayette, IN, USA. His research interests include design of circuits and systems for human body communication, hardware security, and mixed signal circuits design. Shovan is the recipient of the Institute Silver Medal, IIT Bombay in 2014 and the HOST 2017 best student paper award.